Mitigation of stray magnetic fields in MICE

J. Blogs, J. Blogs, J. Blogs, J. Blogs, J. Blogs, J. Blogs, J. Blogs, J. Blogs, J. Blogs, J. Blogs,
J. Blogs, J. Blogs, J. Blogs, J. Blogs, J. Blogs, J. Blogs, J. Blogs, J. Blogs, J. Blogs, J. Blogs,
J. Blogs, J. Blogs, J. Blogs, J. Blogs, J. Blogs, J. Blogs, J. Blogs, J. Blogs, J. Blogs, J. Blogs,
J. Blogs, J. Blogs, J. Blogs, J. Blogs, J. Blogs

Editors:

- **KL:** Sections 1, 5 and 6;
- **MG:** Section 3 (KL and IT will fill in while MG away); and
- **IT:** Sections 2 and 4.

1 Introduction

The results of an analysis of the stray magnetic field in the MICE Hall presented to the collaboration at its meeting in June 2012 (CM33) showed that, in their original positions, the compressors serving the cryocoolers, the magnet controls and power-supply racks and the tracker readout and control racks would be exposed to unacceptably high magnetic fields [1]. In addition, the analysis indicated that other equipment in the Hall, such as the cold-box of the Linde refrigerator and the hydrogen gas-panel, were at risk of having their functionality compromised.

The Magnetic Shielding Group (MSG [2, 3]) was created at CM33 to develop and then to execute the measures required to reduce the stray fields to acceptable levels. The MSG identified two approaches:

1. *Local shielding*: remove equipment from areas of high field and, if this is not possible for certain items, design bespoke shielding to be mounted locally; and
2. *Partial return yoke*: design a partial return yoke (PRY) by which the stray field is contained within a volume close to the MICE magnets.

In view of the design, schedule and cost uncertainties attendant on the PRY solution, the collaboration adopted the local-shielding approach as its baseline strategy at its collaboration meeting in October 2012 (CM34). To mitigate the risk that the baseline approach would fail to produce acceptable solutions for all the critical equipment, the PRY continued to be developed. The continued development of the PRY as a risk-mitigating option was made possible through the recruitment of additional expertise at Brookhaven National Laboratory (BNL).

Implementation of the first steps of the mitigation programme, moving the compressors to the West Wall of the MICE Hall and the magnet control and power-supply racks to Rack Room 2 (see Section 3) was initiated at the February 2013 collaboration meeting (CM35). The development of the baseline approach continued with the design of local shielding for the tracker readout and control systems and the consideration of other equipment deemed to be at risk. The development of the PRY was pursued in parallel. In addition, a careful analysis of the stray field leaking out of the MICE Hall was carried out. The development of the baseline approach and of the PRY alternative is now sufficiently mature to allow the collaboration to consider whether the implementation of the PRY should replace the local-shielding approach as the baseline. **This document describes the considerations that have led the collaboration to ...**

This document is organised as follows. Section 2 reviews the stray fields that would be present in the MICE Hall in the absence of mitigation and defines the issues that must be addressed. Section 3 summarises the actions taken to site the compressors on the West Wall and the control and power-supply racks in Rack Room

2. Section 4 describes the detailed finite-element model of the MICE Hall that has been developed to allow the mitigation strategies to be developed. Section 5 contains a critical analysis of the status of development of the present baseline (local shielding). The design and implementation of the Partial Return Yoke is presented in Section 6. Finally, Section 8 summarises the action that the collaboration proposes to take based on the analyses presented in Sections 5 and 6.

2 The need for stray-field mitigation

The MICE cooling channel will be built in a number of steps (see Figure 1). The MICE Muon Beam and the beam-line instrumentation (see Figure 2) were constructed to perform Step I, which is now complete [4, 5]. Particles in the MICE Muon Beam travel from East to West. The orientation of the beam line with respect to the points of the compass is shown in Figure 2. The collaboration is now preparing Step IV which consists of two solenoidal spectrometers and a single absorber/focus-coil (AFC) module [6]. The energy lost by the muon beam as it passes through the absorber is replaced in two, four-cavity, 201 MHz linac modules. A large superconducting solenoid (the coupling coil) focuses the beam as it passes through the linac module. The linac/coupling-coil module is referred to as the RFCC module. The full MICE cooling cell will be assembled at Step VI with the addition of two RFCC modules and two AFC modules to the Step IV configuration (see the lower drawing in Figure 1 and Figure 3). The timetable for the implementation of the experiment is shown in Figure 1.

The MICE solenoid magnets will each produce fields of the order of several Tesla. The cooling channel will run either in solenoid mode or in flip mode. In solenoid mode, the magnetic axis of each magnet points in the same direction. In flip mode, the magnetic axis will be reversed at the downstream coil in each of the AFC modules.

The spectrometer solenoids consist of a long solenoid with two trim coils to produce a uniform, 4 T field in the tracking volume. Two "matching coils" are wound on the same bobbin. The excitation of the matching coils is chosen to match the beam from the solenoid to the MICE cooling cell. The focus-coil modules consist of two windings on the same bobbin that can be run in solenoid mode or in flip mode. Each coupling coil is a single winding with a bore in excess of 120 cm. Return yokes were not included in either the spectrometer solenoids, the focus-coil modules or the coupling-coil modules. Each of the magnets therefore produces a large stray field; the large bore coupling-coil making a particularly significant contribution.

Two soft iron magnetic shield walls, the North and South Shield Walls, were built to contain the stray field within the MICE Hall. However, as the design of the experiment evolved it has become necessary to use the space between the Walls to house equipment. A re-analysis of the stray field early in 2012 demonstrated that the strength of the stray field was higher than the original simulations had indicated. The field level between the Walls was sufficient that remedial action was required to mitigate the effects of the field. In addition it was necessary to re-evaluate the effectiveness of the Shield Walls at containing the field within the Hall.

The requirements of the stray magnetic field mitigation programme are:

1. To re-site or shield equipment sensitive to stray magnetic field such that the field to which the equipment is exposed is low enough that reliable operation in Steps IV and VI in both solenoid and flip modes is ensured;
2. To devise a mitigation programme that is practical in the sense that it must not place unreasonable constraints on the ability to operate the experiment either in terms of physical access to the various components or the amount of time it takes to run;
3. To provide shielding such that all equipment belonging to MICE or ISIS and positioned outside the MICE Hall functions normally without additional shielding or with minimal additional shielding; and

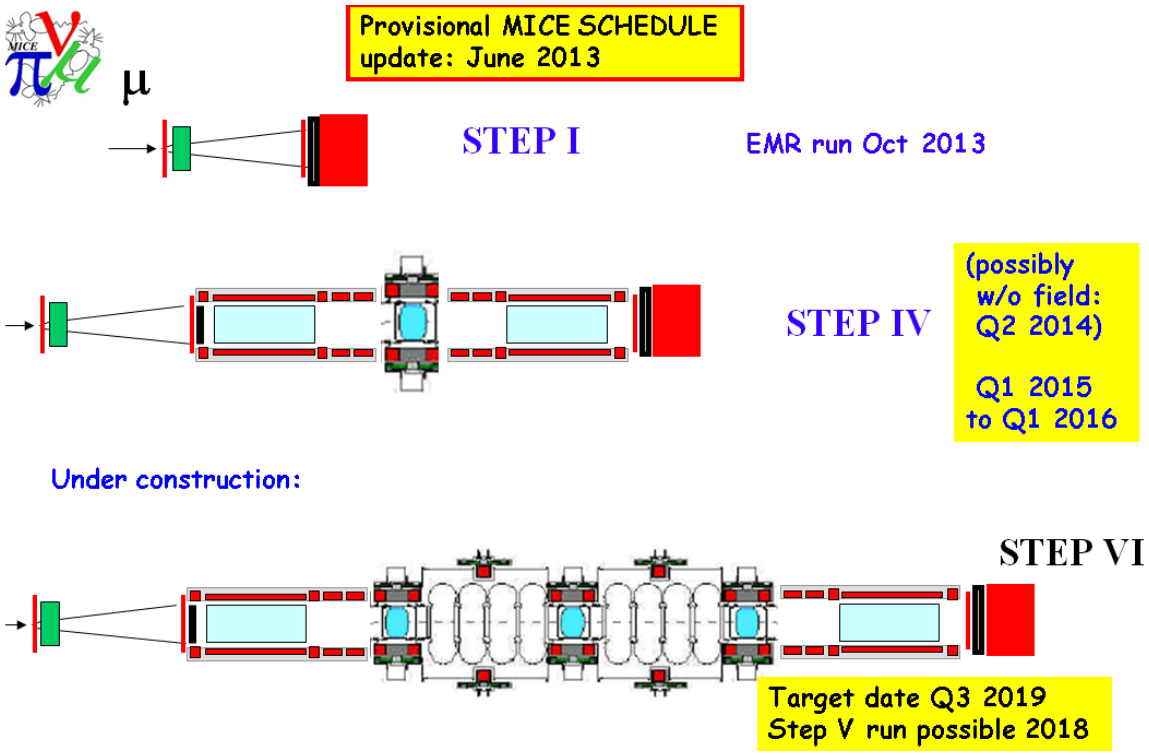

Figure 1: Schematic representation of the MICE Steps (see text). The solenoid coil packs are indicated by the grey rectangles. The individual coils within the coil packs are indicated by the red rectangles. The spectrometer solenoids consist of a long solenoid with two trim coils together with two matching coils wound on the same bobbin. The focus-coil modules consist of two windings on the same bobbin. Each coupling coil is a single winding with a bore in excess of 120 cm. The annotation shows the dates at which the various Steps are scheduled to be complete based on the June 2013 schedule revision.

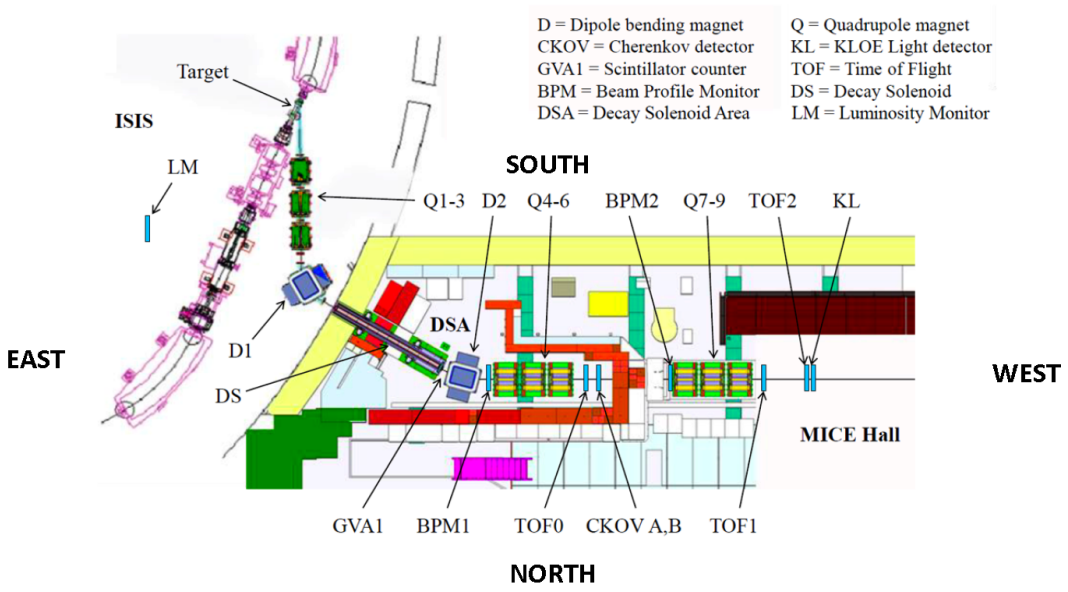

Figure 2: The MICE Muon Beam on ISIS. Protons circulate clockwise in ISIS, producing pions when they intersect with the MICE target. Pions are captured in a quad triplet (Q1–3) and transported to a dipole (D1) which directs pions in the chosen momentum range to the MICE Hall. A superconducting solenoid (DS) causes the pions to spiral, increasing the length of their flight path and so enhancing the number of muons transmitted to the second dipole magnet (D2) at which the muon momentum is selected. Muon transport to MICE is achieved in two quad triplets (Q4–6 and Q7–9). The beam-line instrumentation consists of time-of-flight counters labelled TOF0 and TOF1 and Cherenkov counters (CKOVA and CKOVB) The MICE Muon Beam travels from East to West as shown. The North and South Walls of the Hall are also indicated.

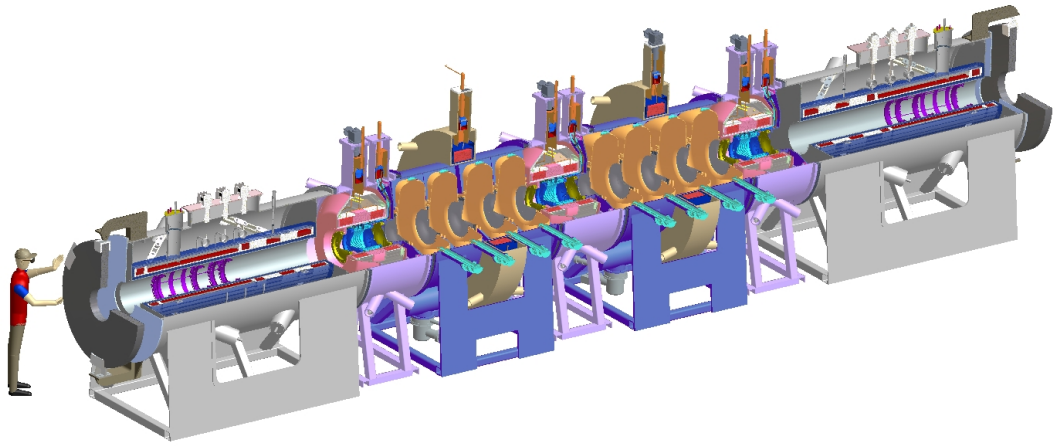

Figure 3: Rendered engineering drawing of the MICE experiment in the Step VI configuration.

4. All health and safety requirements must be satisfied including the limit on the magnetic field in areas accessible to the public. A limit of five Gauss is specified in the RAL and CERN "Best Practice" guides [**?**].

The mitigation strategy was developed under the constraint that its implementation gives as little additional delay to the completion of Step IV as possible. It was considered important, though not essential, that the solution adopted for Step IV be capable of being developed incrementally to serve at Step VI.

3 West Wall Mezzanine and Rack Room 2

The results from the analysis presented in [1] implied that the compressors serving the cryocoolers must be moved from under the South Mezzanine to a location where the stray field is expected to be acceptably low. In the baseline (local shielding) case the move is required because the cost of shielding the compressors was considered to be prohibitively large and, in the case of the alternative PRY solution, the move is required to make space for the support structures and services.

Further, the results of the analysis presented in [1] implied that the magnet power-supply and control racks must also be moved to a location where the stray field is sufficiently low. The advantages to the operation of the experiment if the racks were sited outside the Hall were taken into account.

To mitigate the effect of the stray fields on the compressors and the magnet power-supply and control racks the following steps are being taken:

1. A West Wall Mezzanine to support the compressors is being constructed; and
2. Additional space outside the MICE Hall has been secured to provide "Rack Room 2" to house the racks and to allow the MICE Local Control Room (MLCR) to be extended.

3.1 West Wall Mezzanine

The analysis of the field in the MICE Hall presented in section 2 showed that the field in the region adjacent to the West Wall was sufficiently low for the safe operation of the compressors. In addition, it was determined that the space available was sufficient and that routings could be devised that satisfied the limit on the maximum length of the high-pressure hoses that serve the compressors.

While the West Wall is a relatively open space, it is not uncluttered (see figure 4). In addition, the floor adjacent to the West Wall will be required for the delivery and preparation of components of the experiment. To maintain floor space, yet gain the space to locate the compressors, a mezzanine platform will be installed [7, 8].

There will be 15 compressors located on the West Mezzanine at Step IV and another 4 on the ground floor at the north end. More compressors will be located on the platform and the ground floor at the later Steps (see figure 5). Additional changes to the west end of the South Mezzanine, including moving the power distribution for the compressors to the South Mezzanine platform, re-configuring the staircase from the South Mezzanine platform and changes to the Personnel Protection System (PPS) are required (see figure 6).

3.2 Rack Room 2 and MLCR

Consideration of possible locations for the power-supply and control racks led to the negotiation of more space opposite the current MLCR. The "Rack Room 2" (RR2) layout has been developed and shown to be acceptable (see figure 7) [**?**].

Figure 4: Current West Wall configuration.

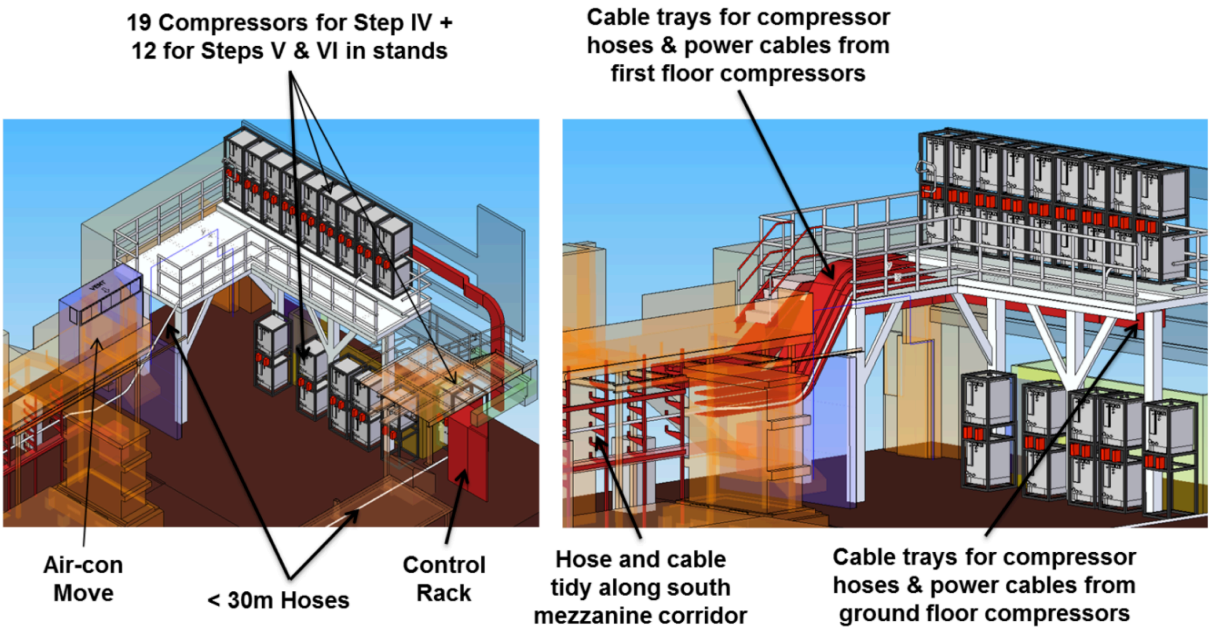

Figure 5: Compressor layout for various MICE Steps.

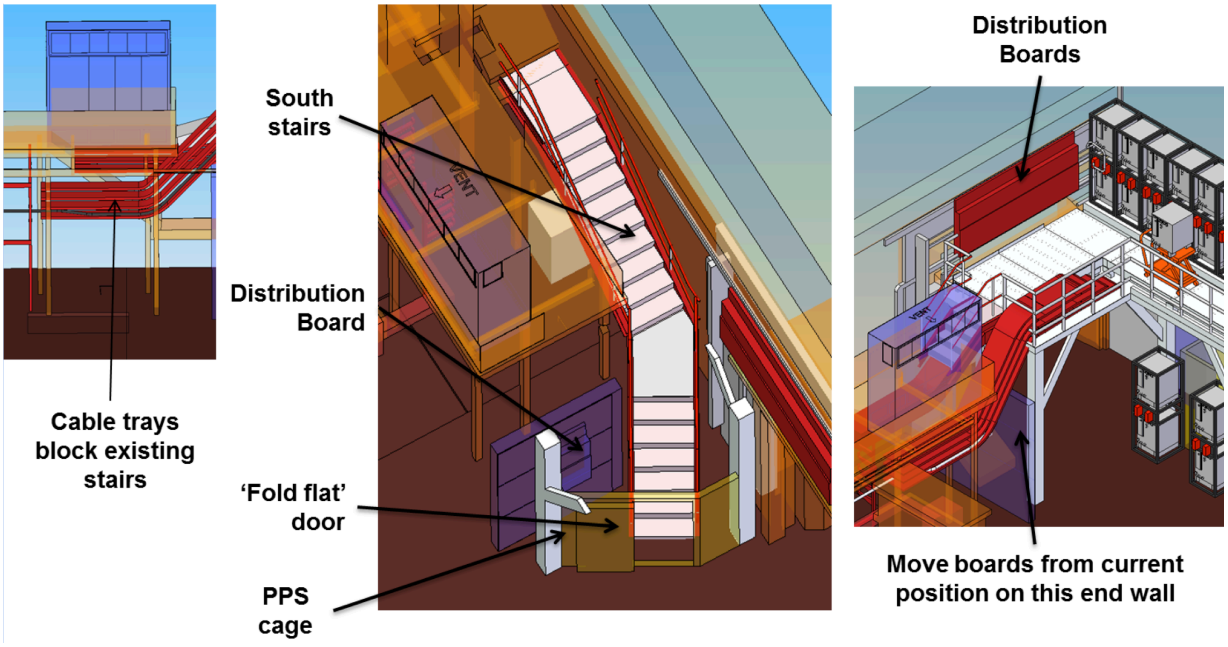

Figure 6: Additional changes for West Mezzanine implementation.

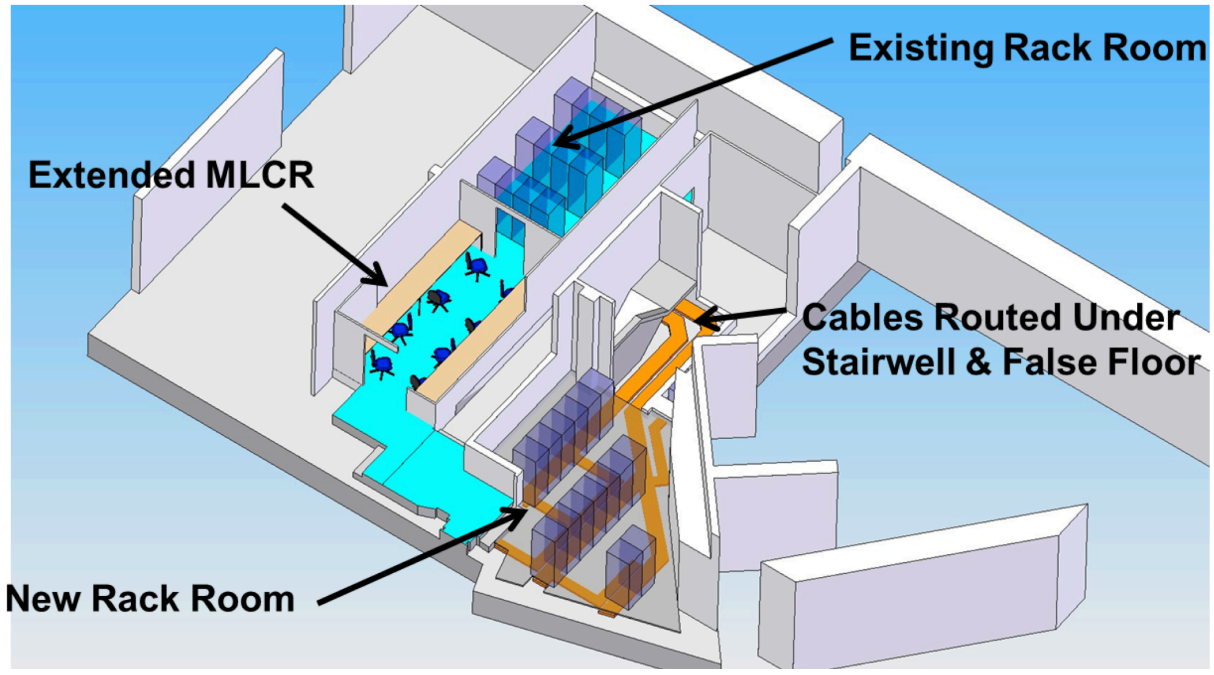

Figure 7: Rack Room 2 and MLCR changes.

The current MLCR supports four people comfortably. There are expected to be up to six people using the MLCR during Step IV commissioning. ISIS have agreed, in principle, that the MLCR can be extended. The current MLCR (as well as the adjoining rack room) is built with Thrislington partitioning so the cost and schedule implication of modification to gain the 2 extra seats will be relatively small. The extension of the MLCR raises issues with access to the ISIS plant room and the ISIS Control Room Power Distribution boards which have to be resolved with ISIS (see figure 7).

These issues aren't visible in the image (at least to the untrained eye).

4 Magnetic model of the MICE Hall

4.1 Purpose of the Model

In order to further understand the issues with the stray field of the MICE magnets, a magnetic model of the MICE Hall was prepared, providing a prediction of the stray field throughout the MICE Hall and surrounding buildings. This model is capable of producing field maps for multiple operating modes of the MICE magnets (two magnet layouts, Steps IV and VI, convolved with two magnet current configurations, solenoid and flip modes, provide four combinations). A range of muon momentum configurations are also possible, but the 240 MeV/c operating mode has the highest magnet currents and therefore the highest stray fields, so was the only configuration modelled. This report is predominantly focussed on the next Step of the experiment, Step IV.

The primary goals of the model are to:

1. Produce field maps that allow a better understanding of potential issues arising from the stray fields, and guide the necessary mitigation work for the baseline design.
2. Provide field maps as input into other, smaller but more detailed models.
3. Provide members of the collaboration with estimates of the magnetic field strength in air, in the vicinity of their equipment.

4.2 Modelling Technique

The model of the MICE Hall is produced using a commercial software package, OPERA 3D from Cobham / Vector Fields [**?**], which relies on finite element analysis (FEA) techniques to estimate the magnetic field. FEA modelling can be a very computationally intensive task, depending on the extent and the required granularity (mesh size) of the model.

The MICE Hall represents a significant volume, approximately 40 m $\times$ 12 m $\times$ 12 m in size, and contains a significant amount of ferrous material. Unfortunately, there is no symmetry to exploit. We also need to simulate how the fields penetrate beyond the confines of the MICE Hall, particularly into the MICE and ISIS control rooms, and a significant additional volume is required to ensure that boundary conditions do not influence the solution. The total volume of the model is approximately 120 m $\times$ 80 m $\times$ 80 m.

Building an FEA model on this scale requires a careful balance between detail and mesh size. To make the problem tractable, certain ferrous objects have not been modelled and others have been simplified geometrically. Despite these best efforts, the model is still large and takes significant computing resources to solve.

The OPERA package breaks the FEA into tasks run by three modules:

1. The 'modeller' module is responsible for defining the model and geometry, as well as meshing the complete model. The user prepares modular .comi files, written in an OPERA–specific scripting language, which define the layout of the hall and all of the constituent elements. This allows for a modular definition

of the model (with elements being added, removed or adjusted as required) and provides documentation of each model run.

2. The 'solver' module applies the actual FE analysis, iteratively finding a solution to the problem.
3. The 'post-processor' module allows for analysis of the solved problem, including evaluation of the field and production of plots. This is independent of the other modules, allowing a solved problem to be evaluated by multiple users in parallel.

4.3 Objects in the Model

The model contains the magnets and both ferrous and non-ferrous objects. The non-ferrous items will have no effect on the magnetic field, but in a model of this size and complexity, they provide a useful reference structure. The geometric description of these items need only be sufficiently accurate to help place the magnets and ferrous objects.

We will describe the ferrous items in the model to a reasonable degree of detail, and some of the non-ferrous items where helpful. The most complete description of the model is available from the technical drawings and .comi files provided at [3].

Throughout this document the various walls and components of the MICE Hall are referenced via their geographic location, i.e. North, South, East and West. These directions were shown on Figure 2. To help aid the reader Figure 8 also shows the these directions with respect to an illustration of MICE Hall Model 91.

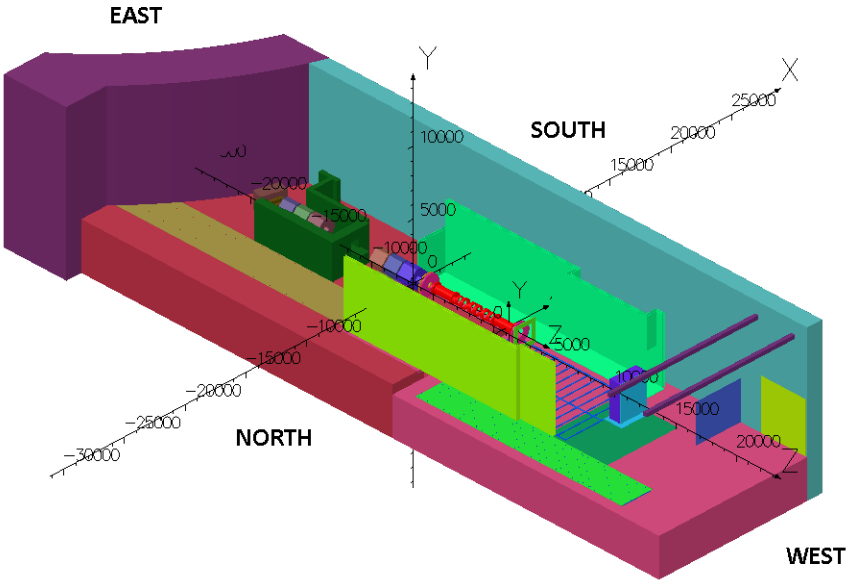

Figure 8: Relative orientation of the MICE Hall superimposed onto Model 91. Note that some structures from this model have been removed in this figure.

4.3.1 Cooling-Channel Magnets

The cooling-channel magnets for the hall model were taken from a set of conductor files that had been used in previous models of MICE. They are visible in Figure 8 in red. These files define the geometry for the Step IV and Step VI magnets and the currents through them for solenoid and flip modes for 240 MeV/c operation. As

mentioned, all modelling has used 240 MeV/c settings, maximising the magnet currents and, by extension, the stray fields.

The magnet geometries and currents are as set in the MICE Technical Reference Document (TRD) [6]. These values may differ from the 'as-built' magnets slightly, as construction of the magnets has in certain cases led to small discrepancies in the geometry and current densities. However, as MICE will tune these currents to produce fields matching those in the original design, this should be of no real consequence to the modelling.

4.3.2 Ferrous Objects

This is a list of the main ferrous objects which have been included in the model, with brief descriptions of their locations in Figure 8. Full details of their location and function within MICE, and any relevant simplifying approximations made in the model, can be found in Appendix A.

North and South Shield Walls (NSW and SSW)
: Light green, either side of the cooling-channel magnets. They represent the initial attempt at magnetic shielding, and are modelled as continuous double skinned walls of 35 mm AISI 1010 steel.

Floor Web and Floor Web Plates
: A blue grid, visible to the West of the cooling-channel magnets.

Dipole D2
: Brown, at the East end of the beamline. Modelled as a solid lump, producing no stray field of its own.

Quadrupoles Q4-6 & Q7-9
: Various colours, between D2 and the cooling-channel magnets. Also modelled as solid lumps without fields. The bases and baseplates were also modelled.

Virostek Plates and Upstream TOF Plates
: Pink, directly adjacent to the cooling channel. Shield the photomultiplier tubes in the TOF detectors.

The Electron Muon Ranger - EMR
: A light green square, just West of the cooling channel.

Decay Solenoid Area - DSA
: A dark green wall, separating Q4-6 and Q7-9, constructed from a combination of steel and concrete.

Beam Dump
: Purple and light blue, at the West end of the experiment, steel and concrete construction.

South West Distribution Board
: Not visible in image, represents only a small quantity of steel, but potentially important for local electronics.

Linac Shield Wall
: Dark purple, a steel loaded concrete wall, with a reduced BH curve.

Trench Plates
: Light brown, North of the DSA. Only the components running parallel to the field return path have been included in the model.

Cellar
: Not visible in figure. Contains the support structure for the magnets.

North Mezzanine
: Not shown in figure, runs North of the NSW.

Cranes
: Dark purple, approximated as two steel beams at the West end of the Hall.

4.3.3 Missing Ferrous Objects

In a model of this size and complexity, we have been forced to make some compromises. This includes missing a significant number of small ferrous objects, which would have been impractical to document and model. Our belief is that the majority of these objects would have only a localised effect on the field. Some further details are available in Appendix A.

4.3.4 Non-Ferrous Structures

Due to the size of the model many non-ferrous structures were added as reference points in the model. These structures make it easier for users to evaluate the field in a particular volume of the MICE Hall. The main objects of note are:

Floors, Walls and Roof of MICE Hall
: Only the South wall and floor are visible in the Figure. Other walls will be visible in other figures, and are placed at the edges of the floor as seen in Figure 8.

Trench
: This sits in the floor at the East end of the MICE Hall, below the tan plates. A significant amount of equipment is contained within, which has been evaluated in Section 5.3.

South Side Buildings
: The building to the South of the SSW houses a number of important rooms, specifically the MICE Local Control Room (MLCR), the current MICE Rack Room and a proposed Rack Room 2, the hydrogen room, the ISIS plant room and the three ISIS control rooms. Modelling and evaluating the fields in these rooms is a vital outcome of the modelling work. Each room will contain equipment that could be sensitive to the stray field, and they are public spaces, which imposes an additional SHE limit on the field.

4.4 Solution Files

Solution files for each model are stored on the web, complete with the source code which generated the model. This allows anyone with access to OPERA to download the solutions and evaluate the fields.

For those who don't have access to OPERA but need to see results from the model, or for quick and standardized information to compare different models, an autogen script generates many images of BMod, Vector Field Plots and Error Plots over the x, y and z planes of the model at 1 m and 2 m spacing (axis dependent).

All of this information is available from [3].

4.5 Model Validation

Given the importance of the work done by the modelling group and the inability to test the full MICE Hall model until all of the cooling-channel magnets were installed, two separate validation processes were carried out. The first was an arranged consultancy with the Vector Fields division of Cobham, who were asked to evaluate the model and confirm it conformed to the best practices of using the OPERA program. The second was a comparison of a smaller model, of Focus Coil 1 (FC1) in the R9 building, with measurements taken during the FC1 training runs.

The consultancy with Vector Fields produced two reports; the first covers their work validating the MICE Hall model itself, and the second discusses the issues of using the MICE Hall model as a basis for sub-modelling

areas of the Hall. Both reports are available from the modelling website [**? ?**]. In this section, we will discuss the main conclusions of the reports.

4.5.1 Validation and Improvement Suggestions for MICE Experimental Hall Modelling

For this report Vector Fields used Model 91, which corresponded to Step IV, 240 MeV/c, solenoid mode. Their report goes into sufficient detail of the validation methods they used, that it would be possible to repeat the process for other configurations within the MICE collaboration. However as we are primarily concerned with Step IV this step has not been taken to date.

The report commented on five items, each of which will be briefly summarised.

Comparison of fields in free space

A representative estimate of the error introduced by the finite mesh was found, by solving the model with all elements set to air. The fields produced are then solely a factor of the magnet inputs and FEA process, and were compared to Biot-Savart calculations of the same magnet inputs. Comparisons used two lines through the model: $x = 0$, $y = 0$, $-7500 < z < 1500$ and $x = 2000$, $y = 0$, $-7500 < z < 1500$, and a plane (referred to as a patch): $-4800 < x < -2000$, $-1000 < y < 1000$, $z = -3000$. The error was found to be less than or equal to 0.21%. The patch was designed to intersect the return path of the flux. This is indicative of the error introduced by the finite mesh, with the caveat that some areas could potentially have larger errors. Still, 0.21% is small in the current scheme, and a satisfying result.

Adding ferromagnetic components to the model

In this study the ferromagnetic components were grouped into six groups that were spatially/functionally related. A model was run with all components set to air and then successive models were run with each group of components having its native BH curve switched on. For each model the effect on three patches was investigated; the patch defined in the previous item, a second behind the NSW (YZ plane at $X = -5300$), and a third behind the SSW (YZ plane at $X = 3920$).

Once again, the location of the patches has an influence on the results of the study and so care must be taken in interpreting the results for other areas. This is particularly true if the area of interest is likely to be near a ferromagnetic object.

There were two results from this study which are copied verbatim from the report:

> *'This investigation shows that the most significant components are those which substantially affect the return path of the flux. While the results presented have been necessarily reduced, they are representative of important areas in the model where sensitive equipment is potentially to be mounted. The models produced for these studies can be used for field recovery in any other area of the meshed space.'*

> *'It is probable that the MICE Hall model already contains enough of the significant components for the fields in free space to be accurate within 1 or 2% - remembering of course that all fields may be at least 0.2% of the 'all free space' value in error anyway. From Cobham's knowledge of the MICE Experimental Hall, there do not appear to be any major components that have been omitted that will further significantly affect results'*

Investigation of material property variations

In this study, the magnetisation values of the BH curves of the steel were reduced by 10% and the effect on the three patches defined in Item 2 was calculated. The observed changes were usually well below 5%. The reduction in the magnetisation of the shielding walls means that they are not performing quite as well as hoped, but as they are generally far from saturation in Model 91 the effect is quite small.

The conclusion was that the uncertainty about material properties in the structures should only be of a minor concern. Note however that this result only applies to the Step IV models.

Investigation of mesh quality

The Hall model has been run using quadratic elements throughout as this is the safest and most accurate method of calculating the fields. Unfortunately, quadratic elements impose a heavy cost in terms of the number of equations that need to be solved, hence increasing both the size and solve time of the model. To investigate whether the use of quadratic elements was necessary, two models were run, one with mixed elements and one with all linear elements. The integrated fields on the patches were compared with the results from the quadratic model.

The results showed that on the patches examined, the benefit of using quadratic elements was marginal yet the solve time improvement was significant.

Care needs to be taken in switching to running models with linear elements. The quadratic elements are of use where the field gradient is high or where high accuracy is sought. So for the general solution, where the solution file could be taken by anyone to ascertain the field anywhere in the model, a quadratic solution is the safest option, although a mixed solution may be sufficient.

However, this result could be of much use for speeding up the process for finding fields for sub-models, as discussed in Section 4.5.2.

Substructure modelling in model 91

This final item considered using field values from the MICE Hall as a source field for a more detailed sub-structure model.

A comparison was made between running the Hall model with a model of a rack in situ, and using the Hall model without a rack in situ but extracting a source field from the Hall model and using these fields as a source for a sub-model that contained the rack.

The integral of the field over a patch was examined. The results from this showed that there was a significant difference between the integral on the patch from these two approaches and this leads to the conclusion that:

> *'The field from an overall model not containing that substructure should not be used as a driving field for a detailed sub-model of the substructure.'*

This has significant implications for any sub-modelling effort.

4.5.2 A Further Investigation of Sub-Structure and Simplification Modelling for the RAL MICE Hall

The following has been copied verbatim from the introduction of the second report:

> *'As shown in the report on Validation and Improvement Suggestions for MICE Experimental Hall Modelling, omitting substructure from the model altogether is not valid when the source fields are obtained. However, a simplified model of the substructure can be included. In this report, different options for simplified substructure models are investigated and some indications of probable error associated with the simplification are obtained.'*

The report goes into great detail about how to implement substructure models, which does not need to be repeated here. However there are a number of recommendations in the report that are worth repeating. These too have been copied verbatim from the reports.

1. *'The effect of solving the magnetic fields in free space using a truncated finite element mesh appears to give about an average 5% error in the 'far field' in the test model. The error will be smaller closer to the solenoid coils and larger near the boundary of the model. This inherent error from using finite elements*

should be considered when making judgements about maximum flux density levels in critical areas of the MICE Hall by repeating this type of calculation for the complete MICE Hall model and investigating the error in the volume where a substructure model is required.'

Our Comment This follows on from the comments made in Section 4.5.1 that the errors had only been calculated on specific patches and so each individual situation needs consideration.

2. *'Structure inside the MICE Hall that consists of a steel outer 'cabinet' with internal ferromagnetic structure can be adequately simplified to either a hollow structure of approximately the same dimensions as the outer cabinet, or an approximate cabinet with a single, appropriately dimensioned, ferromagnetic block placed at its centre. If the existing model includes structure where the block is already in place, don't bother to remove it. But, if future cabinets are added, the outer cabinet should be sufficient to get source fields for a detailed substructure model.'*
3. *'Element size in the free space surrounding a substructure should not need to be reduced to the level that may be needed for a detailed substructure model in order to adequately capture the source field from the complete MICE Hall model.'*
4. *'When trying to examine the shielding effect supplied by magnetic walls, the outer boundary of the model should be made as large as practically possible to avoid image sources.'*
5. *'If substructure modelling of shielding walls is undertaken, the discretization of the wall and supports only needs to be at a reasonable level to capture the geometry. A fine mesh is not needed to capture variations in flux density as these will be small.'*
6. *'A quick way to assess how effective shielding will be whether it is real shielding constructed for the purpose of reducing field or the outside cabinet of some equipment is to determine where the steel is operating on the magnetic characteristic of the shielding material. Tangential components of magnetic field strength and the normal component of magnetic flux density will be continuous at the material surface, so this will also give an indication of the flux density just behind (or inside) the shielding wall.'*
7. *'Simplified models of the shielding walls in the model should be adequate to determine if the flux density is low enough for equipment to be mounted behind them, unless the sensitive equipment is very close to discontinuities in the wall occurring because it is constructed from a finite number of plates. Substructure modelling will not be beneficial. An assessment of the error in the source field associated with the finite element representation should be made in the same vicinity to determine whether the reduction of the field due to the shielding can be considered accurate.'*

Conclusions from the 2nd Report

The 2nd report ends with the following conclusions, which have again be copied verbatim. These directly influence the work described in Section 5.2.

1. *The effect of the meshing and truncation of infinite space should be assessed in any area where it is important to determine if sensitive equipment can be mounted. This should be achieved by comparing Biot-Savart calculated fields with fields recovered from the mesh, assuming all materials have free-space permeability.*
2. *Detailed substructure models can use the overall MICE Hall model to derive a source field providing:*
   (a) *There is a simplified representation of the steel container and its contents included in the MICE Hall model.*
   (b) *The differences in the source field from the solenoids caused by using finite elements compared with Biot-Savart is not larger than the source field values for the sub-structure.*
3. *Hollow tanks, or tanks with an equivalent centralized volume of magnetic material, offer a better approximation than tanks completely filled with a dilute magnetic material.*

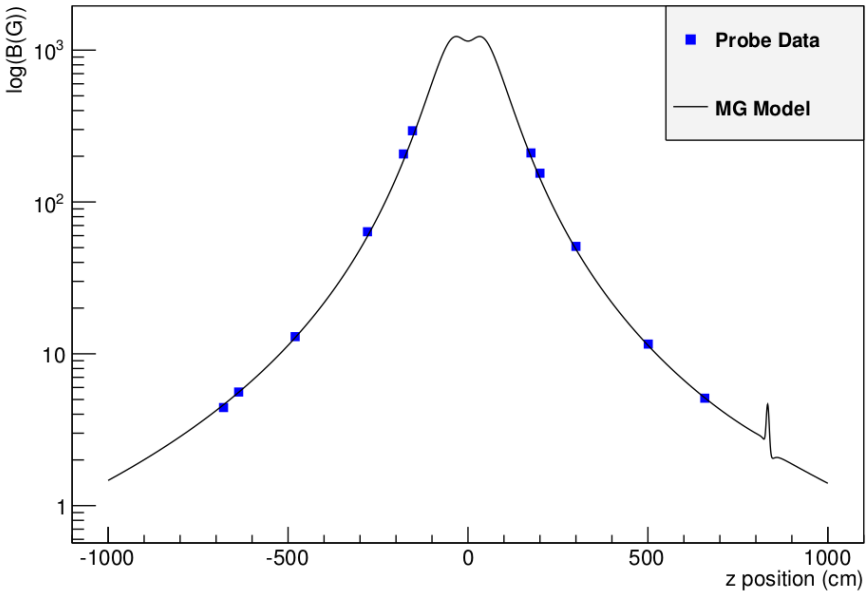

Figure 9: A comparison of some of the measurements made in R9 against predictions from an OPERA model. The feature at $z = 825$ cm is due to a steel wall which has been included in the model.

4. *It is not accurate to extract the source field for a substructure model from a model of the MICE Hall that does not include a simple representation of the structure; see the earlier results obtained in the other MICE Hall report for including the rack in Model 91.*
5. *Substructure modelling behind shielding walls should not be necessary unless the sensitive equipment is placed very close to discontinuities in the wall. The differences in source field associated with truncation of the mesh will probably be larger than the error introduced by simplification.*

4.5.3 R9 Modelling and Measurements

The final validation effort was to compare measurements from the only available cooling-channel magnet, Focus Coil 1, with a simpler model. The FC is currently situated in R9 at RAL, undergoing magnetic training runs. The work space is relatively clear, with only a minimal amount of ferrous material; specifically one control rack and three compressors approximately eight meters from the FC, and mild steel walls. This allows for a smaller and simpler model, using the same techniques and methodology as for the MICE Hall model.

The training runs also allow for the possibility of measurements of the field produced. Measurements were made with a three-axis Gaussmeter, with a resolution of $\sim$1%. The probe was placed into a specially constructed stand, allowing for measurements at a range of heights, covering most of the Hall floor, with a spacial resolution of $\sim$2 cm.

Figure 9 shows the agreement between the produced model and the data taken, along the z axis, through the bore of the magnet. The agreement is sufficiently accurate for the purposes of the MICE experiment.

The next stage is to introduce extra ferrous objects into the field, to study the distortion of the field and the effect of the field on potentially sensitive objects. A $100 \times 100 \times 100$ cm^3 region of air was measured to have a field varying between 20 G and 2 G. After inserting a CryoMech compressor into the centre of the region, the measurements were repeated at the same location, with the expected effect on the field. Unfortunately, the updated models for this work are still being prepared.

5 Baseline magnetic mitigation scheme

5.1 Overview

5.1.1 Introduction

An overview of the fields within the MICE Hall and the neighbouring buildings is given for the Step IV, 240 MeV/c solenoid-mode configuration in figure 10 and for the Step IV, 240 MeV/c flip-mode configuration in figure **??**. The magnetic field is plotted in a horizontal plane at beam height. At this scale a lot of detail is lost. To emphasise the areas of low field, field is plotted over the range 0 G to 5 G. Note that the field is is not plotted for in regioins for which it is greated than 5 G.

All 2D plots are produced using Nodal interpolation with integral fields. This may be slightly less accurate than using a full integration method but given the number of elements in the Hall model the full integration method will not produce 2D plots in a tractable time.

5.1.2 Field Outside of the MICE Hall

Estimates of teh field that will be observed on teh external serfaces of the MICE Hall at Step IV in solenoid mode at 240 MeV/c are shown in figures 12 to 16. The images shown are for Step IV solenoid mode only as this mode of operation produces the highest external fields for step IV as there is less field cancellation in the cooling channel. No images have been shown for the East wall as this is far enough away not to be of concern.

The only area external to the MICE Hall where the calculations indicate that fields above 5 G will be present is on the roof. The effects of any stray fields upon equipment installed on the MICE Hall roof has yet to be established.

5.1.3 Mice Hall West Wall

Figure 17 shows a drawing of the proposed location of the compressor locations along the West Wall [7]. Various attempts were made to introduce approximate representations of the ferrous content of the compressors in the model. Although not insignificant the overall iron density is quite low and, in such an extended volume, the compressor detail made it difficult to include the ferrous mass in a meaningful way. To create these objects and mesh them would require a fine mesh that would make the Hall model time consuming to solve. It is likely that the effect of these iron boxes on the model would be to partially shield the inner contents and locally distort the field. However, given their relative distance from the bulk of the iron in the Hall it is unlikely that there is enough iron in these compressors to significantly affect the magnitude of the field in this region. For this reason the iron mass of the compressors was excluded from the hall FEA model and it is acknowledged that this is a known but unquantified error in the results. Figures 18 and 19 show the predicted field at z=17,000 mm and z=19,000 mm.

5.1.4 ISIS Control Rooms

The ISIS Main Control Room, Operations Room and Diagnostics Room are located adjacent to the MICE Hall South wall at first-floor level and are partly shielded from the MICE magnets by the South Shield Wall. No iron mass is assumed to exist in the ISIS control rooms, although in reality there is likely to be some structural steelwork and racks. Figure 20 shows the relative location of these rooms with respect to the MICE hall in the

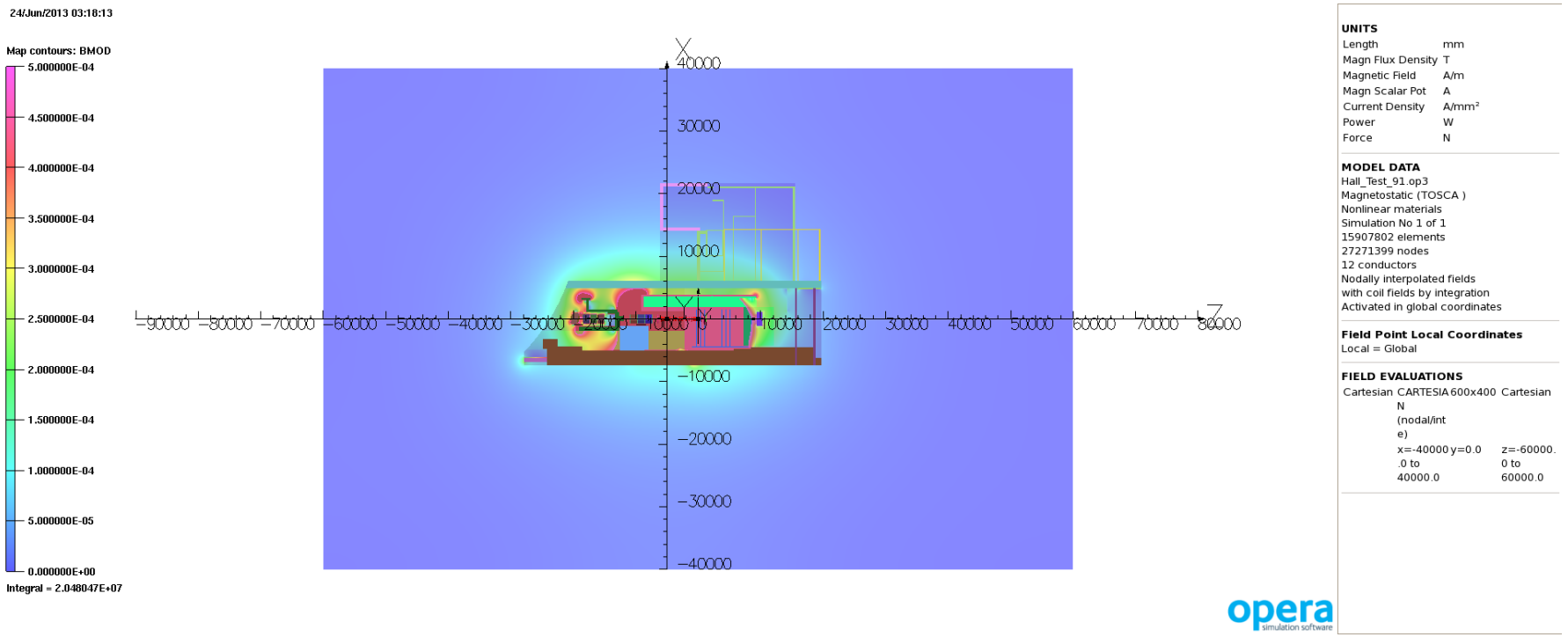

Figure 10: Bmod 5 gauss scale. Step IV 240 Mev/c Solenoid Mode. Overview of Model Volume at Beam Height from Model 91. The Model is shown with structures turned on. One can immediately see that the majority of the stray field is contained within the MICE hall.

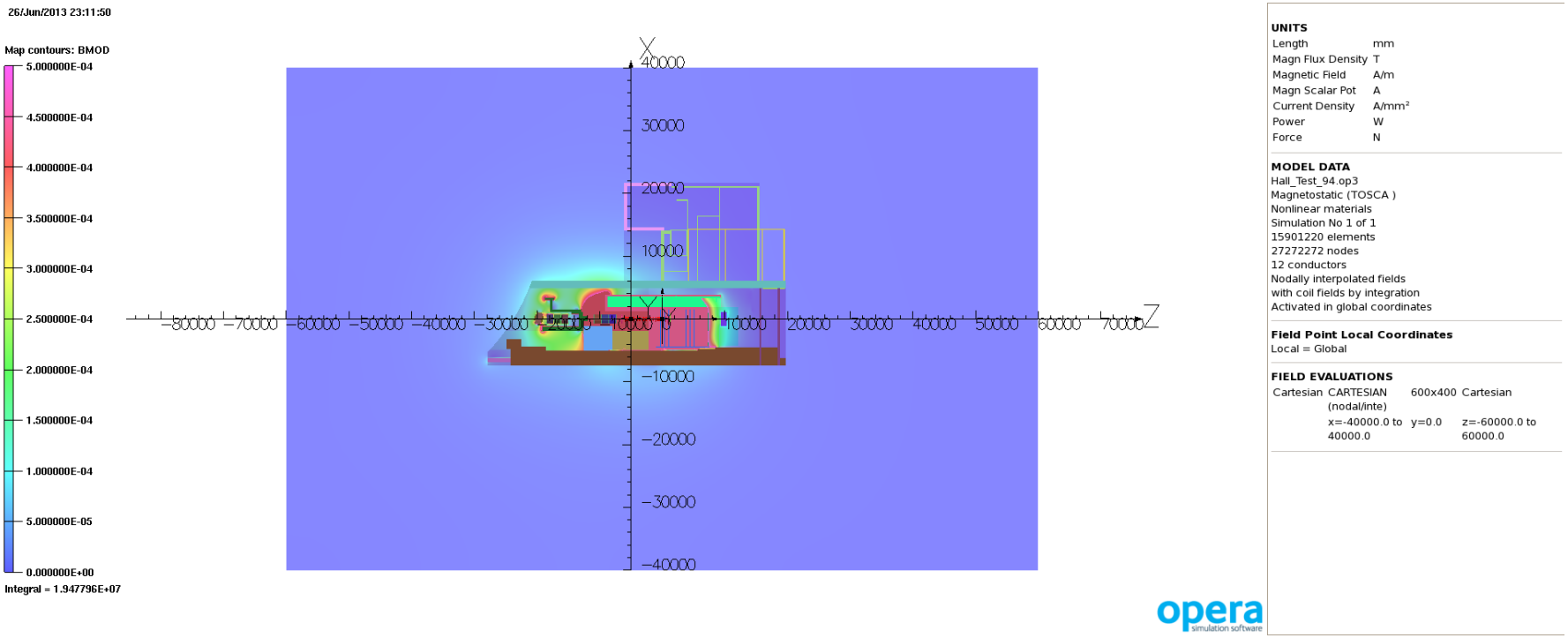

Figure 11: Bmod 5 gauss scale. Step IV 240 Mev/c Flip Mode. Overview of Model Volume at Beam Height from Model 94. The Model is shown with structures turned on. One can immediately see that the majority of the stray field is contained within the MICE hall.

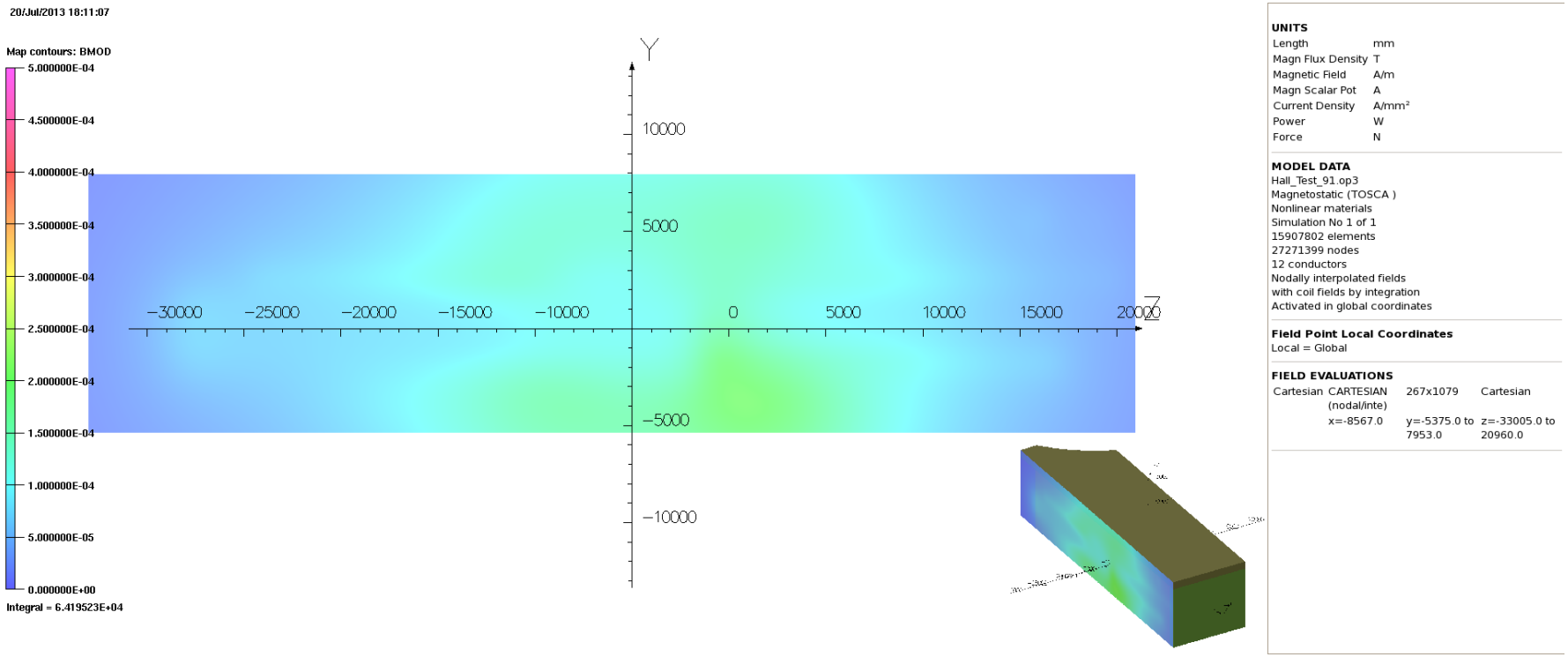

Figure 12: Bmod 5 gauss scale. Step IV 240 MeV/c Solenoid Mode. North Wall Side view.

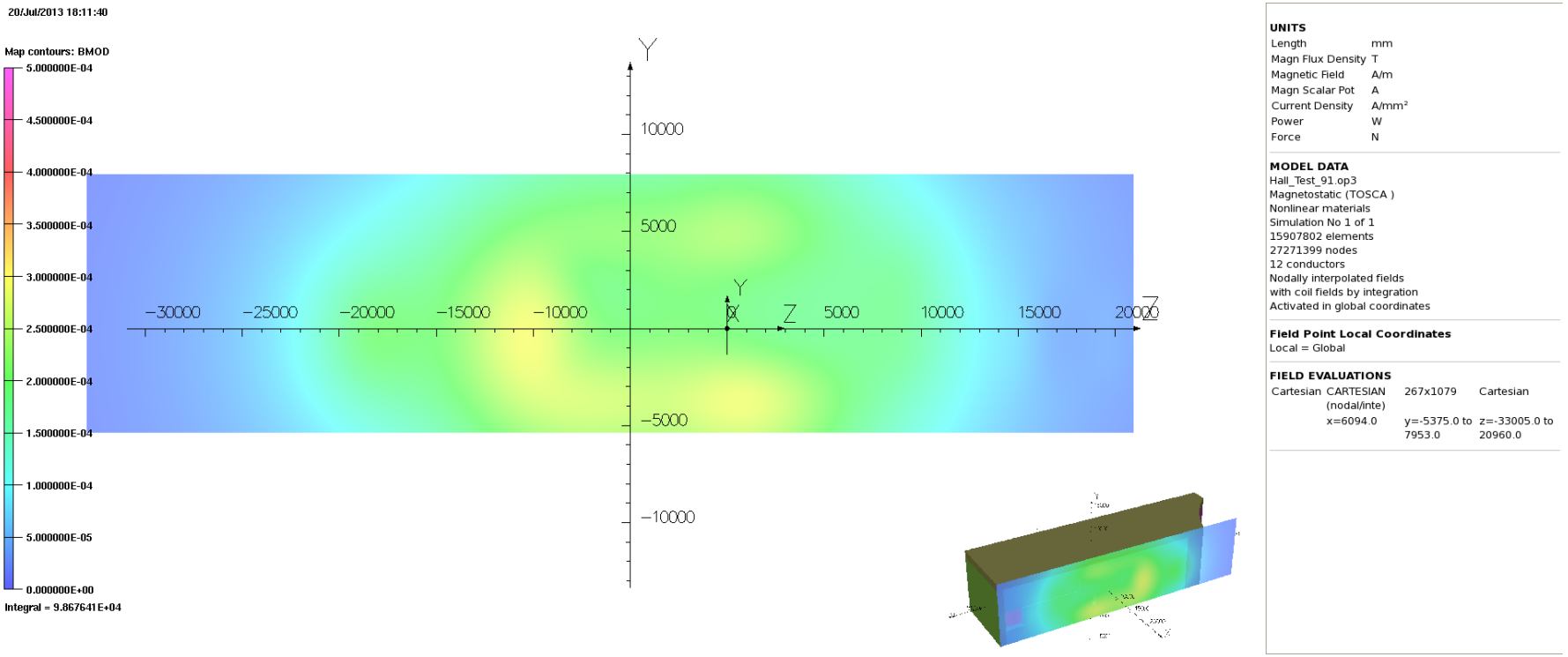

Figure 13: Bmod 5 gauss scale. Step IV 240 MeV/c Solenoid Mode. South Wall Side view.

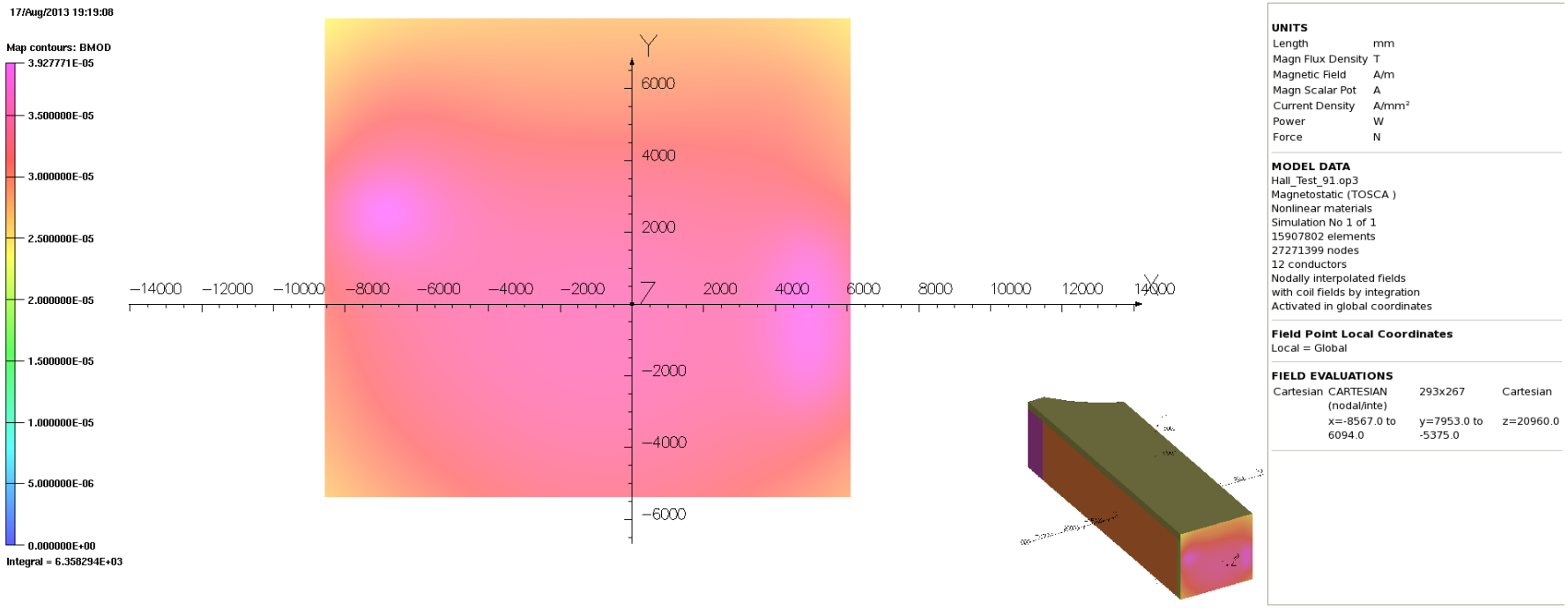

Figure 14: Bmod. Step IV 240 MeV/c Solenoid Mode. West Wall Isometric view. The predicted field is the same magnitude as that of the earth's magnetic field.

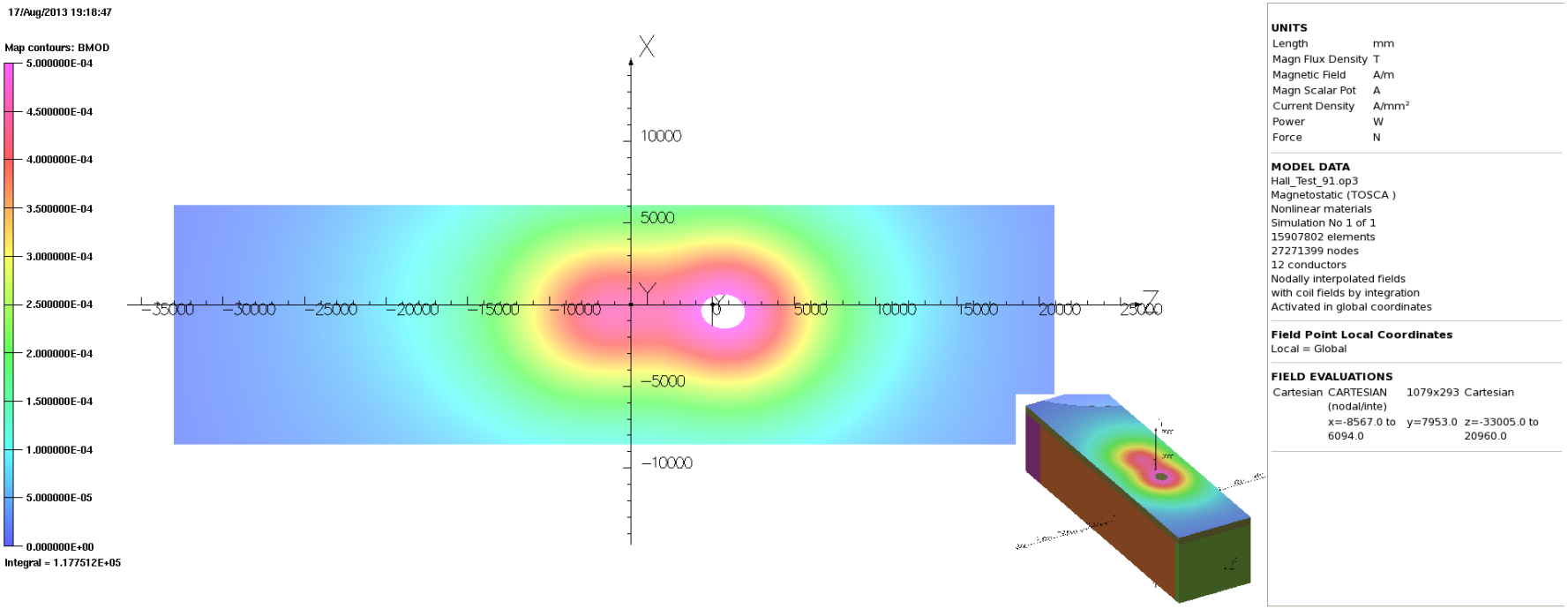

Figure 15: Bmod. Step IV 240 MeV/c Solenoid Mode. External to Roof. This is the only plot where the external field goes above 5 gauss.

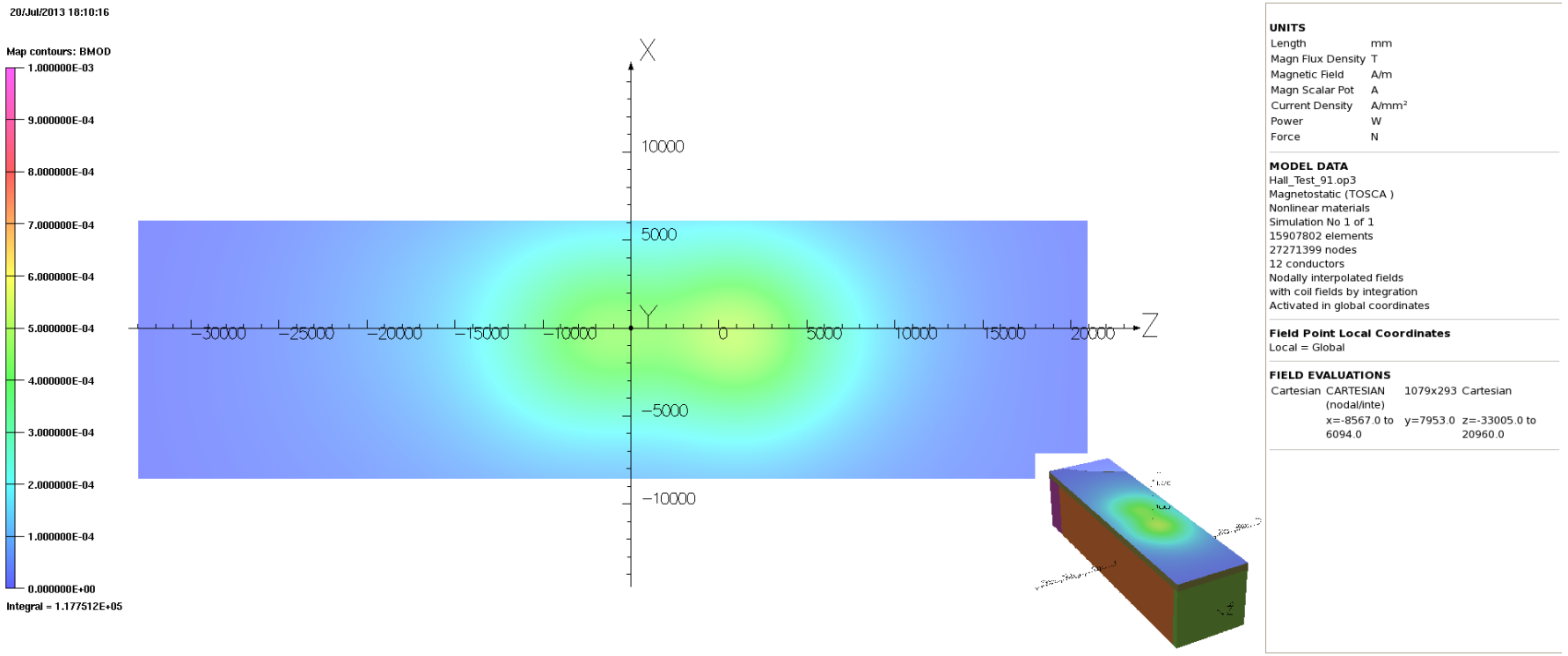

Figure 16: Bmod. Step IV 240 MeV/c Solenoid Mode. External to Roof. This is a 10 gauss plot of the roof. The peak areas are only just above 5 gauss.

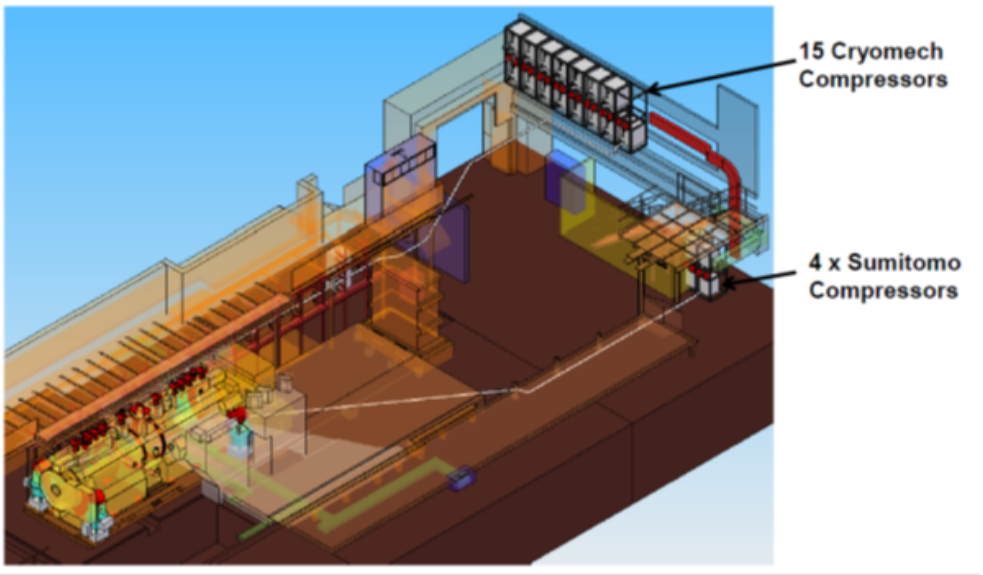

Figure 17: Location of the the Sumitomo and Cryomech compressors against the West Wall for Step IV. [***Does this need a REF to Jason's Document?***]

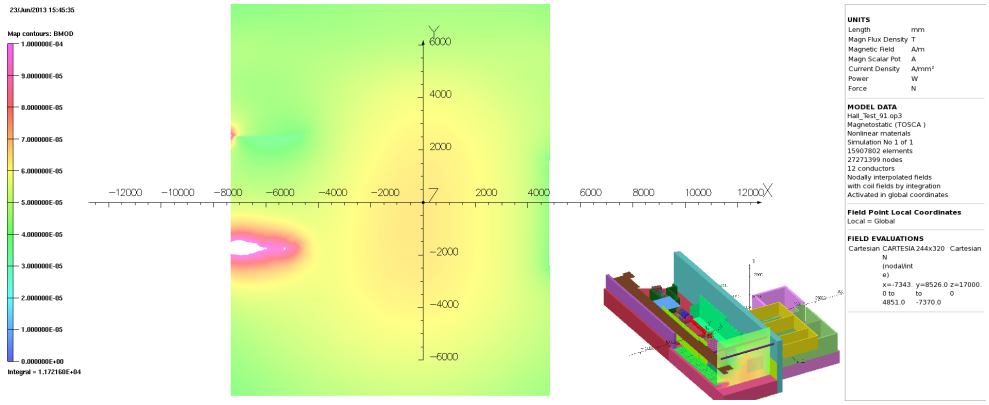

Figure 18: Bmod Field Profile towards the West end of the MICE Hall at z=17,000 mm, 1 gauss Scale. Even a couple of metres within the hall the field level is not much above the earth's magnetic field. The hot areas are where there are ferrous objects.

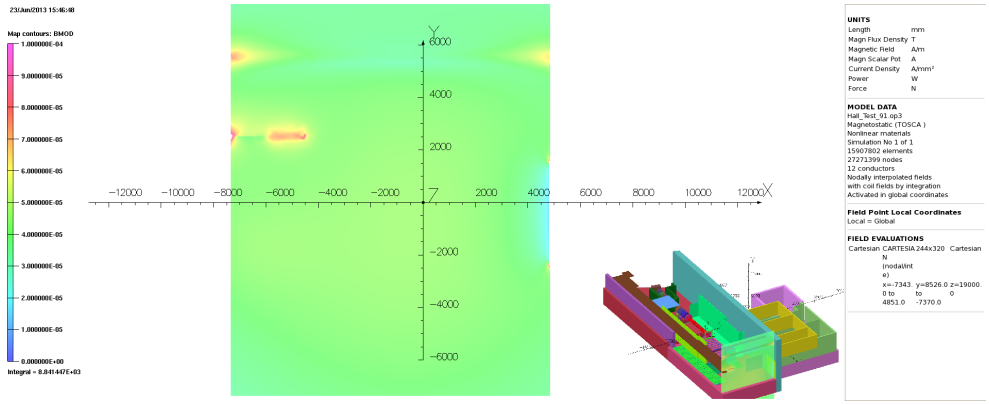

Figure 19: This is on the same scale as the previous plot but the plot is taken 2 m further away from the magnets, z=19,000 mm, close to the West Wall. (736 mm away from the wall itself.)

MICE hall model. Figures 21 to 24 show the field predicted on the outer boundaries of these rooms for step IV solenoid mode 240 MeV/c.

5.1.5 MICE Local Control Room (MLCR)

The MLCR is currently split into two sections. The section of the control room closest to the MICE Hall contains much of the controls equipment and DAQ including the PPS interlock system. The section further away serves as the MICE Local Control Room. Figure 25 shows the location of the MLCR with respect to the MICE magnets. Figures 26 through to 31 show the predicted field strength on the boundaries of the volume for Step IV of the experiment (240 MeV/c solenoid mode). These field maps were produced assuming no iron in the MLCR which is only an approximation as the racks are magnetic and so will draw some flux. The effect of this missing iron is unknown but given that the racks will represent small localised volumes of iron they are unlikely to significantly alter the field map, only localised effects would be expected. As anticipated the area closest to the hall will experience the largest air field, although typically for Step IV the field is no greater than $\approx$2.5 G.

5.1.6 Rack Room 2 (RR2)

Rack Room 2 is located in the South East Corner of the South Side Buildings and is indicated by the volume enclosed by magenta coloured wall in figure 25. The shape of the room as indicated in the model is only an approximation of its true shape, which is quite complex. However, the volume shown by the FEA model encompasses the whole of RR2.

RR2 is far enough away from the beamline that the additional fields imposed from Step IV running are negligible. Figure 32 shows a cross section of the field through this region at a height of y=-1000 mm below beam height level. As the predicted field strength is of the order of $\approx\leq$0.5 G there are therefore no concerns with putting equipment into this room for MICE for Step IV.

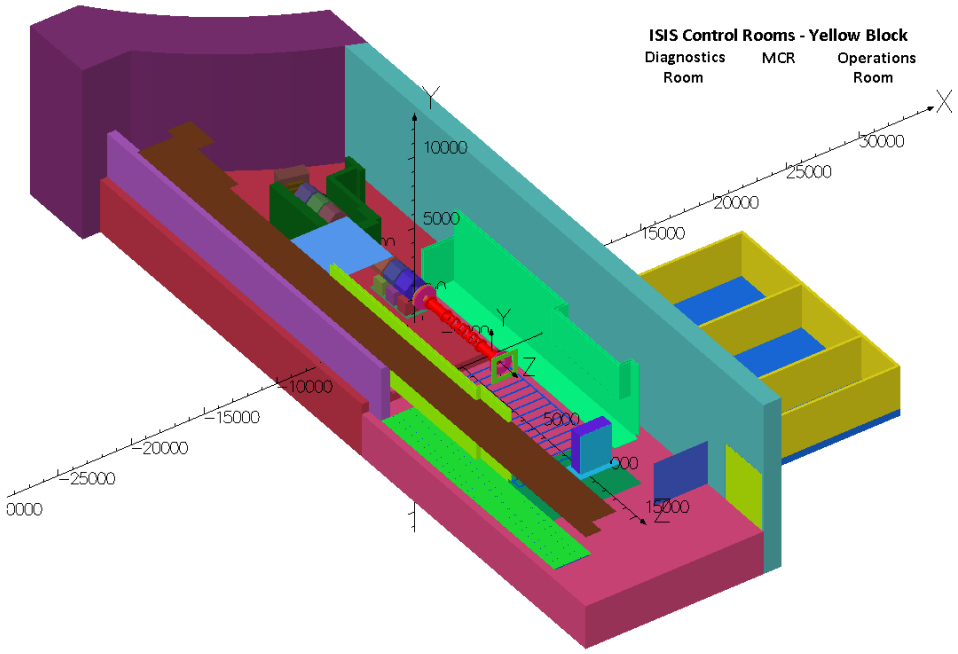

Figure 20: This shows the relative location of the ISIS control rooms to the MICE hall. The South Shield wall partially covers the diagnostics room.

5.1.7 Behind the North Shield Wall (NSW)

The North Shield Wall is of interest because there are a number of electrical systems that sit behind this wall. Beyond Step IV the RF tubes, amplifiers and their associated electronics will be placed here. The North shield wall also partially shields the sub-station transformer, although this will be dealt with seperately in section 5.2.3.

The MICE fibre trackers sit inside the bore of the largest superconducting magnets; however the associated DAQ electronics are constrained to be within 10 m of the tracker due to the length of the leads. The length of these leads means that it is possible to place the tracker racks behind the North Shield Wall. ***LINK TO CRAIG'S PHOTO*** This will only work if several other key components of the tracker system can be successfully shielded against the magnetic fields from MICE which are particularly large in this area due to their proximity to the magnets. The section [*** INSERT LINK TO KIRIL'S WORK ***] shows the work done to understand the local shielding requirements that would be necessary if global sheilding was not to be employed.

*** CRAIG CAN WE HAVE A COPY OF A DRAWING THAT SHOWS WHERE THE RACKS COULD BE PLACED? (and can this be included here?)***

Before showing these plots it is once again worth pointing out that the MICE hall model assumes that the shield walls are dual skinned contiguous sheets of magnetic AISI 1010 steel. In reality these walls are not contiguous but are constructed from plates built onto an I-beam frame and unfortunately there are signficant gaps between where these plates join onto the beams. These gaps lead to flux leakage, which means that the performance of the shield wall may be worse than that indicated in these models. This issue is looked at in more detail in section 5.2.2. It is worth commenting that without the advantage of any measurements to compare with these models, the magnitude of this effect remains an uncertainty.

Figures 33 and 34 give some indication of the expected field strength behind the NSW. Note that both of these plots are on a 10 gauss scale.

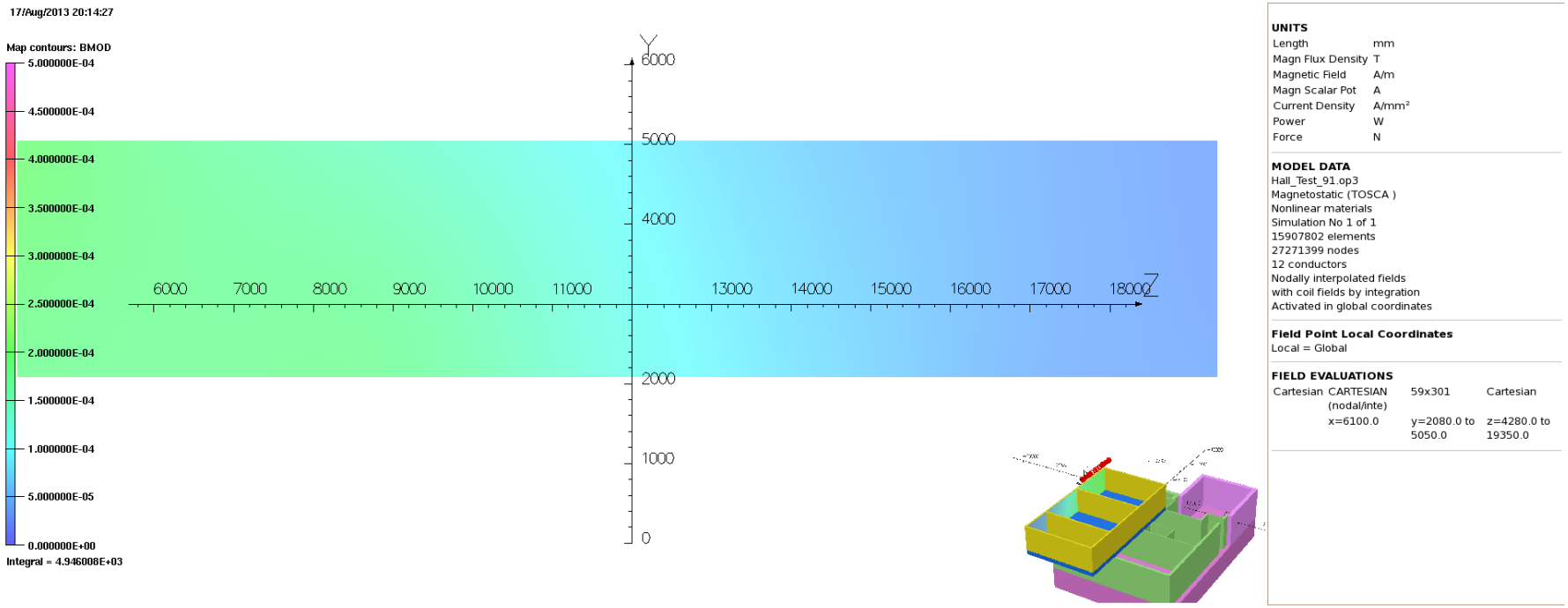

Figure 21: Bmod. Step IV 240 MeV/c Solenoid Mode. South Side of the ISIS control rooms.

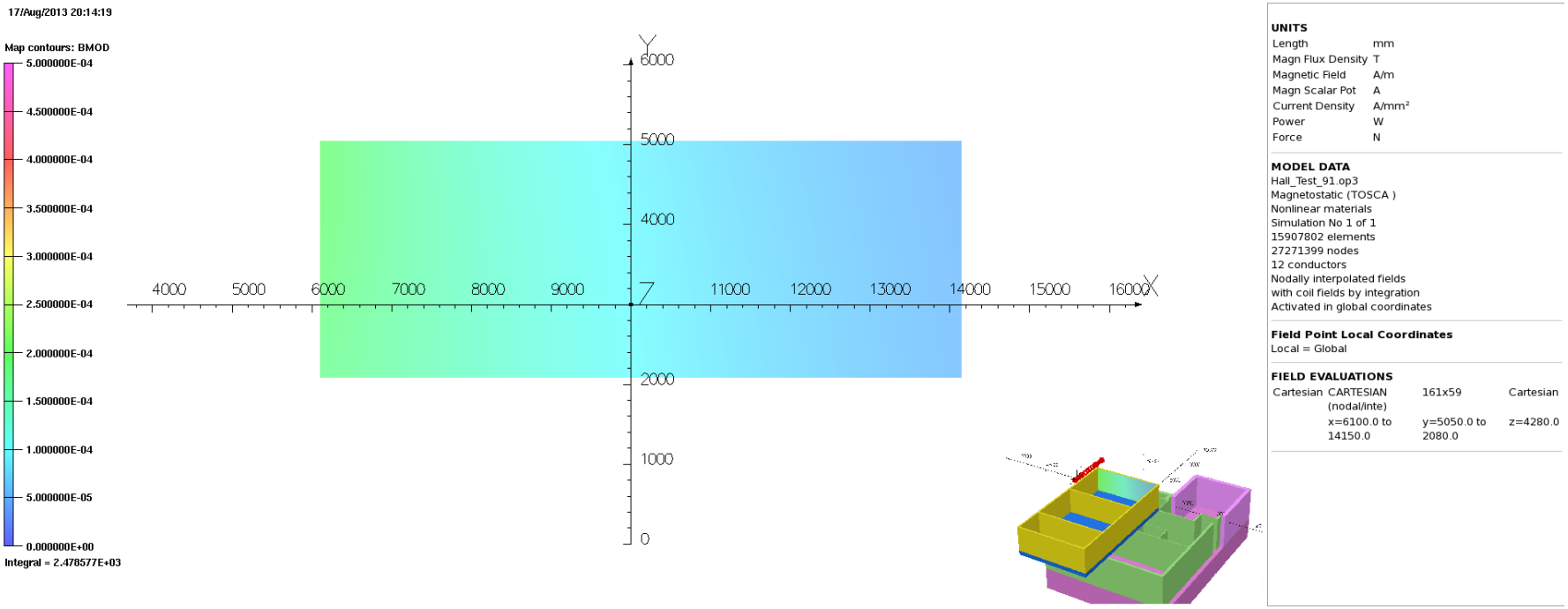

Figure 22: Bmod. Step IV 240 MeV/c Solenoid Mode. East side of the ISIS control rooms.

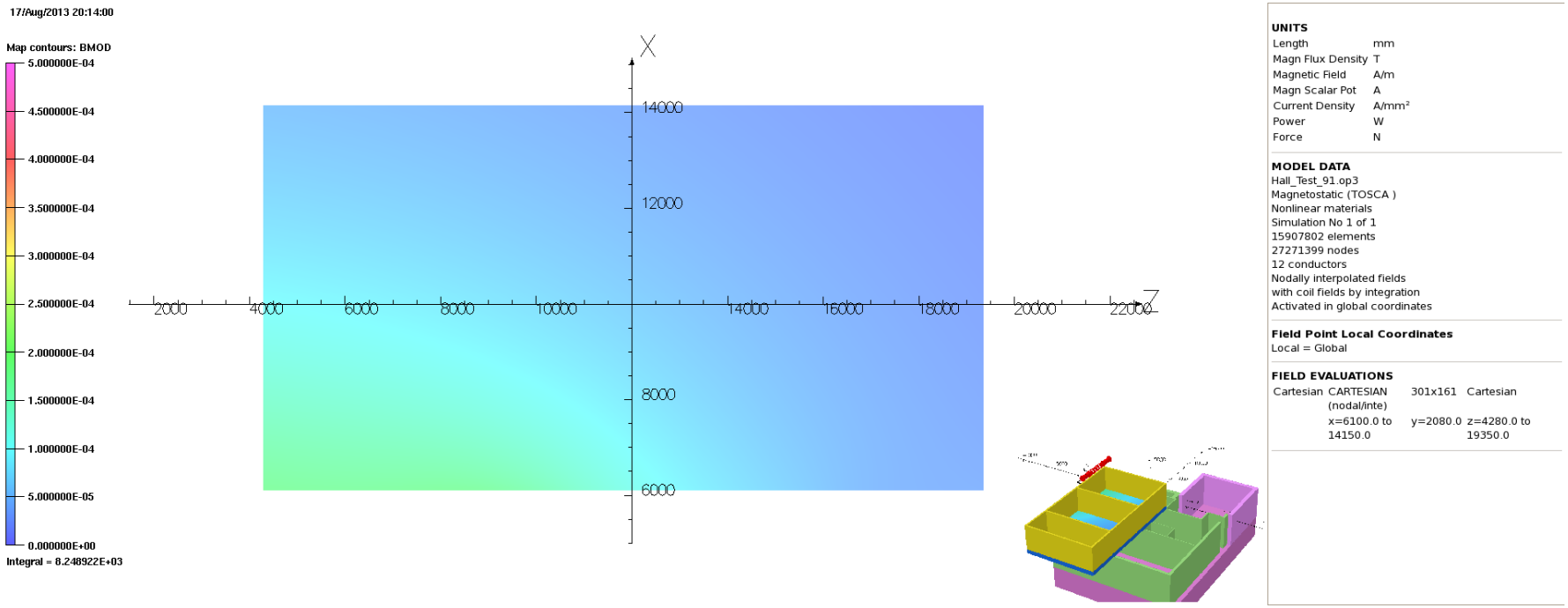

Figure 23: Bmod. Step IV 240 MeV/c Solenoid Mode. Floor of the the ISIS control rooms.

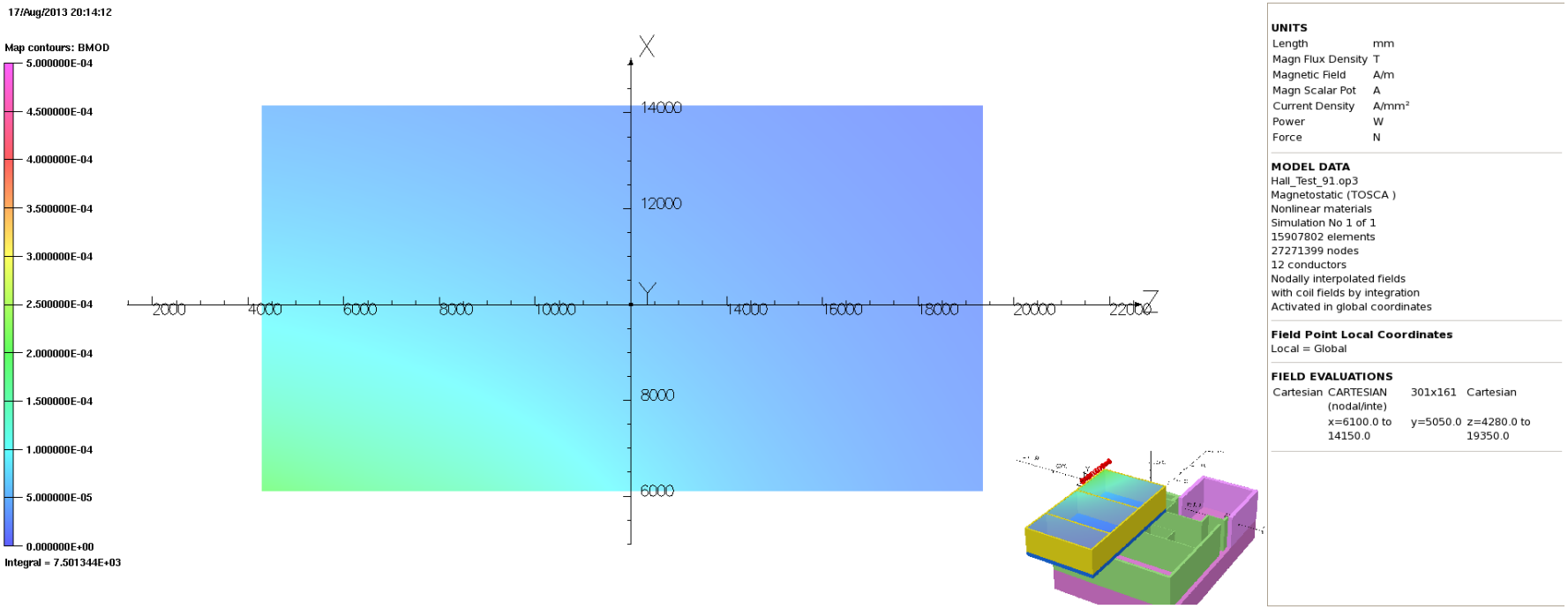

Figure 24: Bmod. Step IV 240 MeV/c Solenoid Mode. Ceiling of the the ISIS control rooms.

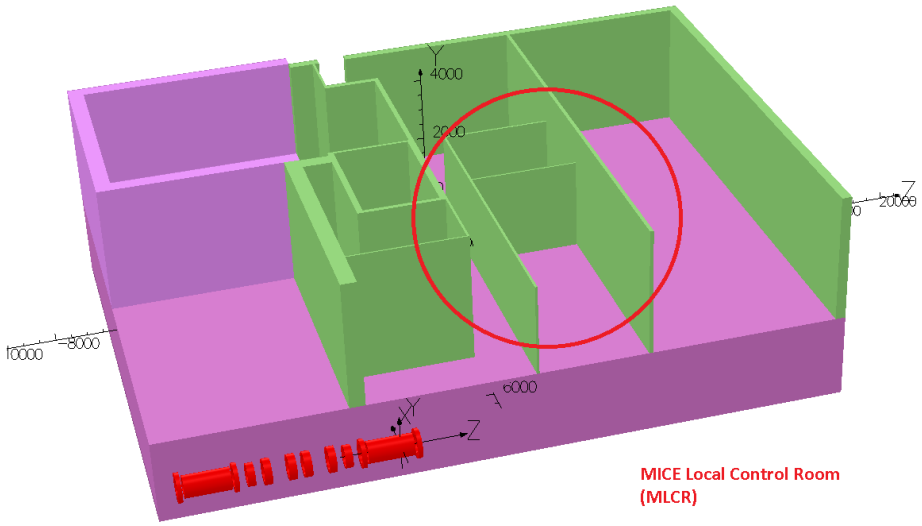

Figure 25: Location of the MLCR with respect to the MICE magnets

*** CRAIG IS THERE A CONCLUSION THAT WE WISH TO DRAW FROM THESE PLOTS? FEEL FREE TO INSERT YOUR OPINION ***

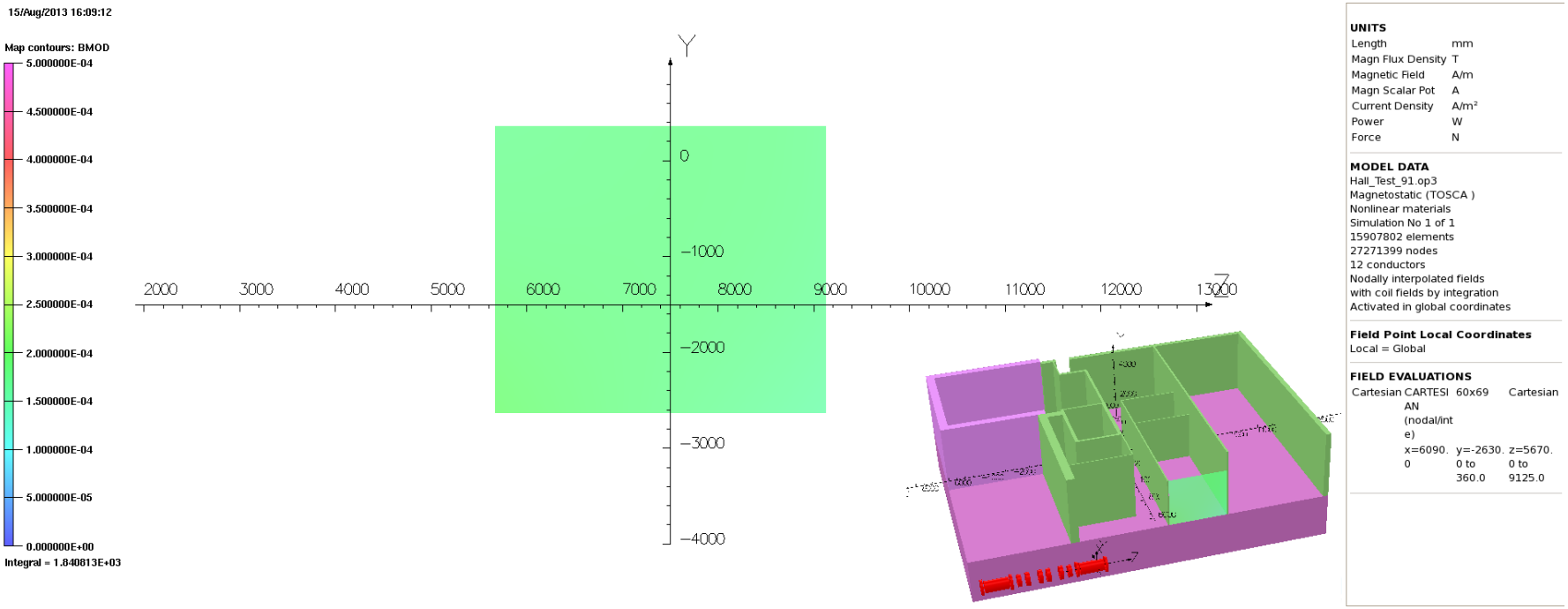

Figure 26: Bmod. Step IV 240 MeV/c Solenoid Mode. MLCR North Side.

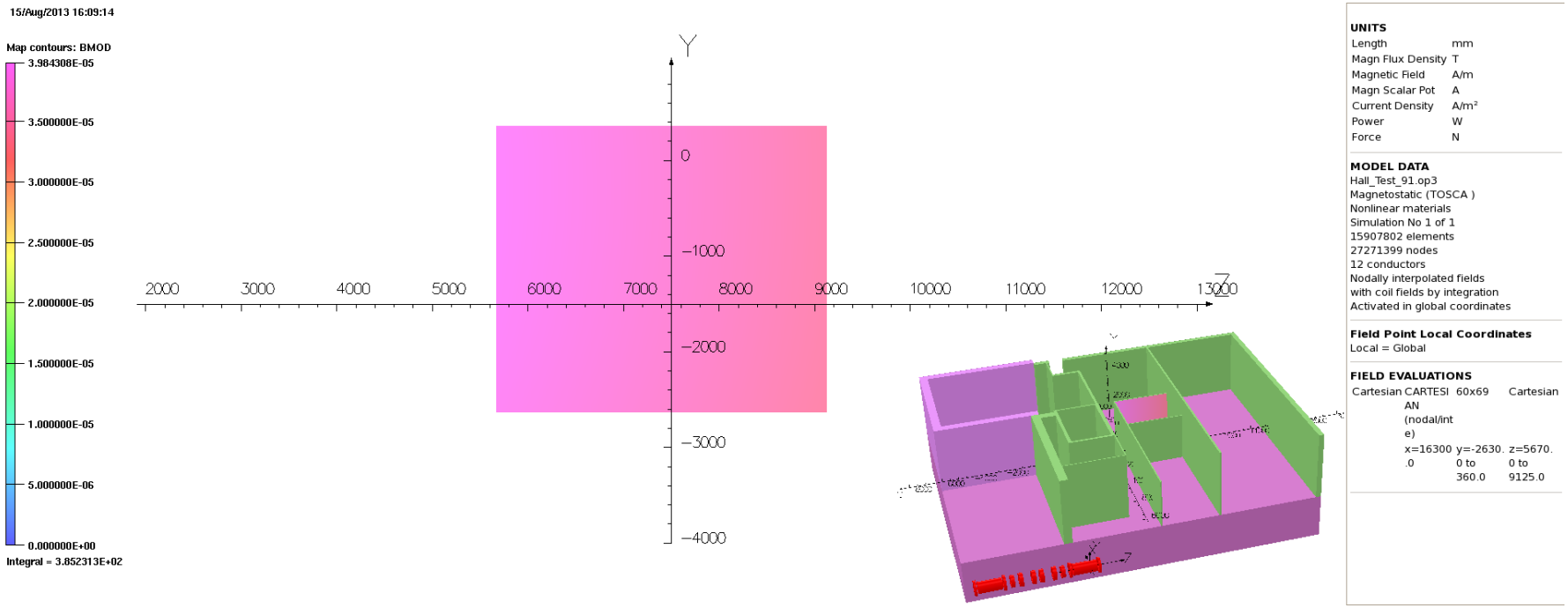

Figure 27: Bmod. Step IV 240 MeV/c Solenoid Mode. MLCR South Side. Note the different scale on this plot!

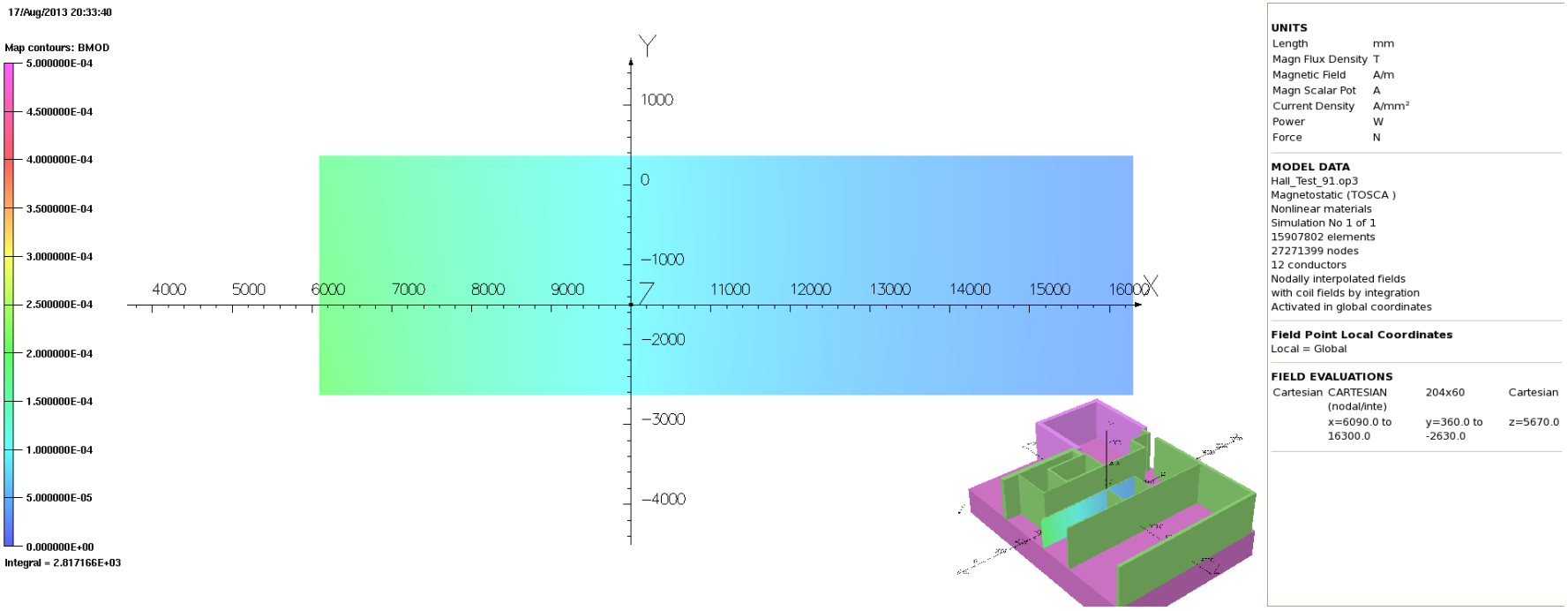

Figure 28: Bmod. Step IV 240 MeV/c Solenoid Mode. MLCR East Side.

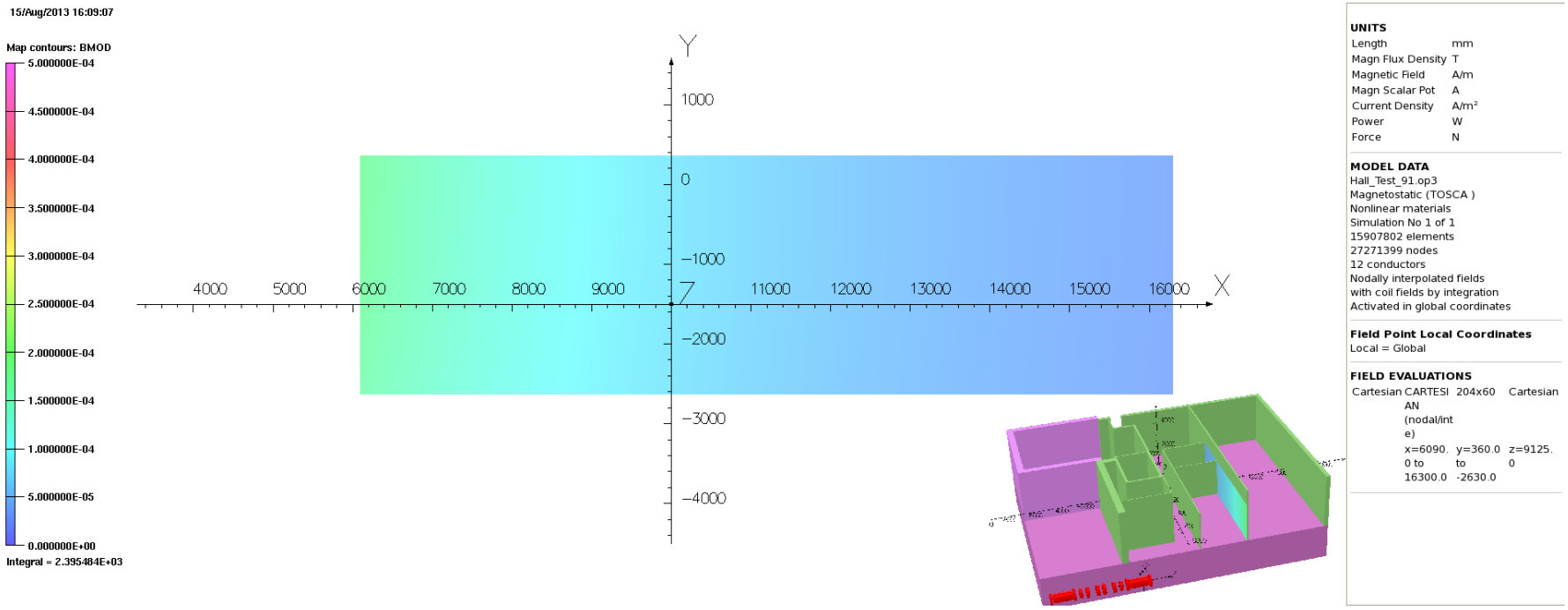

Figure 29: Bmod. Step IV 240 MeV/c Solenoid Mode. MLCR West Side.

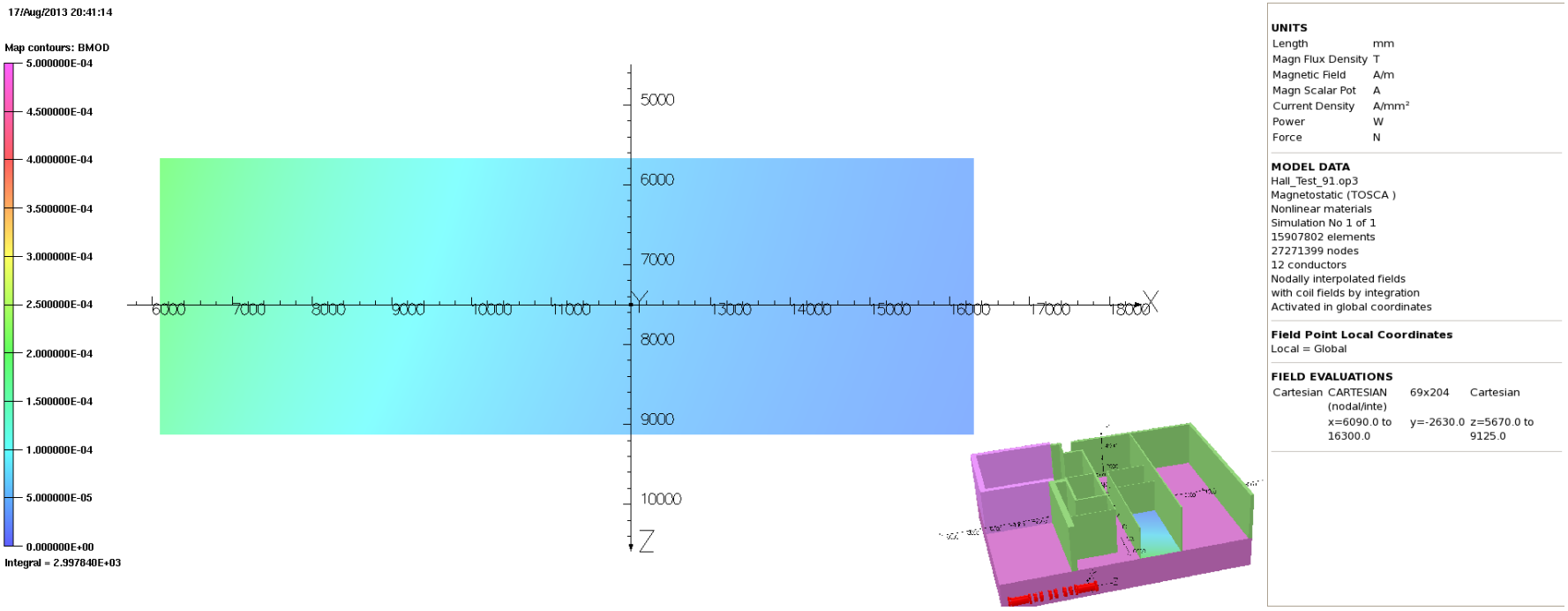

Figure 30: Bmod. Step IV 240 MeV/c Solenoid Mode. MLCR Floor.

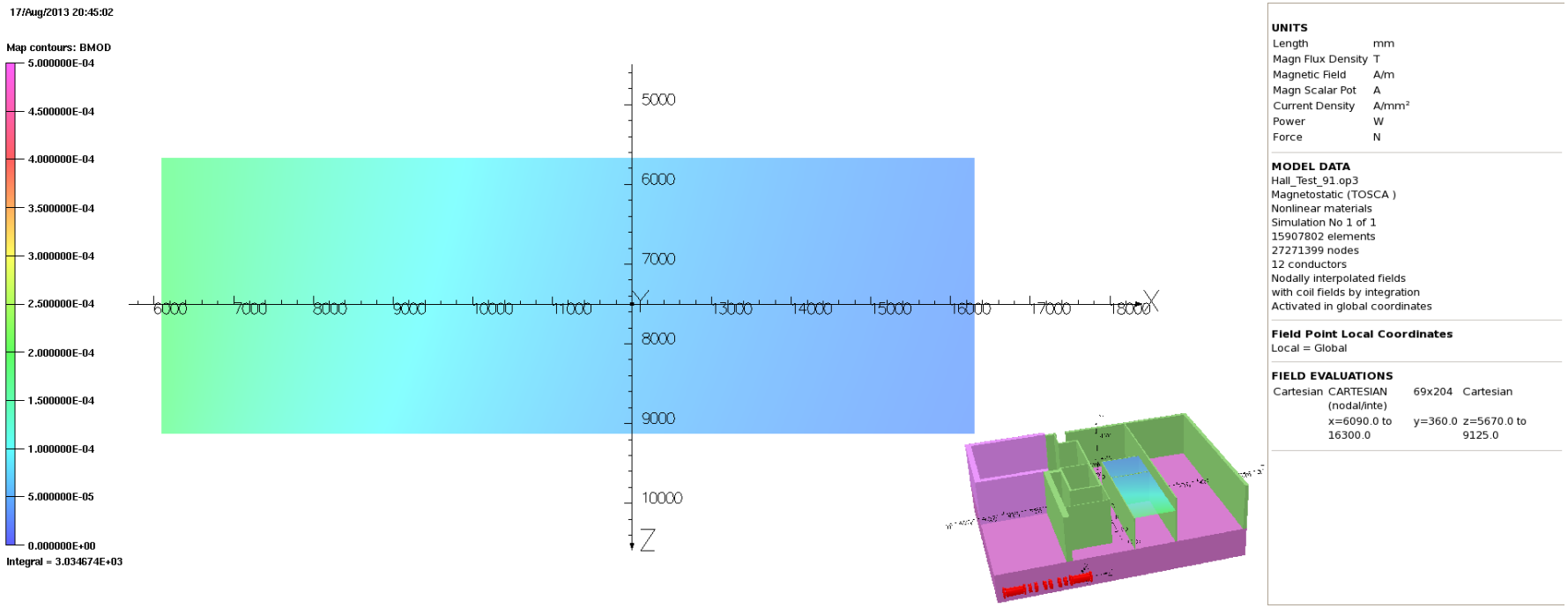

Figure 31: Bmod. Step IV 240 MeV/c Solenoid Mode. MLCR Ceiling.

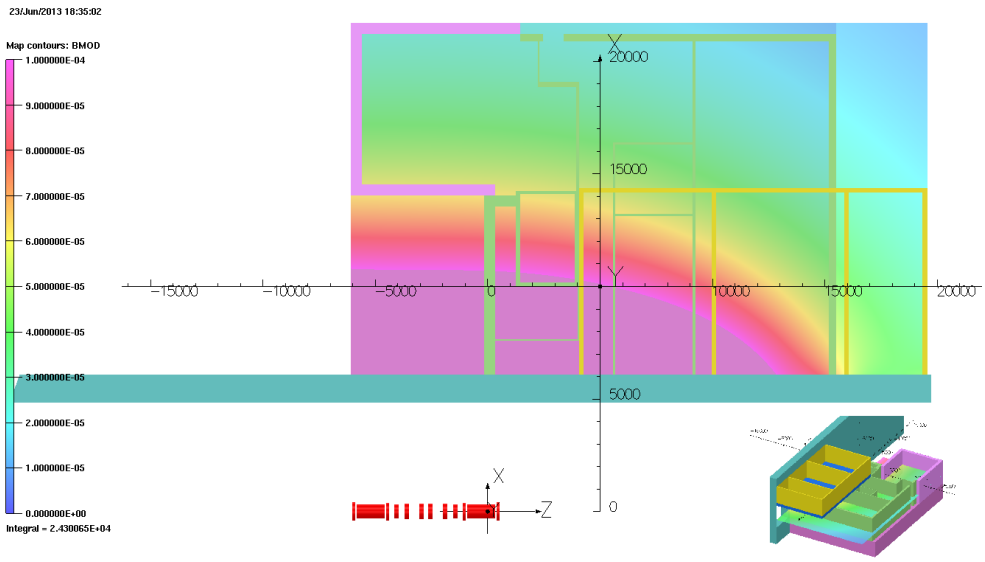

Figure 32: Bmod at y=-1000 mm. The fields through RR2 are negligble for Step IV. Note the scale on this plot is 1 gauss.

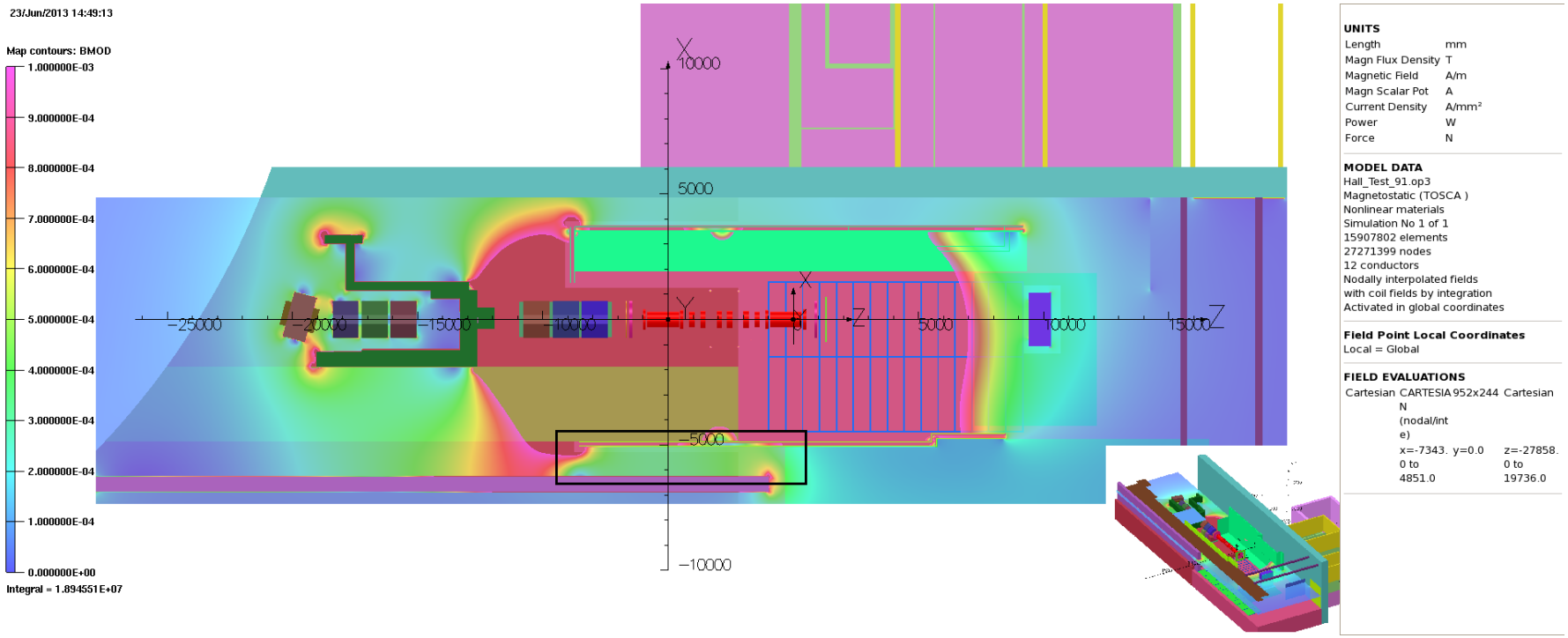

Figure 33: Bmod. Step IV 240 MeV/c Solenoid Mode. 10 gauss Scale. This is a plot at beam height. The area behind the NSW that sits between the Linac wall, marked with a black box, is noticeably warmer than the area behind the west end of the NSW.

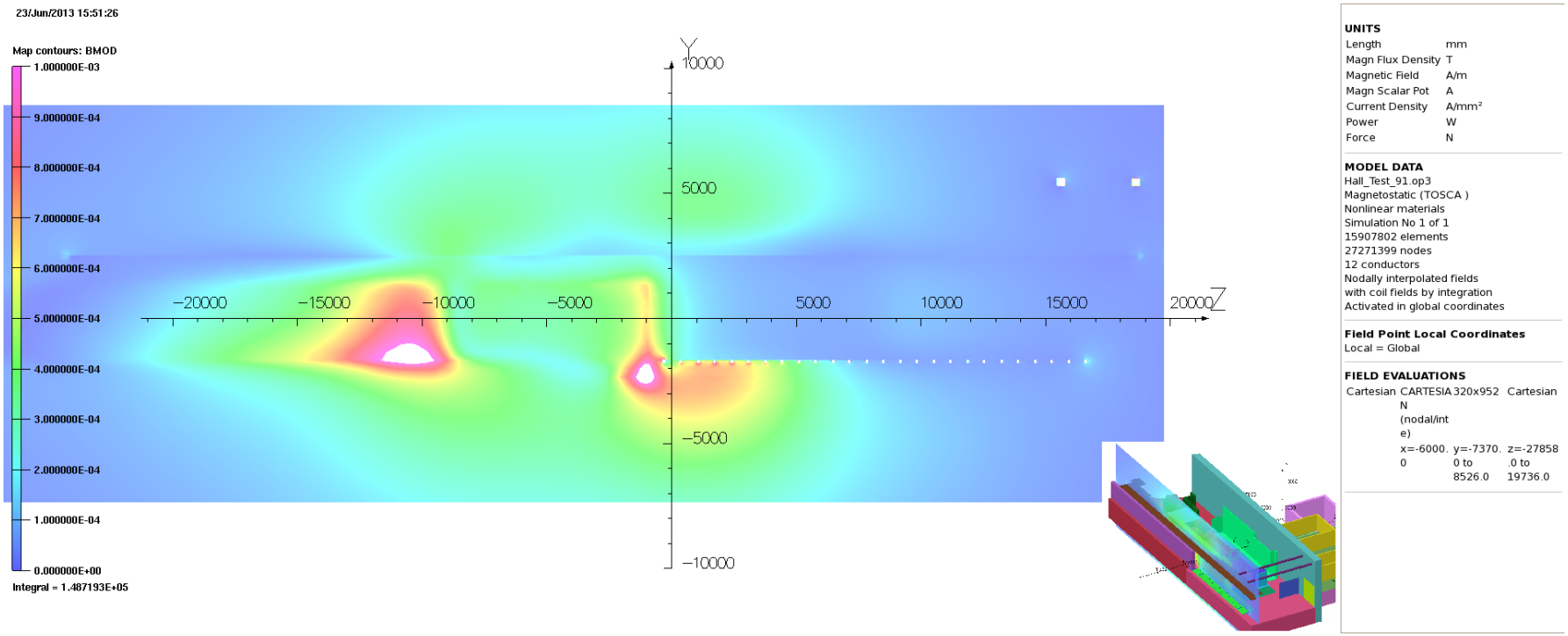

Figure 34: Bmod. Step IV 240 MeV/c Solenoid Mode. 10 gauss Scale. This is a plot at x=-6000 mm. See figure 33 to reference the plane. Once again it is clear that the area between the Linac wall and the NSW is seeing higher fields than behind the rest of the NSW

5.1.8 Quads Q7-Q9

Without the addition of a return yoke the Quads Q7-Q9 will see a significant magnetic field. In the hall model the quads have been modelled as a solid lump of iron, which clearly is an inaccurate overassumption, but on the scale of the hall model this simplification was necessary.

Figures 35 through to 36 show the effect that the quads are having on the field produced by the MICE magnets. There are a few points worth noting.

Firstly the downstream face of Q9 sees signficant magnetisation, however without a more realistic representation of the ferrous mass of a quad it is difficult to know whether this is a signficant real issue or not.

Secondly in the hall model the line of quads act as a low reluctance path to the flux providing a path to the DSA and the fridge plates on the South Shield Wall. This path to the fridge is unintended and has the effect of shifting the field further upstream. Once again the sensitivity of this to a real quadrupole ferrous mass is unknown.

In conclusion if a return yoke was not to be employed this is an area that would require further refinement and study.

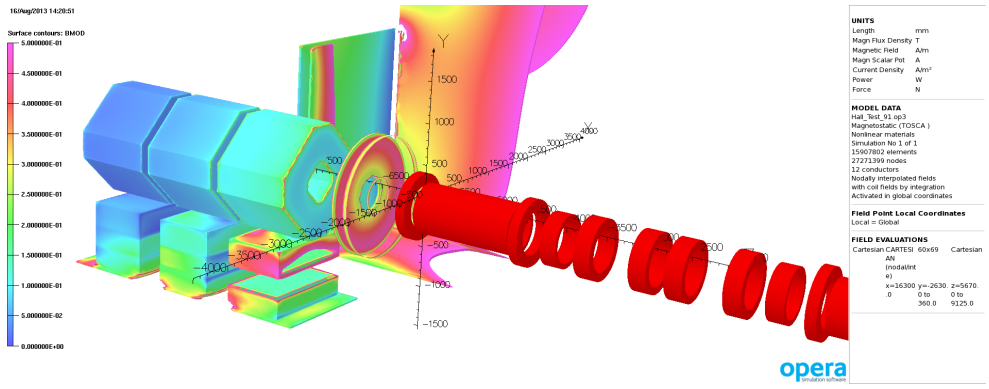

Figure 35: Bmod. 0.5T scale. Step IV 240 Mev/c Solenoid Mode. This shows the induced magnetisation in the ferrous components close to the magnets. The Quads, Q7 to Q9 left to right, have each been modelled as a solid ferrous lump, so the amount of iron has been overestimated. It is unclear what effect a more realistic model would have but it is clear that Q9 will see a large field from the cooling channel.

5.2 Sub Models

In order to study some features in further details, some sub-models were built. This section details these submodels and the results obtained from them.

5.2.1 Trench

*** I have added this subsection as I think Mike Courthold may have done some work on this and might wish to add something. If not then remove. *** Note I haven't yet asked him about this!

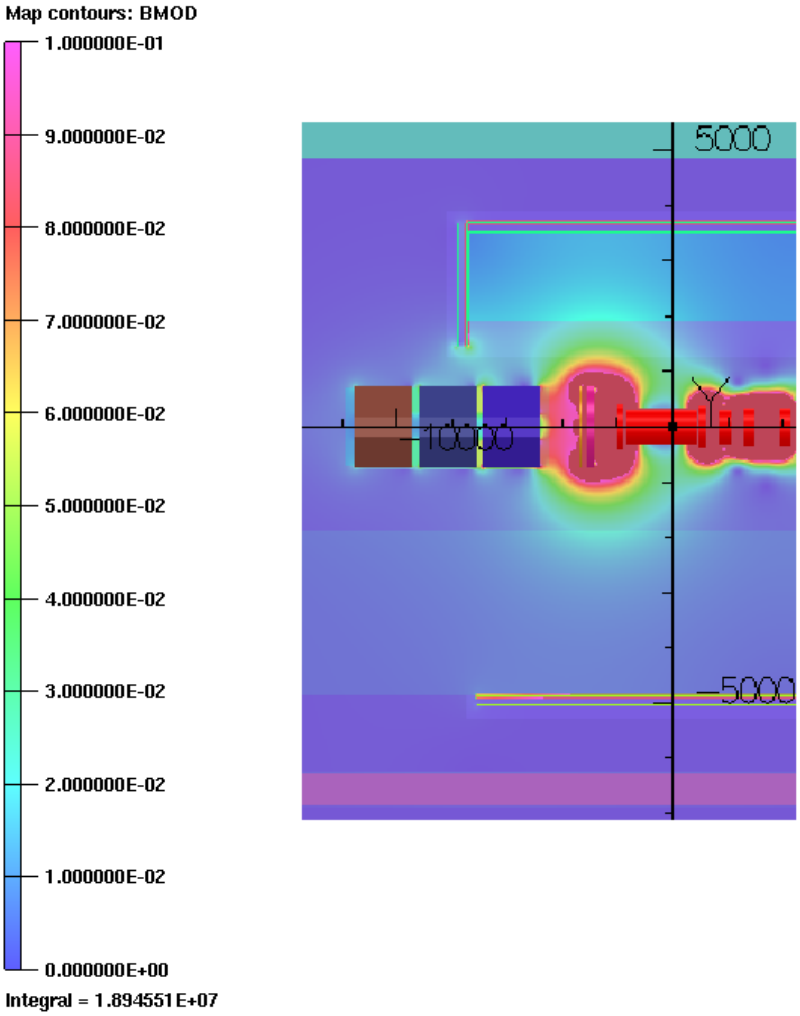

Figure 36: Bmod. 100mT Scale. Step IV 240 Mev/c Solenoid Mode . This plot shows how the quads pull the field from the magnets and how there is a hot spot around the end of the fridge plates; these are the plates that are part of the SSW and are perpendicular to the second quad, Q8, in the figure.

5.2.2 Shield Wall Model

Both the north and south shield wall are constructed from plates of AISI 1010 steel bolted onto a steel frame, however in the MICE hall model the shield wall is modelled as a contiguous sheet of AISI 1010 steel with no supporting framework.

In principle this should be a reasonable approximation, however it has been noted that the plates from which the real steel wall are constructed have significant gaps between the plates. Given that the structural steel behind the plates (I beams) has poorer magnetic properties than the face plates and that additionally the I beam it is much thinner in cross section there was some concern that the real wall will not perform quite as well as the modelled one. Will there be significant field leakage behind these gaps thereby increasing the effective field behind the shield wall?

In order to understand this issue a separate high resolution model of the shield wall was built incorporating these gaps to see if this effect was significant. The vertical I beams were included in the model, however the horizontal I beams were not included as this would have made the meshing difficult. As the return flux will

Figure 37: Photograph of the north shield wall. The gaps between the plates can be clearly observed.

be dominated by the plates in the horizontal direction the horizontal I beams are less important. The meshing of the model was very fine to capture the detail in the gap and to get an accurate representation of what is happening in the gap region. The model included the Step IV magnets at 240 MeV/c Solenoid mode.

The First section of wall that was modelled was composed of two by three panels. This model demonstrated that gap leakage would be observed but the model was of insufficient size to make suitable comparisons with the model of the shield walls in the MICE hall model. For brevity these results are not included here but are available online.

Subsequently a second model with a larger wall composed of three by seven panels was modelled. This wall is approximately half the size of one of the real shield walls. A 7 mm panel gap was used in all of the models. Figure 38 illustrates how the shield wall looks with respect to the Step IV magnets. The I beams can be seen jutting out from the between the two layers of plates. Figures 39 and 40 shows the magnitude of the field behind the 7×3 shield wall model at a distance of 25 mm and 250 mm respectively behind the shield wall. There are clear peaks behind the location of the I beams where the continuity of the plates are broken. In this particular model the plates are standing off from the I beams by 1.5 mm which is to simulate the fact that the join between the plates and the I beams is not too good. The 1.5 mm is excessive and so represents a worse case scenario but some of the two by three panel models had perfect contact between the plates and the I-beams and an increase in the magnitude of the field behind the shield wall was still predicted, although the magnitude of the effect was much subdued. The models are sensitive to the reluctance of this magnetic connection between the plates and the I-beams and it is difficult to estimate what the reluctance of this connection is. This remains a large uncertainty in the modelling.

Finally plots 41 and 42 shows a comparison with the predicted field behind the South shield wall in model 91. There is a small discrepancy in the location of these two shield walls ($\approx$3%) but the difference in the predicted field due to the gaps inbetween the plates is striking.

*** NOTE: I have included the results that we have but ideally I would like to re-run the shield wall model at

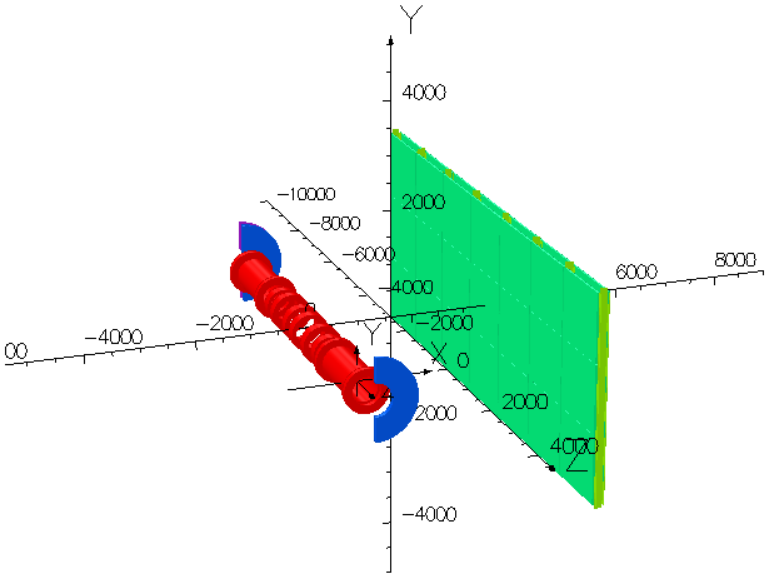

Figure 38: This shows the 7×3 shield wall model. The model is symmetrical in x and y to speed up the solve time. Consequently there is a symmetrical shield wall at the same distance on the -x axis that is not shown in this figure.

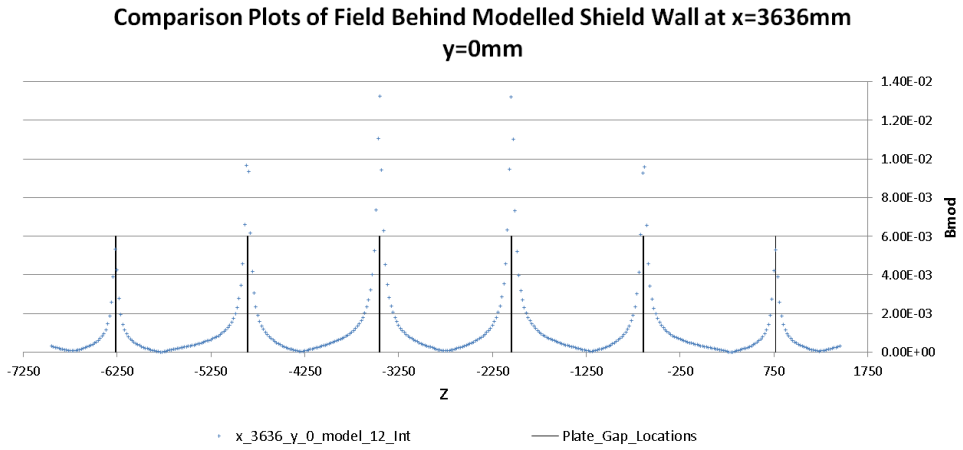

Figure 39: This shows the magnitude of the field behind the 7×3 shield wall model at a distance of 25 mm behind the shield wall. There is a 1.5 mm offset between the plates and the I-beams in this model

the NSW distance with no gap, a 1 mm gap and no gap with a contiguous wall for comparison with model 91. As this is a computationally expensive model I will try to run this model over the summer holidays. If not then we will be stuck with what we have.

(It would also be nice to re-run these models at a distance that is comparable with SSW given that current model has a small offset error in it but this is less important.)

***

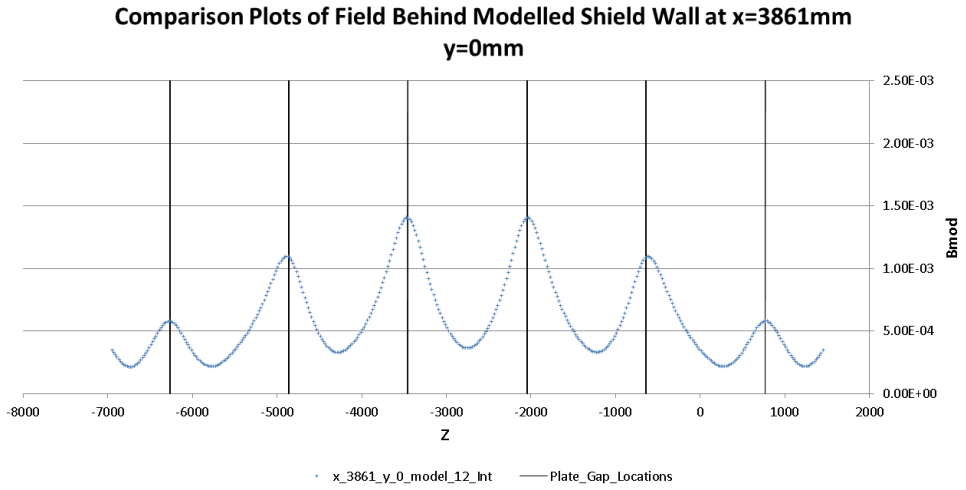

Figure 40: This shows the magnitude of the field behind the 7×3 shield wall model at a distance of 250 mm behind the shield wall. There is a 1.5 mm offset between the plates and the I-beams in this model

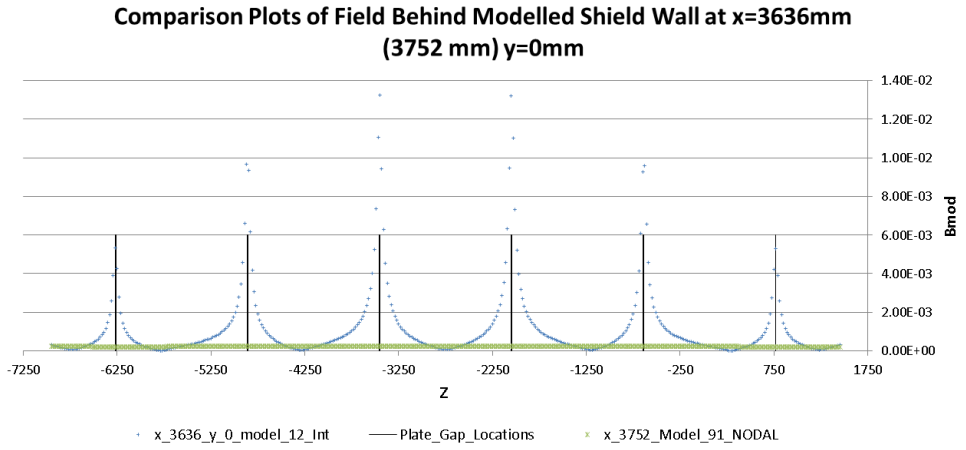

Figure 41: This is a comparison from plot (figure 39) compared with the predicted field 25 mm behind the South Shield Wall from model 91. The South shield wall is slightly further away from the magnets than the standalone shield wall model so the south shield wall data is taken slightly further away from the axis (3752 mm vs 3636 mm). Despite this small discrepancy in distance to the shield wall (≈3%) the difference in the predicted field behind the wall is striking.

Conclusions

The shield wall models have indicated that for the case where the shield walls are not contiguous that any gaps in the shield wall do have an effect upon the field that is observed behind the shield wall. The increase and the localisation of this increase in the field are dependent upon a number of assumptions that are implicit within the model. It would be difficult to further quantify or justify these assumptions without recourse to some magnetic measurements. As we would be unable to obtain such measurement until the MICE magnets are in-situ and turned on this leaves us in an uncomfortable situation that we have a known problem that is difficult to quantify.

This does leave several questions unanswered.

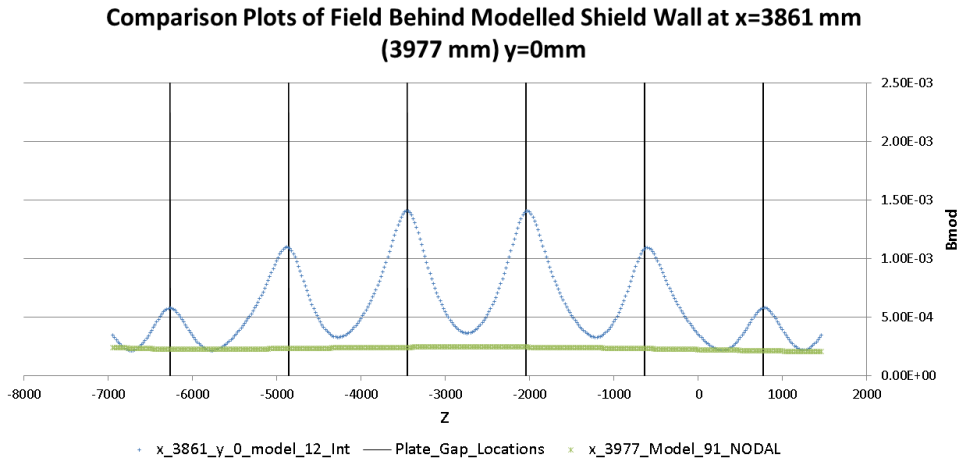

Figure 42: This is an identical comparison from plot (figure 40) compared with the predicted field 250 mm behind the South Shield Wall from model 91. As previously, the South shield wall is slightly further away from the magnets than the standalone shield wall model so the south shield wall data is taken slightly further away from the axis (3966 mm vs 3861 mm).

Is there a global increase in the field behind the shield wall due to the gaps (as the shield wall is less effective than anticipated) and how far does this extend?

How far do the local incursions extend?

Do these incursions affect any equipment? If we don't build a return yoke is the shield wall considered to be a safe haven for the tracker racks?

Do these incursions affect any walkways that were assumed to be safe?

It was already anticipated that a return yoke would be needed for Step V/VI of the experiment so on this assumption any magnetic leaks from the shield wall are less likely to be of concern for the RF (which wouldn't be used until any return yoke was in-situ). However even with reduced external fields do these leaks create local non homogenous areas in the field that would have an adverse effect on the RF tubes? Would MICE be better off without the shield walls at all in this area? This is something that will need separate consideration once a decision has been made.

5.2.3 Sub-Station Sub Model

The MICE hall contains a modern substation that provides power for the experiment. This substation sits in the North West corner of the MICE hall and is partially shielded by the North Shield Wall. As the substation is relatively new there is a significant amount of control electronics, including programmable logic controllers, embedded into the substation's front panels. There is some concern that these electronics could be adversely affected by stray magnetic fields.

Figure 43 shows a photograph of the MICE substation. The base MICE hall model did not contain a model of the substation but the substation represents a signficant mass of iron, estimated at ≈5300 kg. In order to ascertain whether the substation would have an impact upon the field distribution in the MICE hall 5300 kg of mild steel in a 14 mm shell that was an approximate cuboidal representation of the substation geometry and location was added to model 91 and run as model 113. The results from this model through the plane y=0 can be seen in figure 47. Other figures can be viewed on-line. Compared with model 91, there is minimal change to the field distribution in the area that the substation is located and it appears that the maximum air field that the

substation will see is approximately 2 gauss, although for the most part the field is much lower. One can also ascertain that a significant field component runs South to North, although there is an East to West component at the West end of the substation. An equivalent model for Step VI of the experiment has not been run.

Figure 43: This photograph of part of the substation in the MICE hall clearly shows that a signficant amount of electronics has been mounted in the front panels.

To understand the effect of an external field on electronic equipment mounted on the surface of the substation panels several submodels were run where the substation was modelled as a series of racks with a 2 mm thick mild steel skin. The first set of submodels contained a single window in each rack that measured 450 mm high by 300 mm wide. The second set contained four windows in each rack, with each window measuring 100 mm by 100 mm on 150 mm width centres and 200 mm height centres. It should be noted that as only the outer panels were modelled these sub-models only give a total mass of 1000 kg but as we are primarily interested in the field level in the windows of these 2 mm thick panels and that by and large the internal iron in these racks is some distance from these windows, this was considered to be sufficient to give a first estimate of the effect.

An external field of 5 gauss was applied to these models, this was a deliberate overestimate of the external field based upon the air field results from model 91; some of the the submodels were completed before model 113 was solved. The submodels were run with both the field in a South to North direction and in and East to West direction for comparison. As none of the steel in the submodels is saturated then the results should to first order scale to a lower air field.

Figure 48 shows a cross section through the substation model at y=0 with a 5 gauss field from +x (South to North). This is a model with a single large window in each rack. One can immediately see that the area around the windows is seeing a field of approximately 5 gauss.

Figure 44 and 45 shows a couple of view of one of the windows in the submodel. The first image shows the steel surrounding the window and it's relative magnetisation. The other plot shows the predicted field strength in the window on a 10 gauss scale. One can see that the field in the window is approximately the same as the applied external field (5 gauss) although there is some intrusion of higher field from the left and the right.

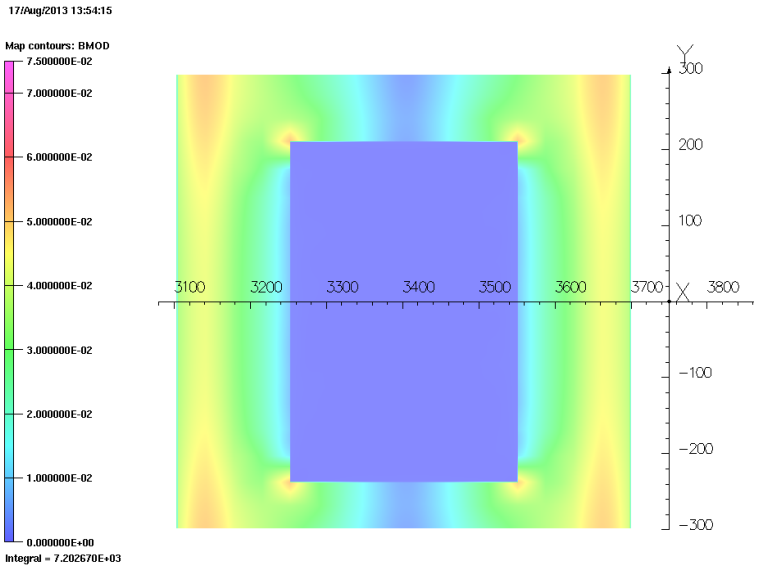

Figure 44: Plot of the steel around the second window from the West end in the substation model. 5 gauss external field running from South to North (from +x). 750 gauss scale.

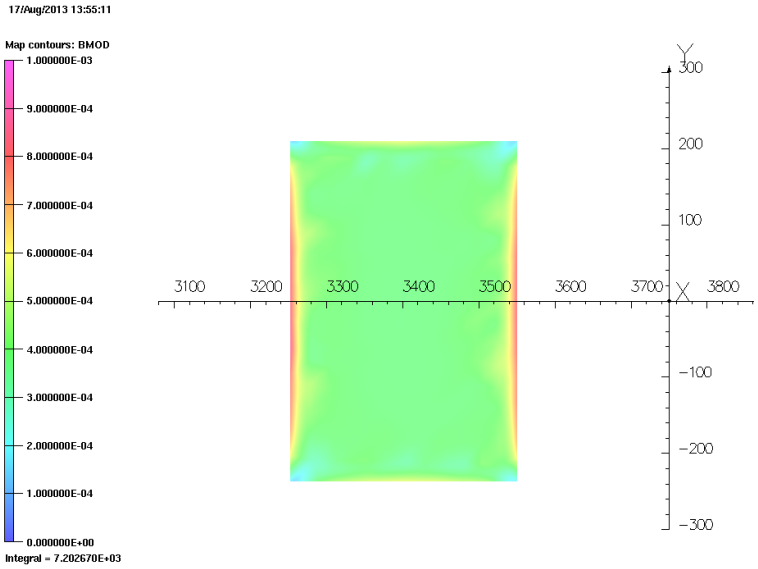

Figure 45: Plot of the air volume inside the second window from the West end in the substation model. 5 gauss external field running from South to North (from +x). 10 gauss scale.

When the external field is applied East to West, a similar picture emerges except that the window plots see a slightly higher field of ≈20% and there is more intrusion of the field from the steel into the window space - see figure 46. A similar picture is seen for models that contain sets of four smaller windows instead of the one larger window.

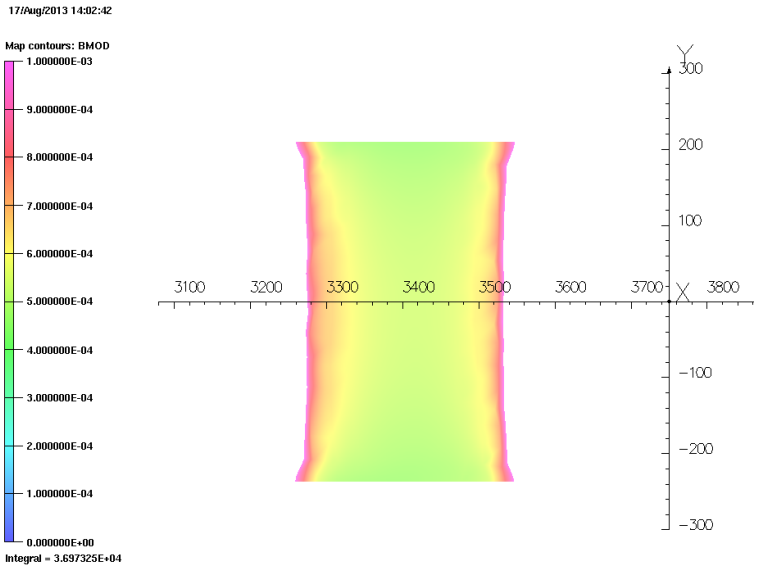

Figure 46: Plot of the air volume inside the second window from the West end in the substation model. 5 gauss external field running from East to West (from +z) 10 gauss scale.

Conclusions

The conclusion from these submodels is that for Step IV the substation does not appear to significantly alter the field profile and consequently the models predict that the substation will see a maximum field of approximately 2 gauss. Further submodelling indicates that any instrumenation mounted in the 2 mm thick steel panels will not see significant amplification of the external magnetic field due to their proximity to these steel panels and that the instruments should only see a level of magnetic field that is consistent with the magnitude of the external air field or slightly above it. A slightly higher level of magnetic field can be expected at the edges of the cutouts/windows.

It should be bourne in mind that these conclusions are based upon the predictions from the model only and these have no grounding in any field measurements. Consequently as the models are only an approximation to both the substation geometry and mass distribution the output from these models should be viewed as a guide.

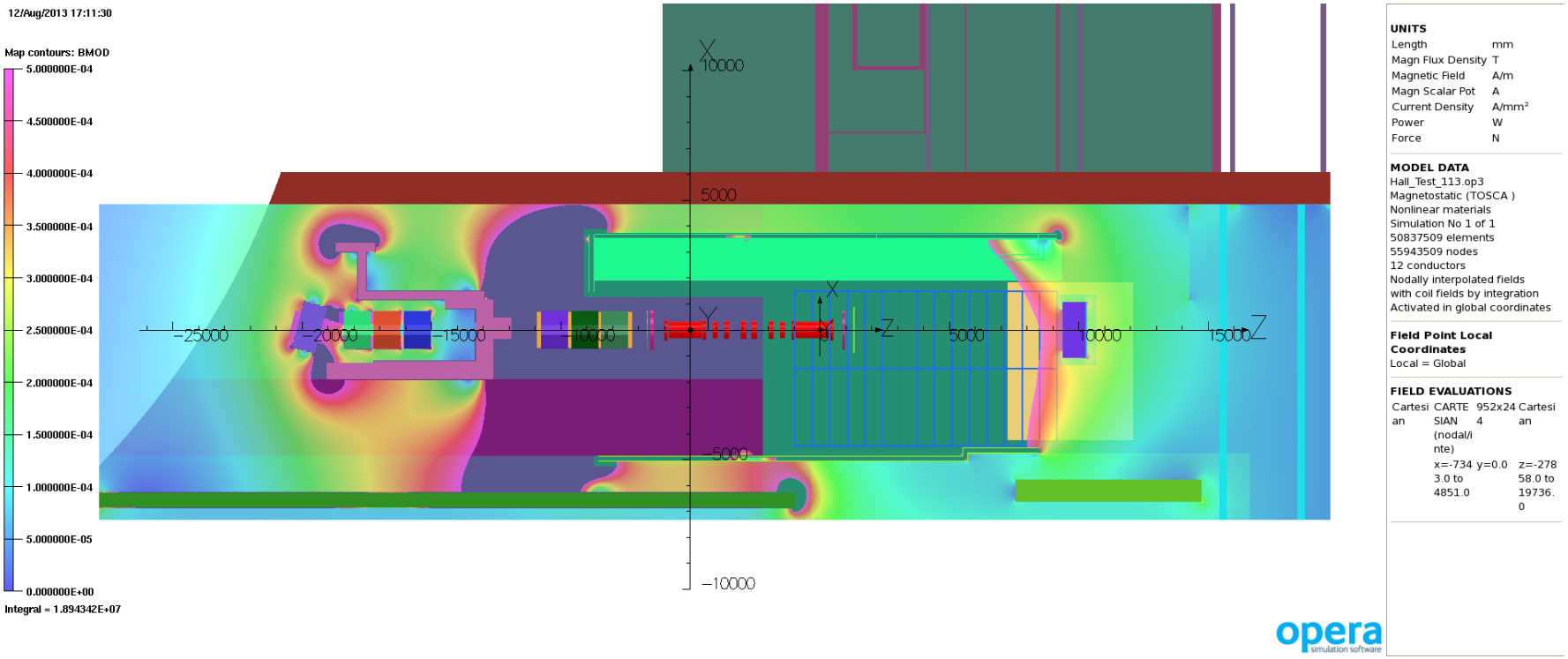

Figure 47: This is an image from the Hall model with the sub-station mass added - Model 113. Step IV Solenoid mode 240 Mev/c. The addition of the substation pulls the field slightly towards the north shield wall but change in the field distribution is minor.

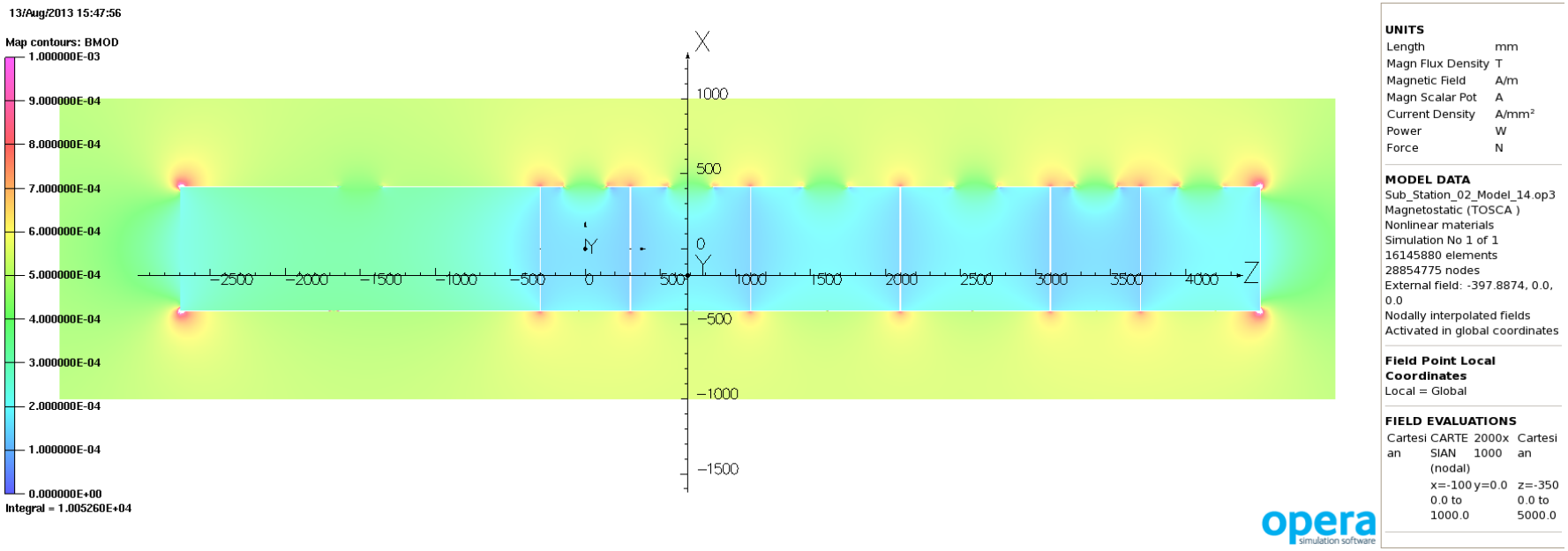

Figure 48: Bmod. Substation model. 5 gauss external field applied from +x (South to North). Note that the model boundary is much further out than the limits of the plot. 10 gauss scale. The field in the vicinity of the windows can be clearly seen.

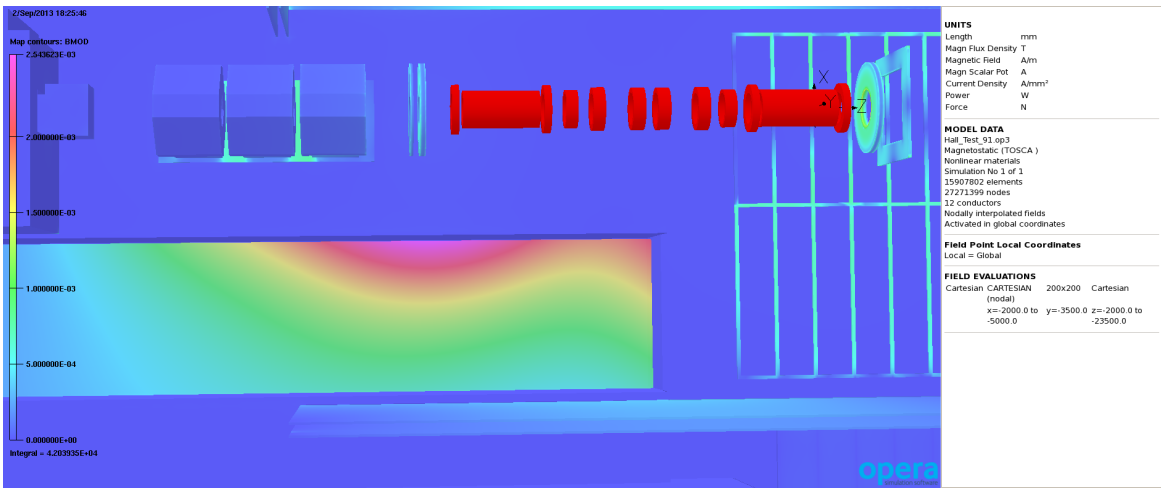

Figure 49: A patch in the MICE Hall Trench, at height $y = -350$ cm, just above the trench floor.

5.3 Inventry of Sensitive Items

The major concerns with the significant stray fields predicted by the MICE Hall model is that they will interfere with the electrical and mechanical operation of components, potentially causing undesired performance or malfunction in certain equipment. As the fields were initially predicted to be lower than current estimates, especially in certain areas where flux has been focussed, some of the equipment which has already been allocated and placed in the hall may be at risk. A full review was started, to log and evaluate all field sensitive items within the experiment, and to understand the operational risk they present.

5.3.1 Method of Evaluation of Sensitive Items

Following a comprehensive inspection of the MICE hall a list was compiled of all the equipment that might be sensitive to magnetic fields and the physical location of such objects. This list is a combination of items installed for the experiment and pre-existing infrastructure. To aid the mitigation effort, each item was allocated to a generalised hall region, e.g. the North Mezzanine, and functional subsystem.

The object of this process is to assess the likelihood of item malfunction or undesirable performance due to the influence of the magnetic field and to ascertain the overall operational risk that such malfunctions would contribute to the experiment. The two elements of understanding the risk are: determining the ‘in air’ magnetic field for each item’s location, and the sensitivity in performance of the item to the estimated external field.

Using MICE Hall Model 91, as previously described in this document, the magnitude of the air field (BMod) was extracted, from either a single representative location or a set of Cartesian patches for the larger items. In each case, the maximum observed field was recorded, as the approach is aimed at considering the worst case scenarios. Figure 49 shows the magnetic field in the Trench, at a height of $y = -350$ cm (just above the trench floor), showing the dynamic nature of the field in that region. Some of the items considered in the trench span at least a factor of two change in local field.

The second factor in this process of evaluation is the sensitivity of the item to a surrounding magnetic field, specifically the value at which the element would cease to function in the intended manner. This is the most difficult figure to ascertain. Ideally, items would be tested; the Focus Coil in R9 presents one possible method of testing, as do magnets operated by UK universities, However, many of the items are already integrated into the MICE experimental area (and too costly for replacements to be procured and tested), others could be moved

Figure 50: Patch used to evaluate the PSU for Q9.

to a test location, but not tested under the full range of working conditions (as an example, a fire alarm control panel cannot be cleared because it is seen to briefly operate in a strong magnetic field, it must be tested under a wide range of inputs and preferably over a prolonged period of time).

Manufacturers are frequently unwilling to publish a field sensitivity figure in their specification. In some instances, objects can be opened and a visual inspection of the individual components can inform an estimate of the maximum field, but this is not guaranteed.

Therefore, the decision was made that a 10 G threshold would be set, between 'low risk' and 'investigate further' categories. This value was based on the sensitivity of relays [**?**] and allowing for a significant margin of error in the FEA model. Relays are one of the most sensitive and commonplace components, found in electronics, control and power supply equipment. This was only a general rule; where items are known to have greater sensitivity, such as those featuring Hall Effect sensors, then they have been moved to the 'investigate further' category.

The final factor for consideration is that of risk with regards to the safe running and reliable operation of the experiment. A highly essential safety component or detector system has been given greater consideration than a general webcam or thermometer.

5.3.2 List of Magnetic Field sensitive items in MICE

Table 1 lists all of the items that were categorized as 'investigate further'. Many other elements were investigated, and potential mitigating steps identified, despite their 'low risk' status. Where possible, these mitigating steps will be taken, provided they do not adversely effect the MICE schedule.

5.3.3 Items Requiring Magnetic Field Mitigation

Conventional Magnet Q9 PSU

The maximum field in this region is evaluated from the model as 27 G, see Figure 50. The equipment features typical controls automation components such as relays, which can show unreliable performance

Table 1

Object	Location	System	Field in Air (G)	Comment
PPS Trench Magnetic Switch	Trench	PPS	9	Evaluated without ferrous mass of trench fence work.
Crowcon Gas analyser	North Wall	Infrastructure	10	Can be mitigated with local shielding.
Linde Helium Fridge	South East Corner	Decay Solenoid	10	
Filtration System	Trench	Water	10	
D10 Board and Isolator	Trench	General Power	15	Board will probably be removed.
208v Transformer	Trench	General Power	15	Transformer can be moved to Rack Room 2.
Cranes	Global	Infrastructure	16	Can require crane isn't used while cooling channel on.
Air Con Units East	North Wall	Air Conditioning	5 to 20	Evaluated without ferrous mass of item.
Fire Bell	Trench	Fire Protection	10 to 20	Dynamic field area.
Grundfos Pumps $\times$ 2 & Control Box	Trench	Water	10 to 20	Dynamic field area. May be affected, relocation being investigated.
Moving Beam Stop	Beamline	Infrastructure	20	System should be unaffected if fully pneumatic.
Web Cam South Wall	Ground	Webcams	20	Can be relocated.
MQ9 PSU	Cooling Channel	General Power	27	Proposed relocation next to MQ8 PSU Rack.
North Mezz Extension Dist Board	North Mezz	General Power	47	Change for Redspot Fuse board.
LH2 Heater PSU	South Mezz	LH2	80 to 200	Dynamic field area. Field sensitivity of item needs to be established.
LH2 Relays	South Mezz	LH2	80 to 200	Dynamic field area. Field sensitivity of item needs to be established.
Pressure Gauge Dial	South Mezz	LH2	80 to 200	Dynamic field area. Field sensitivity of item needs to be established.
D14 LH2 Mezz Power	South Mezz	LH2	80 to 200	Dynamic field area. Field sensitivity of item needs to be established.
LH2 Gas Panel	South Mezz	LH2	80 to 200	Dynamic field area. Field sensitivity of item needs to be established.

from 15 G. The proposal is to move this unit East in the hall, further away from the cooling channel magnets. The proposed region shows a much lower field, $\sim$7 G.

Trench Western End

Many of the items in this area marked as 'Investigate Further' will be moved and replaced, such as the Grundfos water pumps. The only significant high risk item is now the Fire Bell. The type/technology of this sounder needs investigating and, if sensitive to the fields in the area, will need to be moved or replaced.

5.3.4 Areas and Items with Field Risk Insufficiently Evaluated

The South East corner of the hall, under the Linde fridge, is an area that requires further investigation, see Figure 51. The field is very dynamic in this region, with a maximum of 100 G dropping quickly to a more typical 10 G. The region contains controls and vacuum equipment used to operate the Decay Solenoid. Of notable concern here are programmable logic controllers (PLC), known to be sensitive from approximately 25 G and also a water chiller. Mitigation, if necessary, would be to add local screening inside the control cabinet and possible relocation of the chiller.

Another area requiring further analysis is the Liquid Hydrogen gas panel on the South Mezzanine; it is in close proximity to the downstream spectrometer solenoid and the model shows fields of up to 200 G in air (see Figure 52).

The LH_2 gas panel contains three elements of concern; electro-magnetic valves, pneumatic valves and turbo-pumps. The EM valves are fairly robust against magnetic fields, and if required can be moved to a location with a lower field by simply extending the plastic tubing connections. The pneumatic valves contain position indicators that rely on the Hall-effect. If necessary, these will be replaced with alternative types, which use potentiomenters and micro-switches. Finally, the turbo-pumps can be fitted closer to the attached vacuum chamber, and screened with local magnetic shielding. The vacuum gauges in the panel will not be an issue, as they have been identified as a combination of capacitance type, which is immune to the magnetic field, and Penning type, which can be fitted with manufacturer-supplied shields.

5.3.5 Summary

All the listed items in a predicted field over 10 G are capable of being moved or replaced. The majority of the small items could be dealt with quite simply and quickly. The Q9 power supply will not be easy to accommodate elsewhere, and will take some organisation to re-connect and route cable, but the risk can be resolved. The safety related items such as the Fire bell, Gas Analyser and the PPS Magnetic switch could be assessed in more detail, including field tested prior to being placed into active service. The crane would need to be discussed within the operations and online groups, to confirm that it will not be required while the cooling channel is at current. A procedure to inhibit its use while the magnets are at current would need to be developed and implemented.

The major mitigation issues will be the outcome of further analysis of the Liquid Hydrogen gas panel on the South Mezzanine and the Linde equipment. These issues could potentially be quite time consuming and costly to deal with. There are also a lot of valves on the front panel that might need relocating, and the design and testing of local shielding systems is not a task the collaboration has a wealth of experience with.

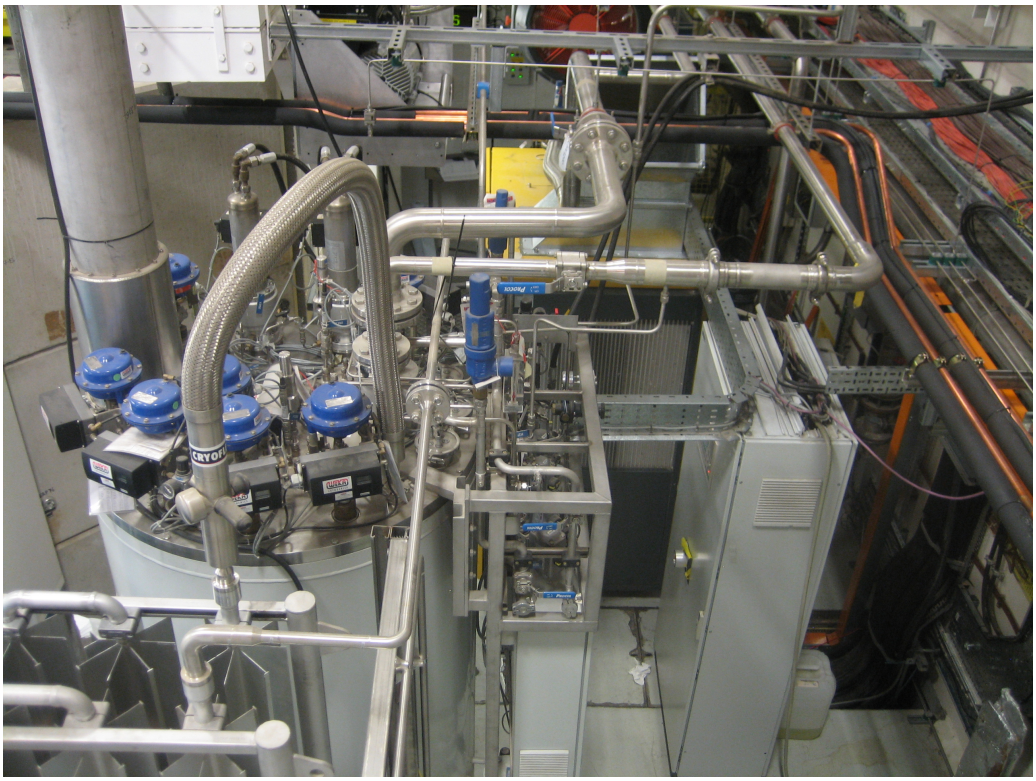

(a) A photo of the SE Corner, taken from the South Mezzanine.

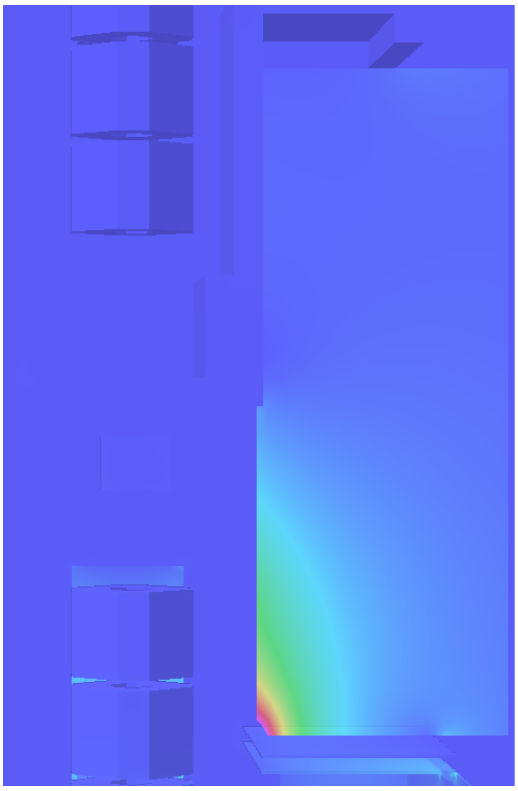

(b) Patch of the SE Corner region, with a scale of 0 - 100 G.

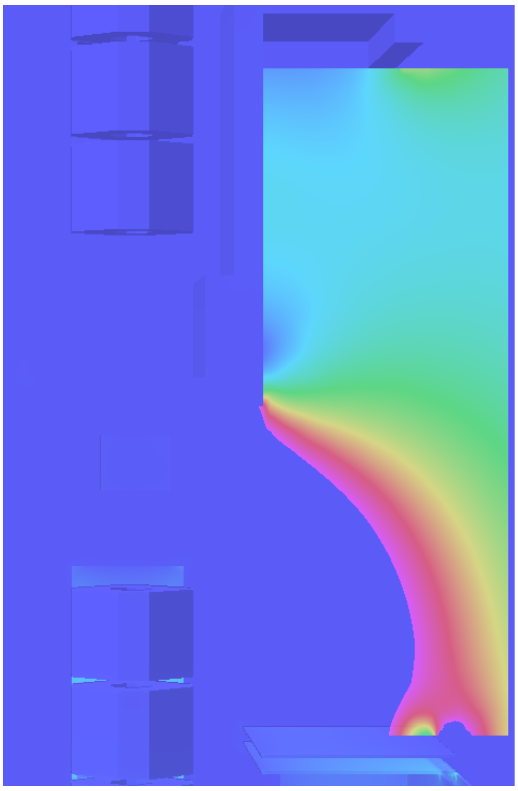

(c) Patch of the SE Corner region, with a scale of 0 - 10 G.

Figure 51: Analysis of the SE Corner, containing the Linde fridge for the Decay Solenoid.

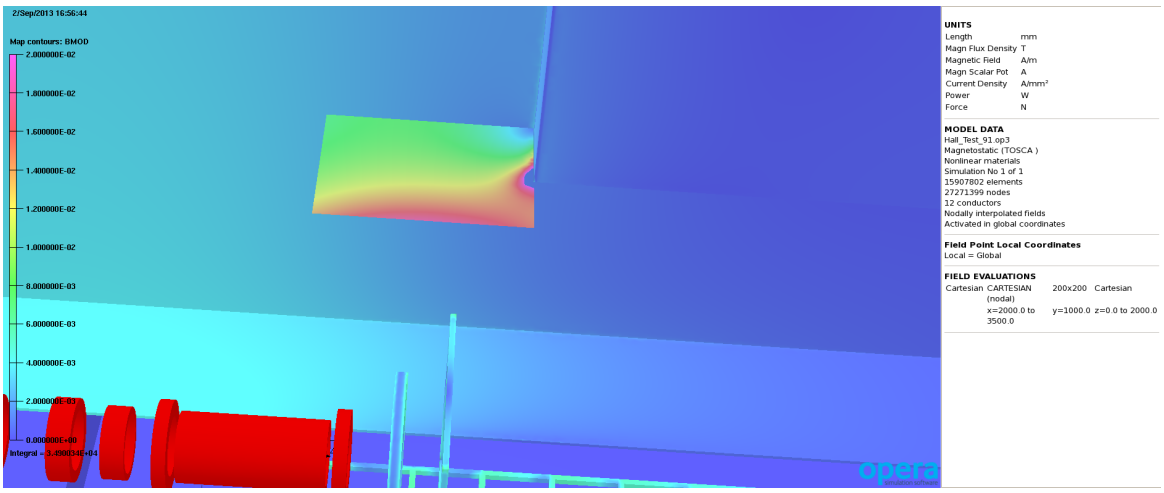

Figure 52: Patch used to evaluate the LH_2 system on the South Mezzanine.

5.4 Tracker readout systems

The four Tracker Cryostats (as seen in Figure 53) are some of the potentially sensitive MICE elements closest to the cooling channel; constrained by the short length of the fibre-optic connection between the Trackers installed inside the Spectrometer Solenoids and the Cryostat bodies. Under the Baseline plan, this proximity necessitates a local shielding solution.

The components of the cryostat that have been identified as being sensitive to magnetic fields are listed in Table 2. The table states the Manufacturer's stated limit on the tolerable field, and the estimated stray fields, according to MICE Hall Model 91.

Table 2: Components of the Tracker Cryostats which have been identified as requiring shielding.

Component	Tolerable Field (mT)	Predicted Field (mT)
Power Supply Unit	25	30
Turbo-molecular Pump	5	40
Vacuum Gauge	10	40
Cryocooler (cold head)	35	70

The degree to which the external field needs to be attenuated, the suppression ratio, varies between components, affecting the difficulty of determining a solution. Evaluation of the potential solutions has been achieved using simplified local models, relying on the MICE Hall model as a prediction of the field and applying a healthy safety factor. A model has been created for each shield solution, with a homogeneous external field applied. The direction of the external field was varied, to ensure that the shield was sufficient in the worst case scenarios. It should be noted that the difficulty of shielding a component is not only defined by the suppression ratio; the size of the volume to be shielded and the access to the area are also key factors.

5.4.1 Single shield solution

The possibility of implementing a single cylindrical shield, to accommodate the whole tracker cryostat, was investigated first. A cylinder of AISI 1010 steel, radius 60 cm and thickness $\sim$10 cm, would achieve a sup-

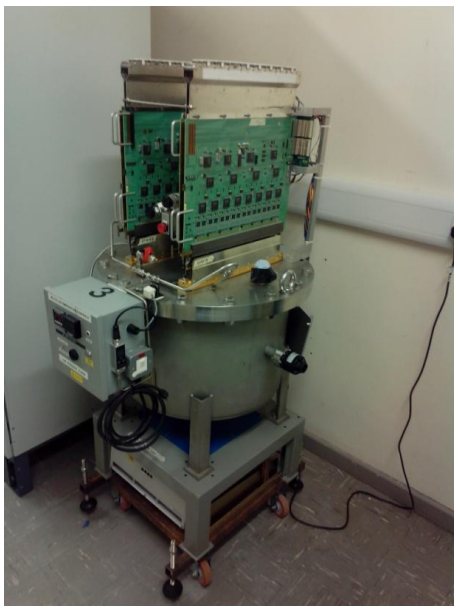

Figure 53: One of four Tracker Cryostats.

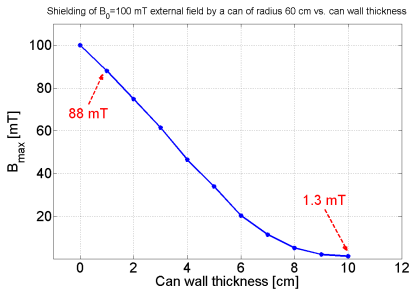

Figure 54: Results for a single cylindrical shield solution, to be placed over each Tracker Cryostat.

pression ratio of order 90 (as seen in Figure 54) when placed in a 100 mT field (higher than the Model 91 prediction). This would be sufficient to shield even the lid heater box, which could tolerate only 1.5 mT, and would be moved away from the Tracker Cryostat under all other shielding options.

The major disadvantage of a single cylindrical shield is the weight of the can, and the requirement to remove the can for any access to the cryostat. Two strategies for reducing the can weight were investigated: a "composite can" consisting of an outer steel layer and an inner μ-metal layer; or several co-axial cylinders with air-gaps between them.

The composite can solution, with 7 cm steel and 1.8 cm μ-metal, was found to have no benefits, due to the discontinuity of B/μ across the μ-metal / steel interface. The μ-metal saturation point of 0.7 T was significantly lower than the 1.5 T of the steel, such that the μ-metal operates in the low-permeability region of its BH curve, offering no advantage over a 8.8 cm all-steel solution.

The advantages of multiple co-axial cylinders for shielding purposes have been known since the late 1800s. A two cylinder solution was investigated; a 4 cm thick inner cylinder separated from a 5 cm thick out cylinder by 2 cm. The solution decreased the weight, but led to an increase in the total radius. A 60 cm radius shield was already difficult to accommodate, due to the very limited space available and the short length of the fibre-optic connections, so a larger but lighter solution was also unacceptable. Due to the large volume and weight of the single shield solutions, this idea was abandoned and individual shields were considered.

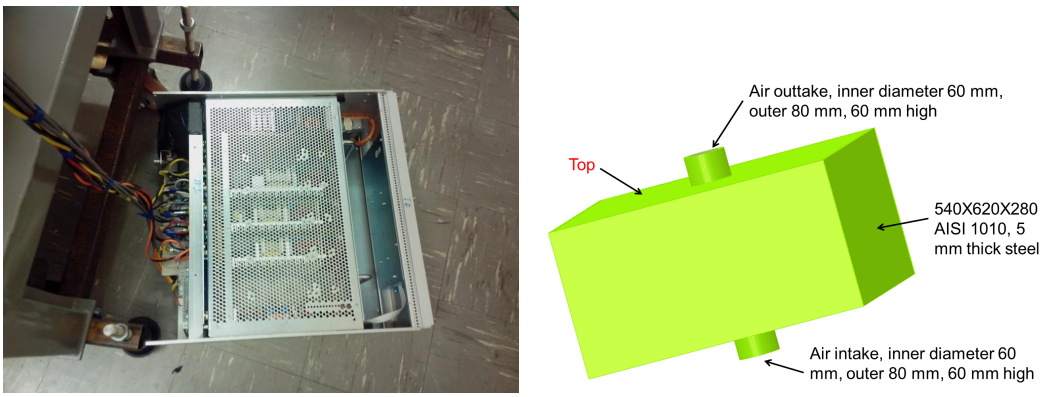

(a) (b)

Figure 55: a) The PSU for the Tracker Cryostat and b) the proposed shield.

5.4.2 Individual shield designs

The alternative to a single shield solution is to individually shield the components sensitive to magnetic fields. An analysis of the feasibility of individual shields follows. Note that the analysis only addresses magnetic shielding performance; mechanical and electrical engineering aspects have not been considered in detail, but brief investigations have identified no major concerns.

PSU Shield

Figure 55 shows the Tracker Cryostat's PSU and the proposed shield design. The shield is a steel box, with 5 cm clearance between the PSU and the shield walls. Two chimneys, on the top and bottom, would allow airflow for cooling and cable access.

The shielding performance of the box was assessed by calculating the field distribution in the shielded area resulting from a 30 mT homogeneous external field. Various field directions were modelled, and a maximum internal field of 10 mT was found. Inside the chimneys, the field drops to $\leq$3 mT; which might allow for the installation of electric cooling fans if required.

As described, the box is capable of shielding the PSU magnetically, but additional design (both mechanical, to permit opening and closing the shield for PSU access, and electrical, to guarantee cable access and sufficient cooling) would be required. Care would need to be taken that mechanical design changes did not compromise the shielding.

Turbomolecular Pump and Vacuum Gauge Shields

The shielding solutions for the turbomolecular pump and vacuum gauge can be seen in Figure 56 and are functionally identical; a capped steel pipe with 1 cm thick walls is sufficient to attenuate an external field of 40 mT to between 3 and 0.5 mT (dependent on field direction), below the safe limit of 5 mT. The two shields would only vary in pipe length and cap inner diameter. The caps reduce penetration of the field, while maintaining air circulation and access. The shields can be installed by splitting the cylinders along a plane containing the axis, fitting the two halves and then re-attaching them together with steel bands.

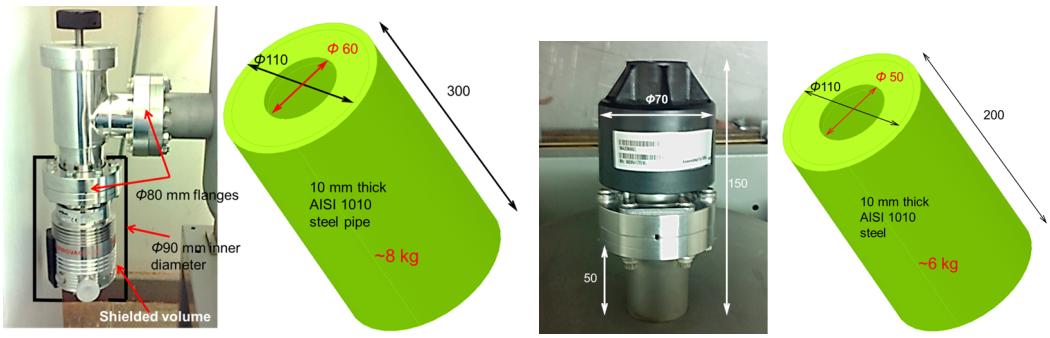

(a) (b)

Figure 56: a) The turbomolecular pump, with proposed shield and b) the vacuum gauge.

Cryocooler Shielding

Of the four components considered in this section the Cryocooler cold head is subjected to the highest magnetic field strength (70 mT). This field needs to be attenuated to below 35 mT. The suppression ratio is low, but there is no easy access to the unit, as can be seen in Figure 57.

Figure 58 shows a proposed solution. A large diameter cylinder with 3 cm thick walls encloses the liquid Helium tank, shielding the cryocooler portion inside the tank. The smaller diameter cylinder has 2 cm thick walls, and shields the external section of the cryocooler. The design does not include access for the cabling and connecting external units; such as the PCBs, vacuum gauge and turbomolecular pump (all visible in Figure 57b). The chimney design, suggested for the PSU shield, would be a general solution for these connections, but the engineering aspects of the work would not be trivial. Installing the shield would also become an intrusive procedure, introducing risk to the components each time the shield is added or removed.

As with the other shield designs various directions of the external field were modelled. In each case, the internal field was well below the target value. Figure 58b shows results for a 70 mT external field at an angle of 45°, with the internal field well below the 35 mT limit, suggesting that further optimization would be possible.

Summary

In conclusion, FEA modelling has demonstrated that local shielding options for the four magnetically sensitive components of the Tracker Cryostats are possible. A complete engineering analysis and design has not been completed, with some aspects of the design clearly needing modifications or additions. While these changes are likely possible, many of them would add elements of risk to the local shielding option. This is particularly true for the cryocooler cold heads.

5.5 Racks and compressors

Lead author: MG

5.6 Summary

Lead author: CM/KL

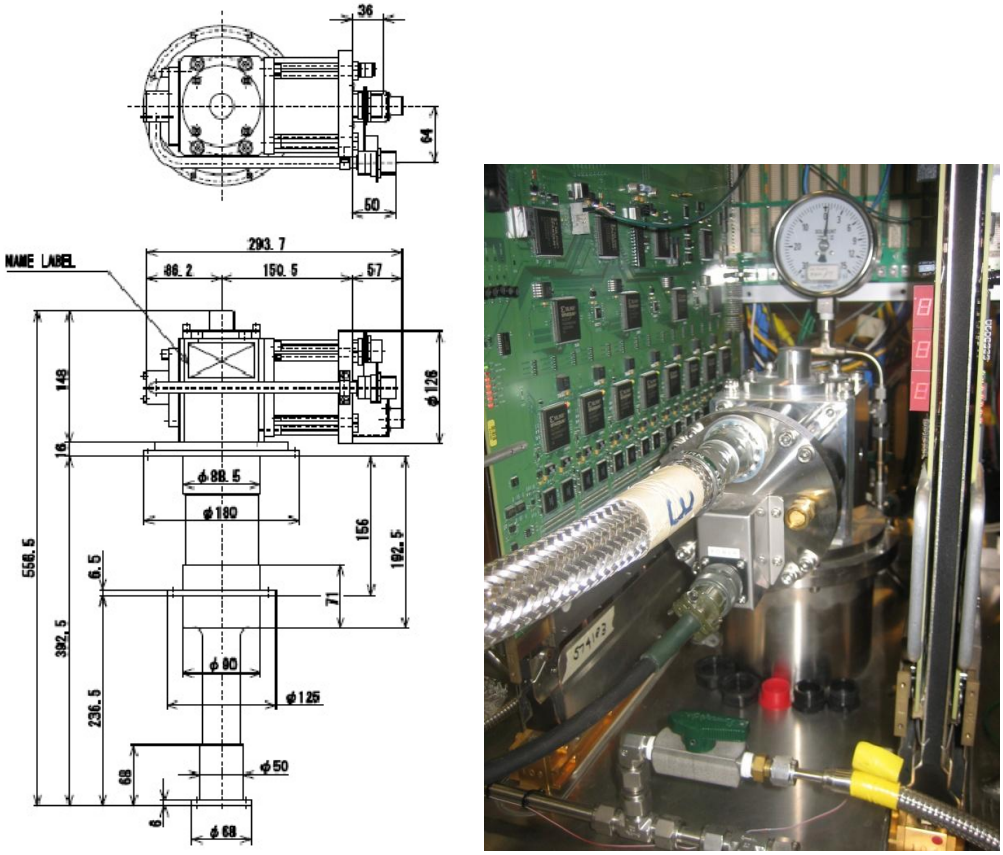

(a) (b)

Figure 57: The Tracker Cryocooler cold head. a) Shows a schematic of the device, and b) shows the top half of the cryocooler, extending out of the cryostat body.

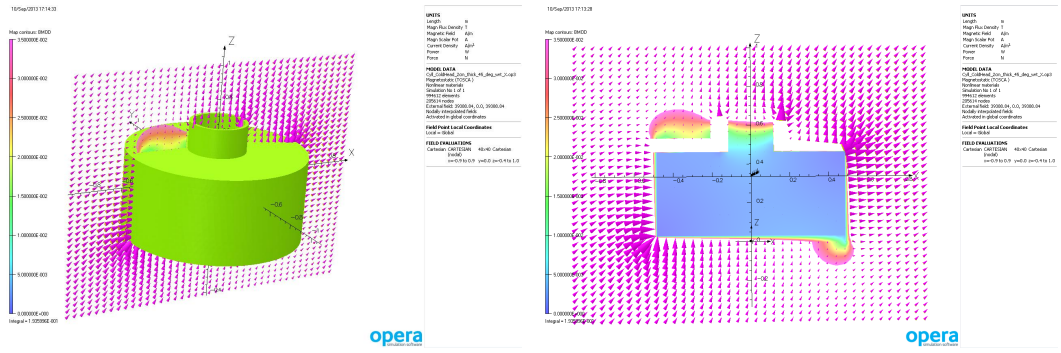

(a) (b)

Figure 58: a) Proposed shield for the Cryocooler, which is partially enclosed inside the liquid Helium tank, and b) the response to a 70 mT external field at an angle of 45°. Scale is 0 - 35 mT.

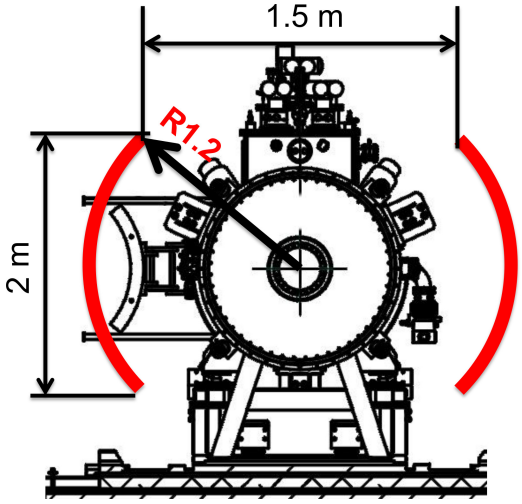

Figure 59: General Concept for the PRY, which is shown in red.

6 Partial return yoke

6.1 Overview

All MICE magnets are large diameter solenoids, which are relatively thin and short. From a shielding point of view an ideal solution is to encase the MICE magnets in a soft-iron cylinder. This approach is of course unrealistic; accessing the cooling channel to provide the required services, and to read out the Tracker detector, would be practically impossible. However, good shielding can be achieved with only a partial return yoke (PRY), as long as it provides an improved return path for the magnetic field. This concept is shown in Figure 59.

As shown in the figure, the initial concept assumed soft-iron, located on a circle with a radius of 1.2 m, covering the $\pm 50^{\circ}$ range on both sides of the cooling channel. Initial studies showed that for Step IV a thickness of about 10 cm is required for good shielding. The weight of such a shield (which is approximately 8 m long) would be 30 metric tons. The performance is shown in Figure 60, which shows the modulus of the stray field on a surface with a radius of 1.5 m. The figure shows that the stray field is reduced to < 1.5 mT in the magnetic 'wind shadow' of the shield; without the shield, the field in the region would be > 30 mT.

During the course of this project the shield has evolved; these changes either improved the performance of the shield or, at a later stage, were driven by engineering considerations. Figure 61 shows an overview of the development history.

The vertical extensions shown in the middle design of Figure 61 were added to provide a better suppression of the remaining stray field behind the shield. Figure 62 shows flux tubes of the magnetic field from the original PRY design, and illustrates how the majority of the flux behind the shield stems from the top and bottom openings in the shield. Adding vertical extensions significantly improves the performance, demonstrated in Figure 63. The figure shows a side-by-side comparison: using vertical extensions the magnetic field can be reduced to < 1 mT.

The final change in design was motivated by construction constraints; an initial engineering source investigation was started on the first design. The majority of vendors were unable to form an arc section of radius 1.2 m and thickness 100 mm. The only vendor who could provide such sections stated that the arcs would need to start and end with straight sections, approximately 200 mm long, and would have a maximum width of 1,219 mm. The addition of the vertical extensions would have been difficult, from a fabrication point of view, but possible.

However, the width constraint would have been a serious disadvantage to the PRY, as it necessitate the yoke be built in six pieces per side, with five vertical joints along the length. Section 6.3.3 discusses the disadvantages

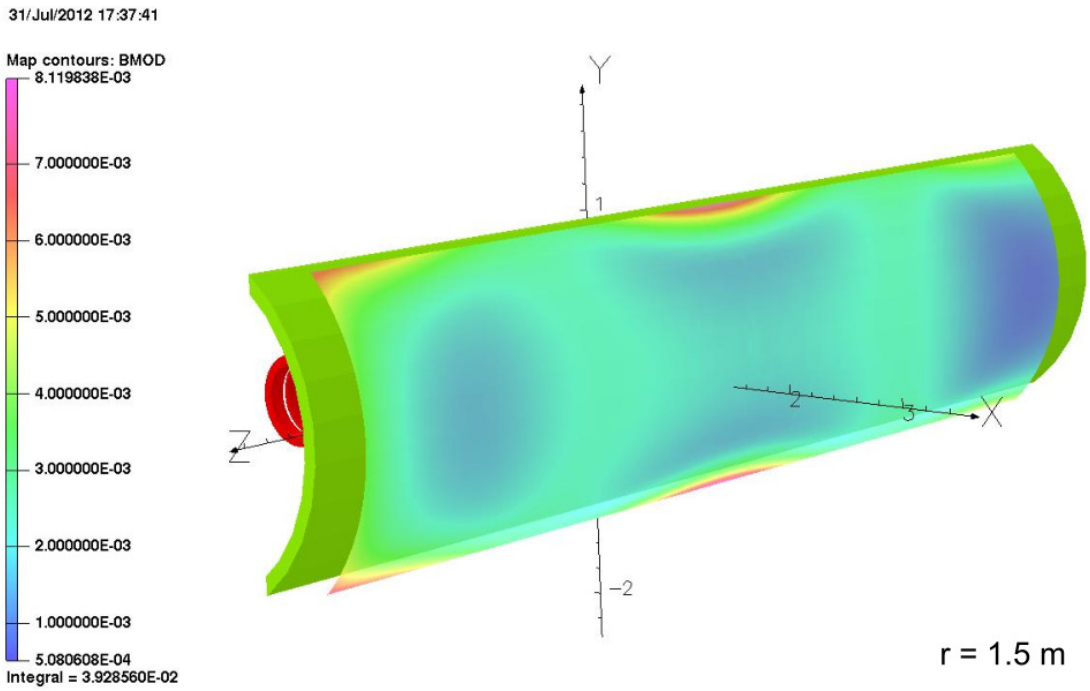

Figure 60: General Concept - Performance.

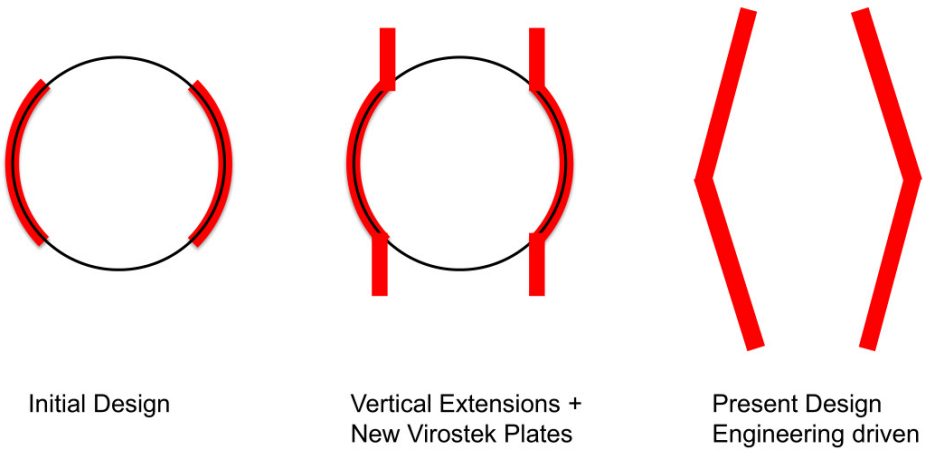

Figure 61: Development History

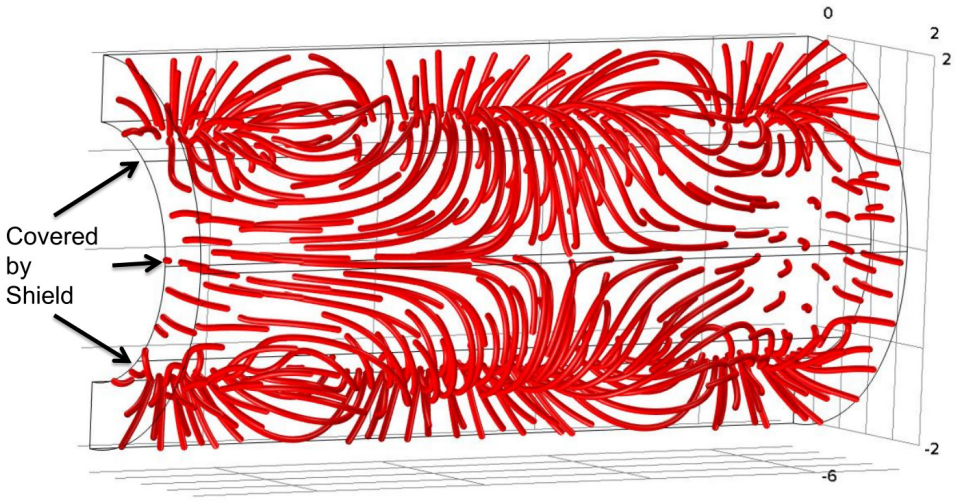

Figure 62: Source of Stray Field.

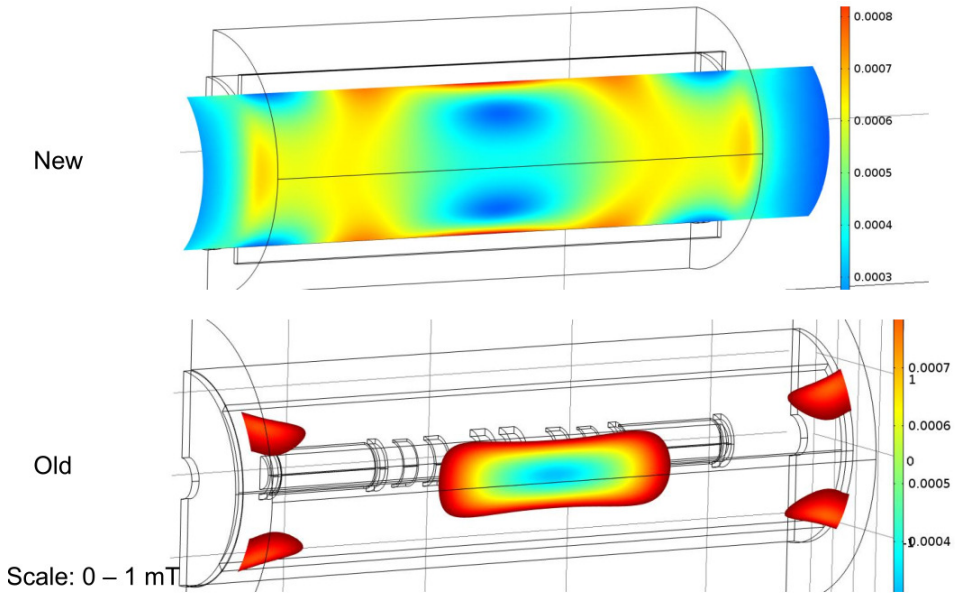

Figure 63: Comparison Vertical Extension. Both images use the same scale for the magnetic flux density, $0 - 1\,\mathrm{mT}$.

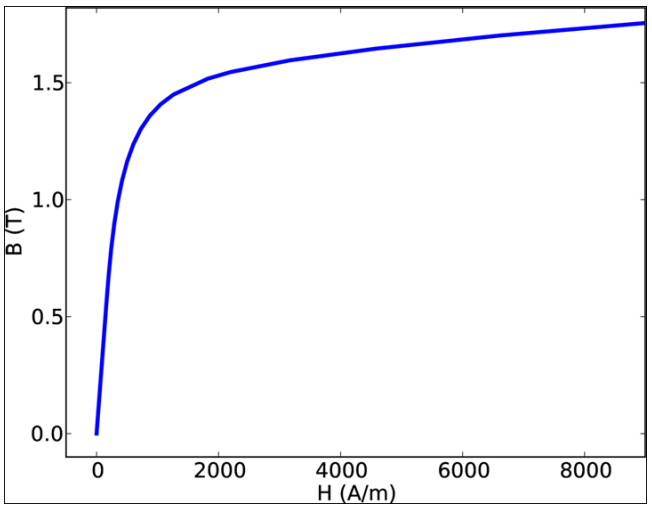

Figure 64: Magnetization curve of AISI 1010 steel.

of vertical joints for the magnetic properties of the PRY.

At this point, an improved design was conceived (the right hand image in Figure 61), where the arc plus vertical extensions evolved into two straight sections, tilted to an angle of $11.5°$. Eliminating the curved central part removed the width restriction, allowing for a design consisting of four flat plates of steel, two at the bottom and two at the top. (Two longer plates would also have been feasible, if not for the weight limit of the MICE Hall cranes). This is the design that has been considered for the rest of this section.

6.2 Magnetic design

6.2.1 Methodology - Computer Simulations

To analyse the problem and estimate the performance of the PRY solution, two commercial FEA packages were used: COMSOL [9] and OPERA 3D [**?**]. In the simulations it is assumed that the yoke is made of AISI 1010 steel; the BH-curve from OPERA was used, and can be seen in Figure 64.

The two software packages use different physics implementations, such that the results obtained from both packages can be compared and verified against each other. COMSOL solves for the magnetic vector potential:

$$\nabla \times \left(\mu^{-1} \nabla \times A\right) = J \ . \tag{1}$$

In this equation μ is the magnetic permeability, A the magnetic vector potential and J a current density. In contrast, OPERA solves for the magnetic scalar potential ϕ:

$$\nabla\mu\nabla\phi - \nabla\mu \left(\int_{\Omega_J} \frac{J \times R}{|R^3|} \mathrm{d}\Omega_J \right) = 0 \ . \tag{2}$$

Contributions to the magnetic field from current carrying structures at a distance R are usually evaluated using Biot-Savart law and integrated over the domain Ω.

The advantage of the scalar potential implementation of OPERA is that it is much more memory efficient: the number of degrees of freedom is smaller (scalar field versus vector field for each point in 3D space). The disadvantage is that problems are somewhat more difficult to setup, as different potentials need to be defined (reduced potential vs. total potential).

A special feature of COMSOL is the thin permeability boundary condition, which allows the user to model thin air gaps in geometries without compromising the mesh quality. This feature was benchmarked in a simulation with a real gap and no significant difference in the results was found. The thin permeability boundary condition can be described by the following equation:

$$n \times (H_1 - H_2) = \nabla_t \times \frac{d}{\mu_0 \mu_r} \nabla_t \times A \ . \tag{3}$$

In this equation H denotes the magnetic field strength and n a vector normal to the boundary.

In both software packages, linear and quadratic elements were used, without observing a significant difference in the results. The final verification was usually carried out using quadratic elements, which results in a slightly better spatial resolution. In OPERA, the coil fields were evaluated by integration and the contributions from iron domains by nodal interpolation. This is the preferred evaluation mode according to the manufacturer. The mesh size chosen was sufficiently small for the areas of interest; this was verified by mesh refinements and choosing higher order elements. For both simulation packages non-linear solvers were employed. Key proof-of-principle simulations were performed in both codes with, for this application, negligible differences in the results.

6.2.2 Expected Performance

For the design, care was taken to keep the magnetization in the PRY around 1.25 T, which is the level where μ_r starts to decrease. Figure 65 shows the typical magnetization in the shield for the 200 MeV flip mode.

The aim of the yoke is to screen large parts of the MICE Hall from stray fields, higher than $\sim$5 G. This level is sufficient for the operation of magnetically sensitive equipment such as cryopumps, power supplies and vacuum gauges located in the tracker cryostat. Figure 66 show the magnitude of the magnetic field at a radius of 1.5 m (just behind the shield) at beam height. The figure shows the magnetic field without shield for flip and solenoid mode (both 240 MeV). The expected stray field with shield is shown for two shield ticknesses, which are 10 and 12 cm. For the shielded case the 240 MeV solenoid mode is chosen, which can be considered a worst case.

The figures show that the stray field is reduced from 30-60 mT to $\sim$1 mT in case of the 10 cm shield and $<$0.6 mT for the 12 cm shield; this is a reduction of factor 30–100, depending on the position and chosen shield thickness. Increasing the shielding iron by 20% doubles the performance of the shield.

Figures 67 and 68 show the extent of the fringe field for the 200 MeV flip mode. The images show 3D iso-surface plots; the green surface represents a field of 5 G. Both figures show a comparison of the unshielded situation versus the stray field extent with partial return yoke. In both scenarios, the models include no iron in the MICE Hall, an approximation which is valid for this comparison. The figures emphasize that the stray field extent is drastically reduced with the magnetic shield: in longitudinal direction the stray field is reduced from about ± 7.5 m to about half of that. Even in the vertical direction, which is not covered by the shield, the stray field extent is reduced significantly from 9 m to about 4.5 m. In the horizontal direction the 5 G line (assuming a 12 cm thick shield) is located directly behind the shield; therefore all of the main floor of the MICE Hall will have a field below 5 G.

Particular emphasis during the development process was on a solution which would ensure that equipment vital to the operation of MICE was shielded. In particular, the electronics within the tracker cryostats are known to be very sensitive to magnetic field. The tracker cryostats are located adjacent to the two spectrometer solenoids. Without shielding, the stray field is $\sim$36 mT, as shown in Figure69. Using the shield this is reduced to 0.6 mT at the position closest to the tracker. The stray field within the tracker cryostat drops quickly with distance, so on the opposite side of the cryostat the field is predicted to be less than half of this (< 0.3 mT).

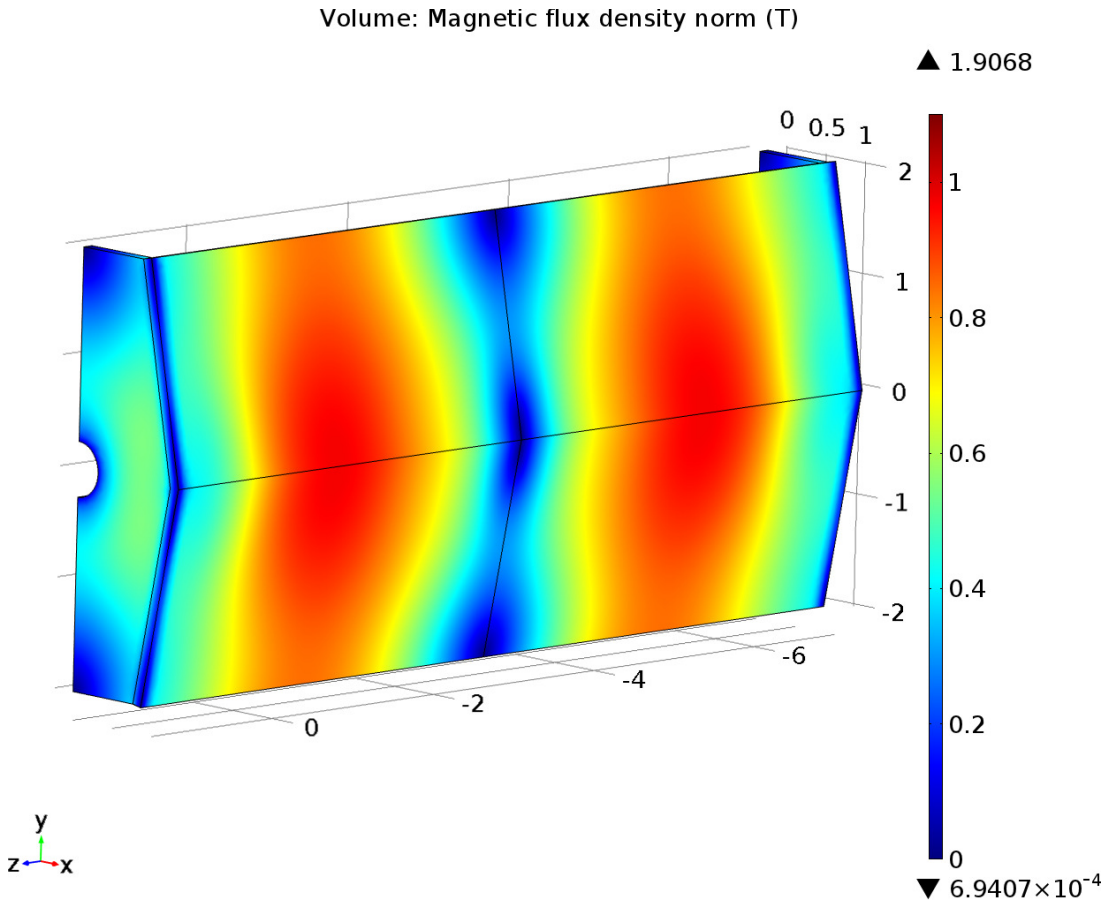

Figure 65: Magnetic field equivalent to the magnetization of the shield for 200 MeV in flip configuration.

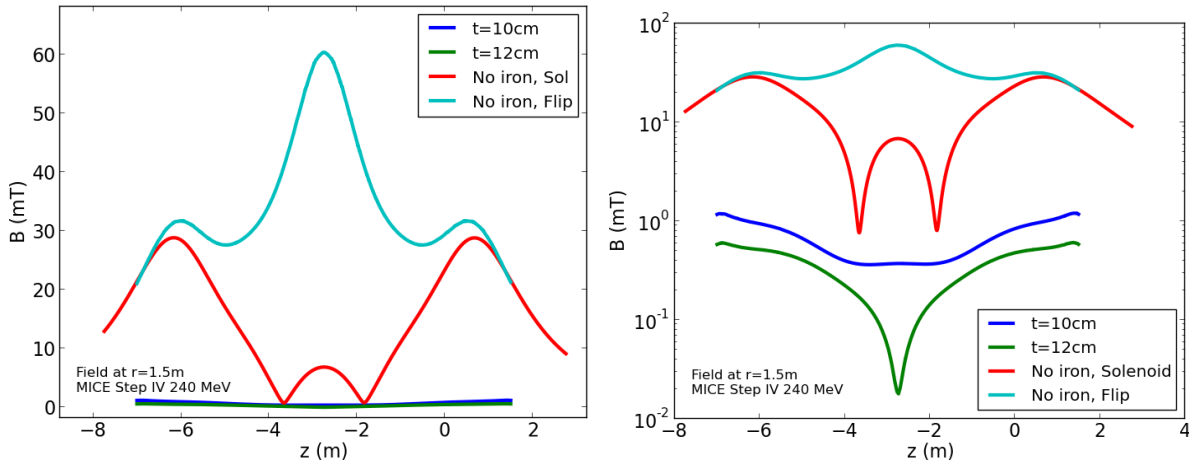

(a) Linear scale.

(b) Log scale.

Figure 66: Modulus of the magnetic fringe field at a radius of 1.5 m at beam height. Both figures show the same data; the right hand figure uses a logarithmic scale.

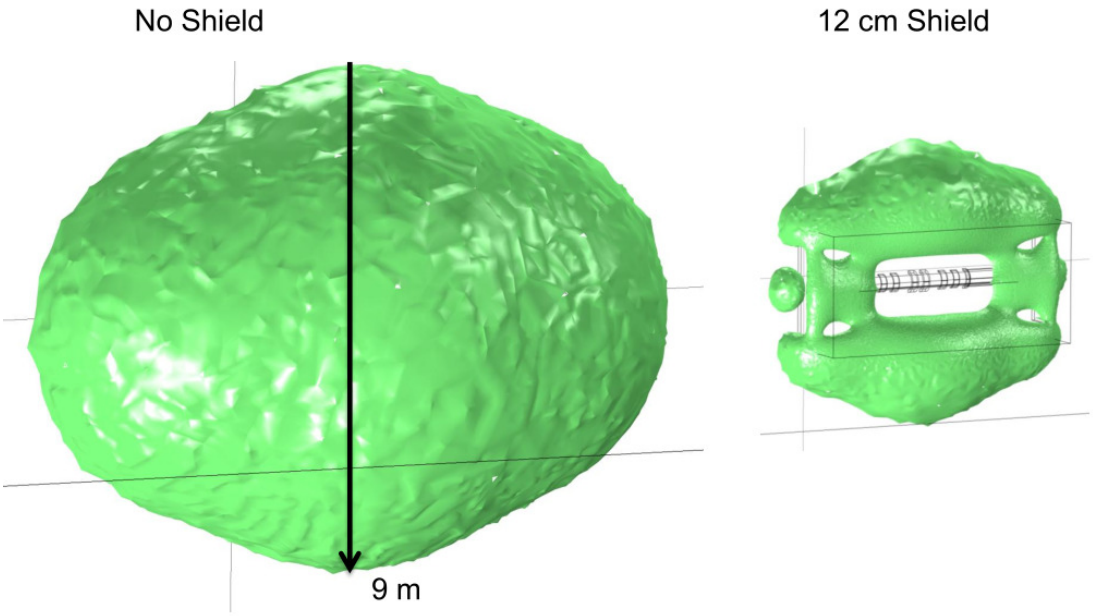

Figure 67: 5 G iso-surface plot of MICE for 200 MeV flip mode. The left figure shows the 5 G surface for an unshielded scenario (no iron present) versus the case where a 12 cm shield is adopted.

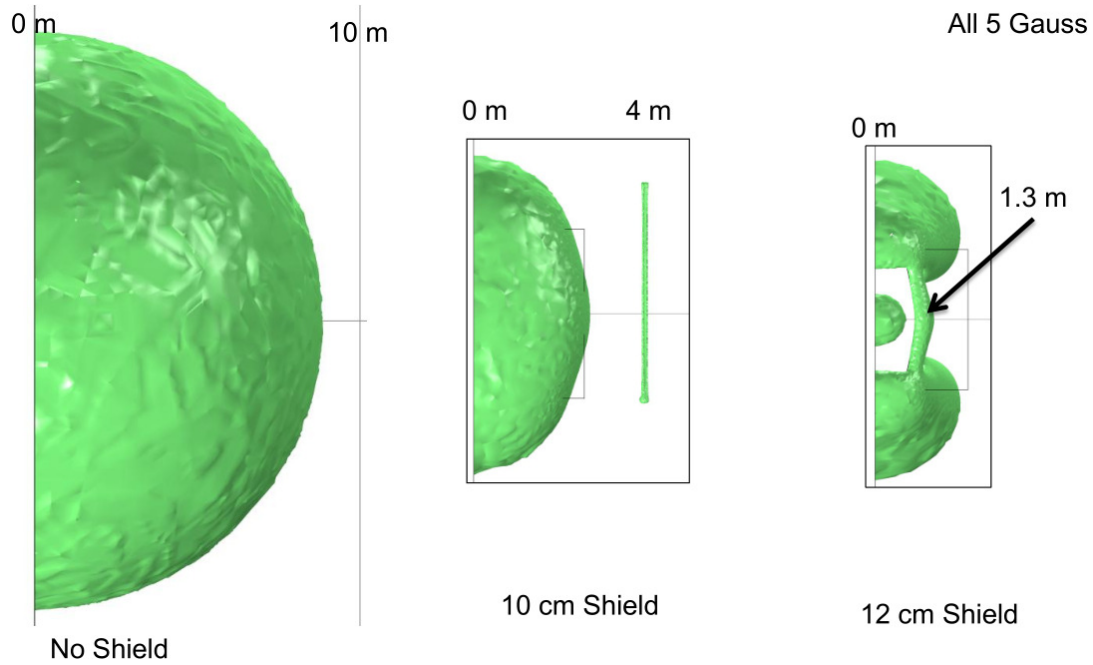

Figure 68: 5 G iso-surface plot of MICE for the 200 MeV flip mode, shielded and unshielded, in frontal view.

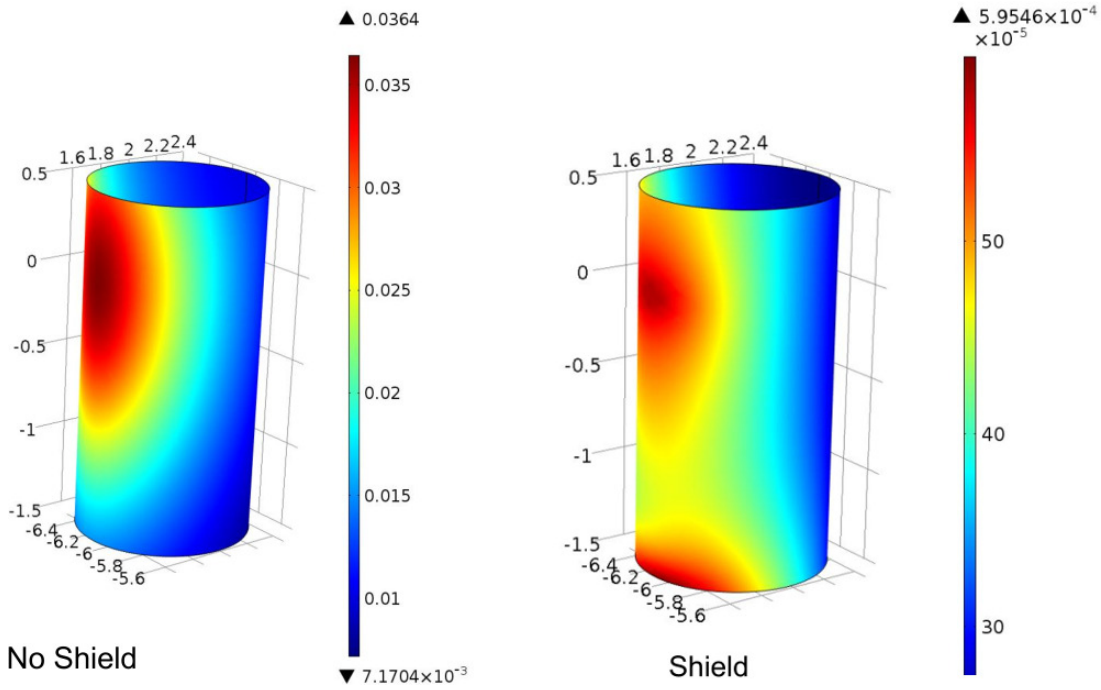

Figure 69: Modulus of the magnetic field at the position of the tracker cryostat. The left figure shows the field assuming an unshielded situation and the right one with a 12 cm thick shield. The scale maximum has dropped by a factor of 60.

6.2.3 Effect On the Beam

The effect of the PRY on the beam dynamics of MICE was studied separately using tracking studies in MAUS. The findings are discussed in more detail in [**?**]; in short, the study concluded that the PRY has a barely measurable effect on the beam travelling through MICE. The main effect is to introduce a slight misfocus to the beam, introducing a slight change in the cooling power of the channel. In summary, there is no reason, from a beam dynamics perspective, not to implement the partial return yoke.

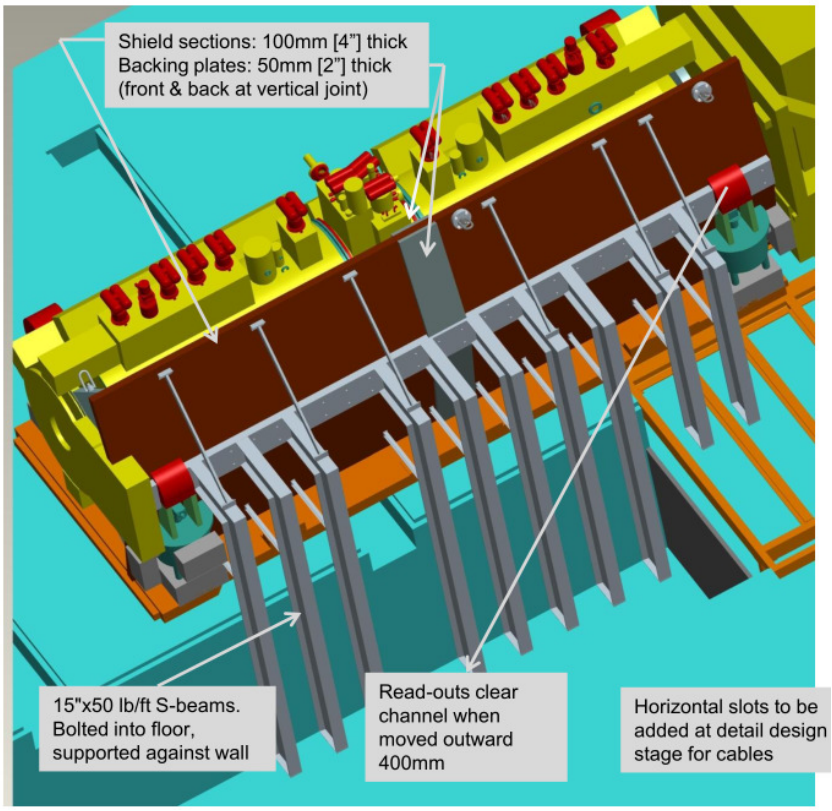

Figure 70: Overview of the engineering design.

6.3 Mechanical design

The engineering design of the magnetic shield was carried out by the Mechanical Engineering group of the Magnet Division at BNL. This section contains a summary the efforts of the initial design phase, which includes the general engineering concept, the support structure, forces on the shield and connection issues.

6.3.1 Engineering Concept

Figures 70 and 71 show the general engineering concept, after the iterative development process described in Section 6.1. The emerged design has a very similar, if not better, shielding characteristics to the initial suggestion with vertical extensions. In total, 8 panels of AISI 1010 are required, each about 4 m long and 1.5 m in width. The thickness of each panel is 10 or 12 cm, depending on the shielding performance required by the experiment. The weight of each panel is approximately 4.5 t (metric) and can therefore be lifted and transported in the MICE hall (the cranes in the MICE hall have a weight limit of 8 t). Each panel is tilted by 11.5° to interfere less with components in the hall and to improve the shielding performance.

Figure 71 shows the shield and the support structure, which consists of several S-beams. The support structure is designed to take the force acting on the shield to the floor. The number of support legs has been adjusted to comply with maximum permissible floor loadings in the MICE hall in this area.

An additional iron structure is envisaged to cover the open space between the Virostek plate and the shield, which further improves the shielding performance by preventing flux leakage.

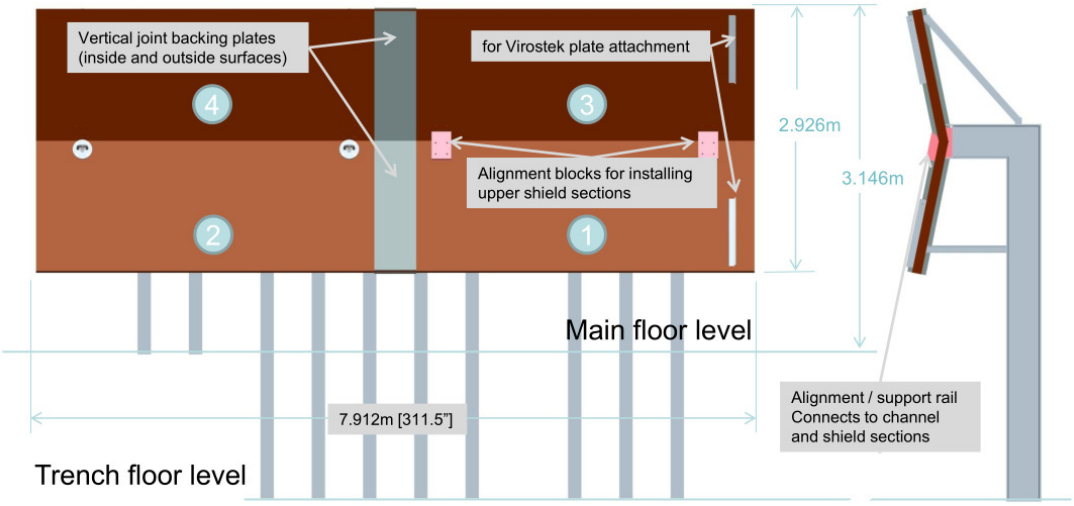

Figure 71: The MICE Partial Return Yoke.

Table 3: Forces on the shield in Newton.

	200 MeV Flip	240 MeV Flip	200 MeV Solenoid	240 MeV Solenoid	Case 5 Solenoid
Section 1 F_x	-7376.33	-8460.42	-2344.79	-2258.92	-3077.52
Section 1 F_y	1432.61	1645.39	436.87	416.73	575.77
Section 1 F_z	-0.47	0.25	-2.54	-3.05	-7.45
Section 2 F_x	-7414.04	-8498.62	-2382.47	-2297.38	-3115.83
Section 2 F_y	1439.29	1651.92	444.02	423.96	582.47
Section 2 F_z	2.22	2.01	2.86	3.32	7.71
Section 3 F_x	-7375.00	-8458.57	-2344.89	-2258.96	-3077.52
Section 3 F_y	-1432.93	-1645.79	-436.75	-416.66	-575.82
Section 3 F_z	-1.49	-0.76	-3.33	-3.74	-7.97
Section 4 F_x	-7415.20	-8500.02	-2382.90	-2297.80	-3116.01
Section 4 F_y	-1441.16	-1654.05	-444.73	-424.70	-583.92
Section 4 F_z	1.92	1.32	3.05	3.49	7.68

6.3.2 Forces on the Shield

The forces on the shield were evaluated for all cases of Step IV. The study was carried out using COMSOL, which allows for the evaluation the force using the Maxwell stress tensor. The force is evaluated for each panel separately (for the panel numbering see Figure 72).

Table 3 shows the results of the analysis. It is worth nothing that there is no net longitudinal or vertical force on the shield due to symmetry reasons. The largest force is in horizontal direction; the direction is such that it acts to collapse the shield onto the MICE channel.

The forces were used to evaluate the stresses and deflection of the shield. The forces were applied as a bulk force in an ANSYS FEA simulation. The results of this simulation are shown in Fig. 73. The maximum deflection is 5 mm, which occurs at the top of the shield. This can be reduced significantly by either doubling up the S-beams (factor of two reduction) or by introducing crossbars (to less than 0.28 mm). Crossbars were adopted for the following engineering design.

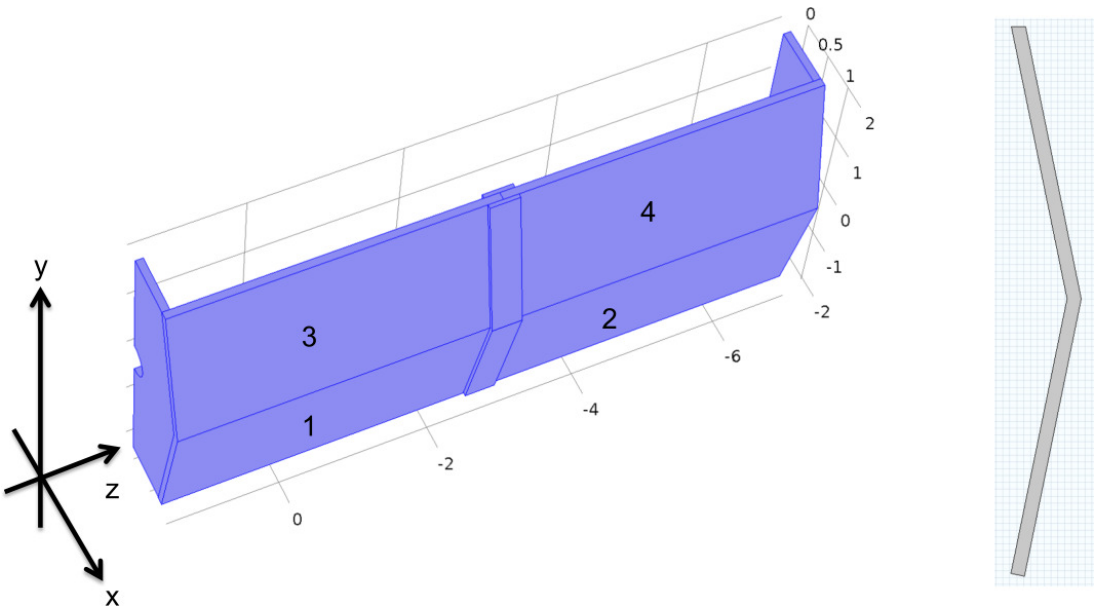

Figure 72: Geometry used to evaluate the forces on the shield.

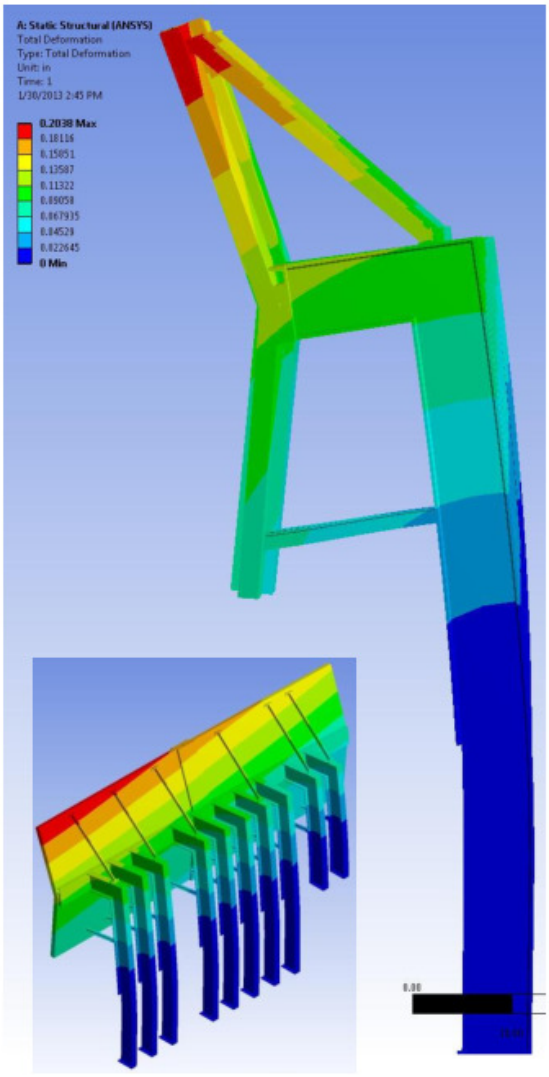

Figure 73: Result of the ANSYS simulation.

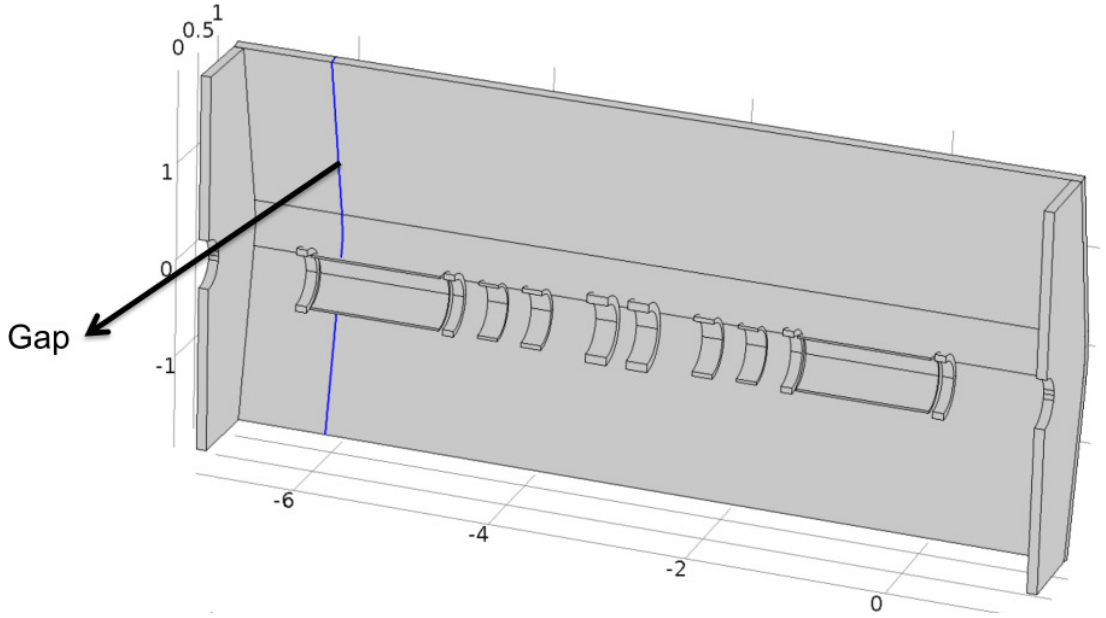

Figure 74: Geometry: Vertical gap in shield.

6.3.3 Vertical Gaps in the Shield

Vertical gaps in the shield occur between two adjacent shielding panels. Initial investigations showed that vertical gaps in the shield are detrimental to the shielding performance. Figure 74 shows the position of a vertical gap in the shield near the tracker region. The simulation result of the stray magnetic flux behind the shield, at a radius of 1.5 m and beam height is shown in Fig. 75. The figure shows that depending on the width of the gap the stray field behind the shield increases substantially.

To avoid performance impacts several potential solutions were studied. An adequate and easy to implement strategy is to double-up the shield at the position of a vertical gap; Figure 76 illustrates the concept. Each of the two backing plates is required to be half the thickness of the shield. The width of each connection piece is 0.4 m. The backing plates work by forming a low magnetic reluctance joint between neighboring shield sections; at the joint the magnetic flux is redirected into the backing plates, thus avoiding the vertical gap. The performance of this concept was evaluated using FEA; in the simulation it was assumed that the air gap between backing plates and shielding panel is 0.5 mm. As shown in Figure 77, the impact on the shielding performance can be expected to be minimal.

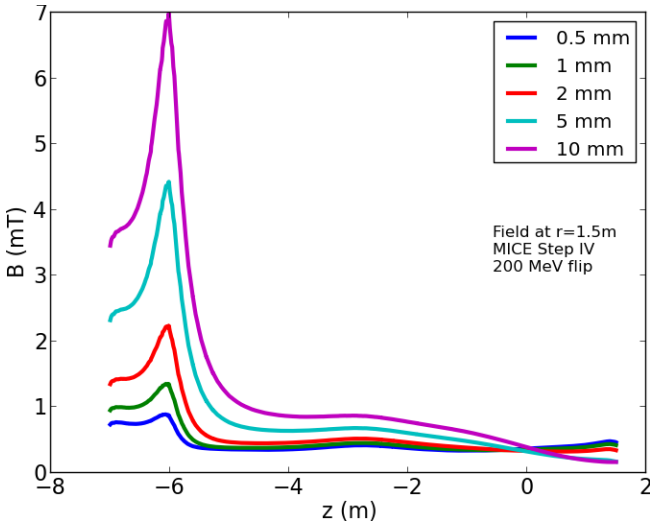

Figure 75: Modulus of the magnetic flux density at a radius of 1.5 m for 200 MeV flip mode assuming a vertical gap at $z = -6$ m.

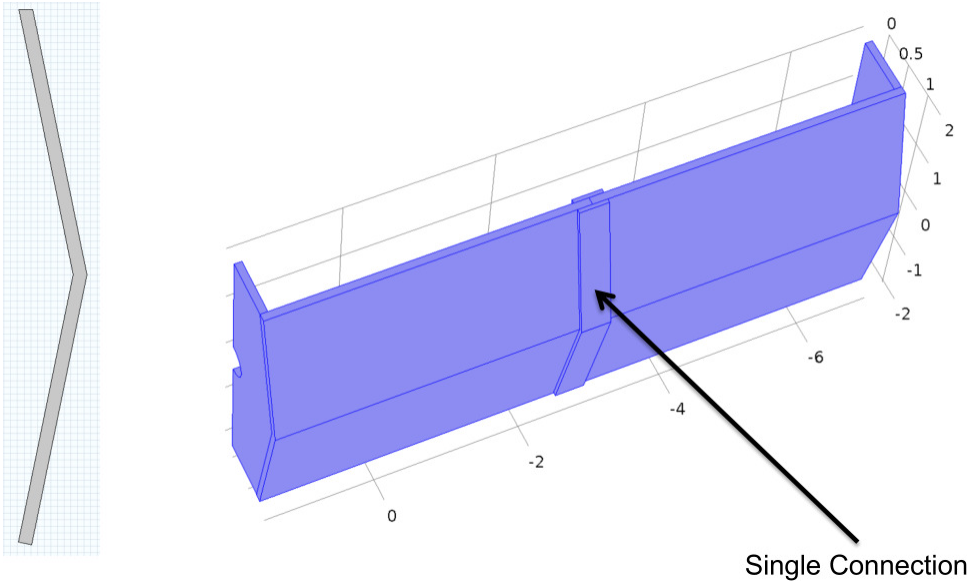

Figure 76: Concept of doubling up a vertical gap.

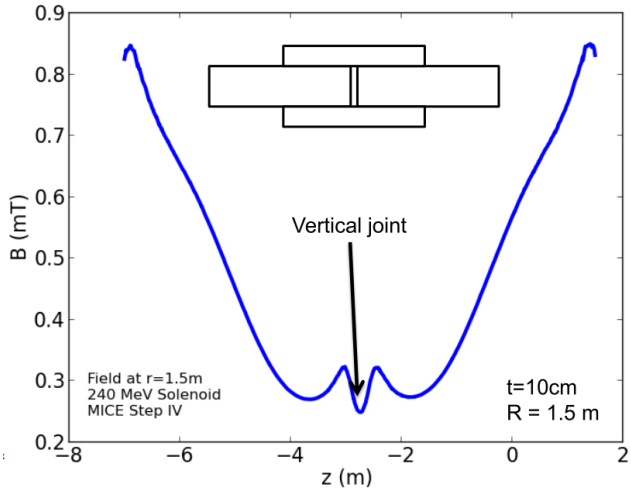

Figure 77: Modulus of the residual stray field at a radius of 1.5 m and beam height for 200 MeV flip mode. The vertical gap is doubled up using two backing plates, each 40 cm long.

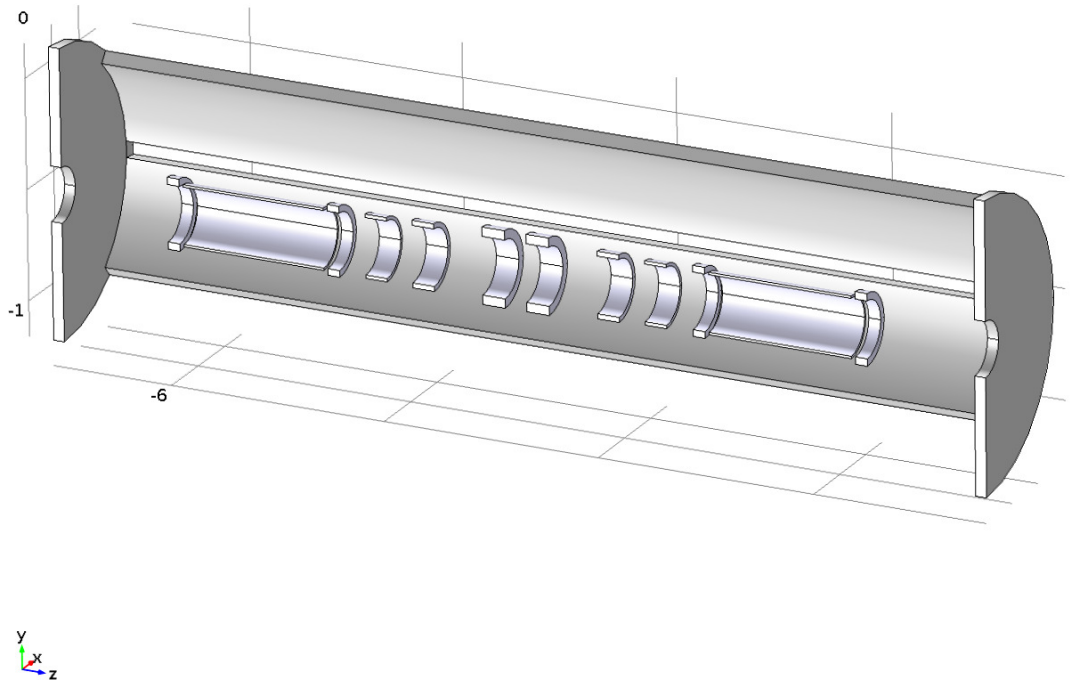

Figure 78: Horizontal gap in shield: Geometry Overview.

6.3.4 Horizontal Gaps in the Shield

Horizontal gaps as shown in Figure 78 in the shield were studied as well. Figures 79 and 80 show simulation results for 200 MeV flip mode. The figures show that the stray field behind the shield by comparison is far less sensitive to horizontal gaps. Even gaps of 20 cm width produce only an increase in stray field of about 1 mT. Horizontal slots in the shield, as shown in Figure81, can therefore be used to feed connections through the shield, instead of around. This is vital in certain situations, for example the waveguides between the Tracker and Tracker Cryostats; which are of set length, and have a limited bending radius.

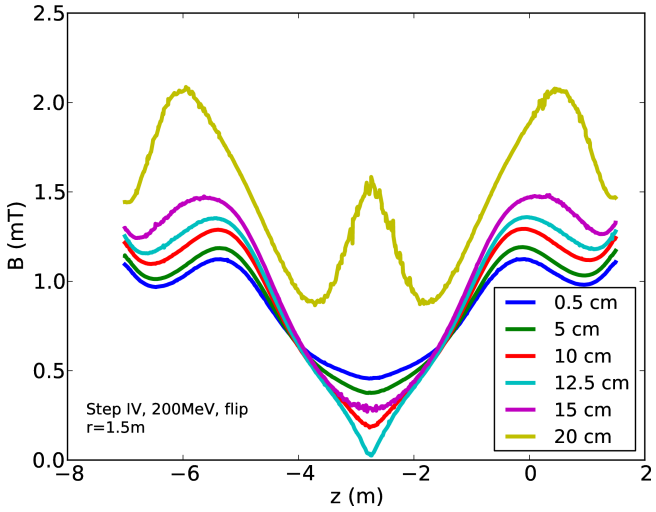

Figure 79: Modulus of the residual magnetic field at a radius of 1.5 m. The simulation assumes a horizontal gap in the shield, at beam height.

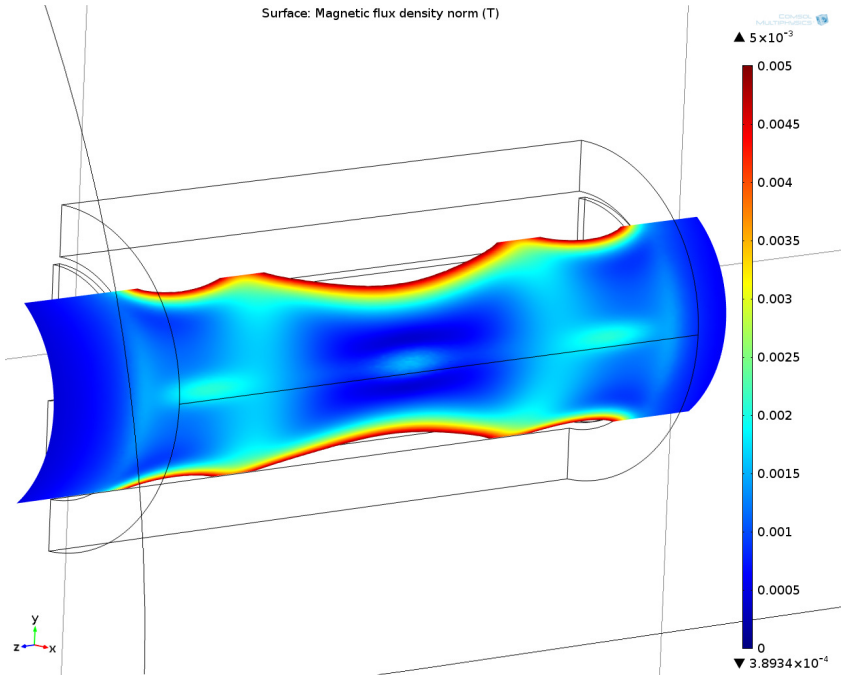

Figure 80: Field at a radius of 1.5 m behind the shield. This simulation assumes a horizontal gap of 200 mm width over the entire length of the shield (as shown in Figure 78).

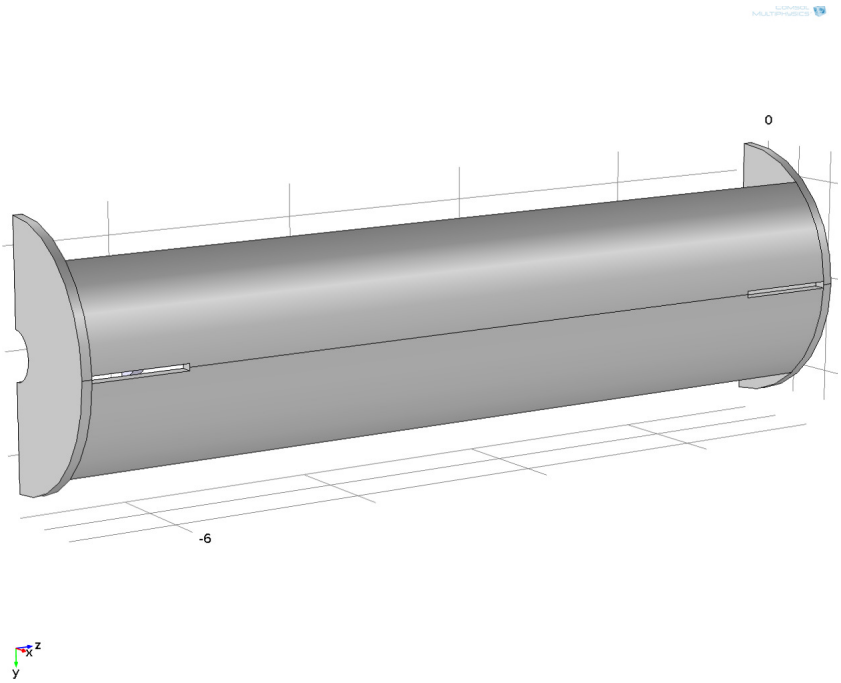

Figure 81: The figure shows a shielding concept with a 1 m long slot near the Tracker region, which can be occupied by the Tracker waveguides to connect the Tracker and Tracker cryostat. The slots are 10 cm wide, which is sufficient for the Tracker waveguide connectors.

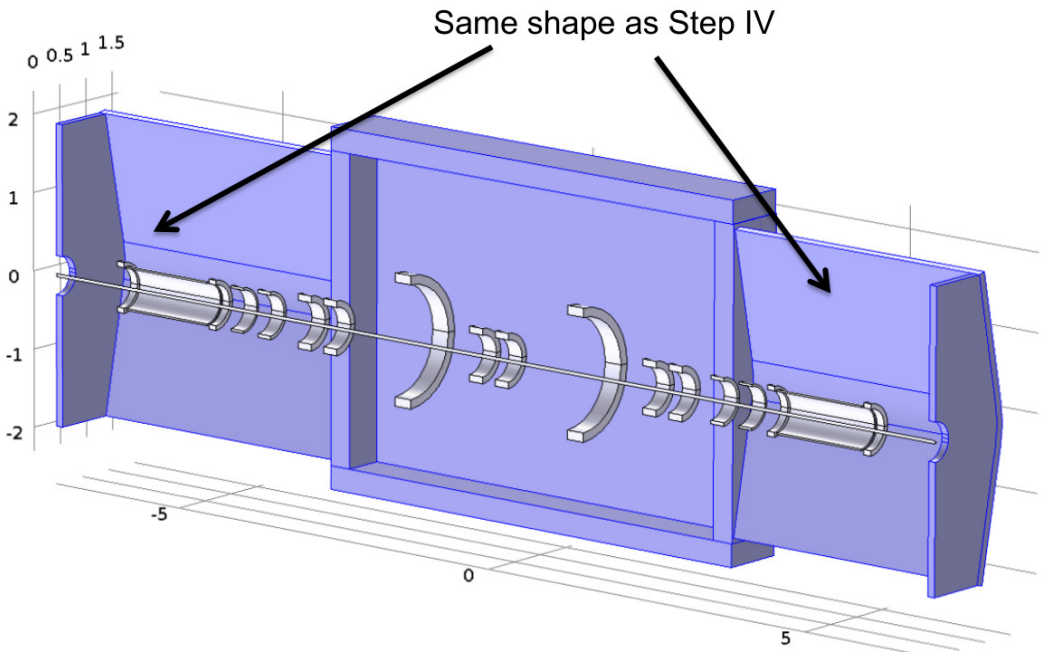

Figure 82: Suggested shield geometry for Step VI.

6.3.5 Extension to Step VI

The main focus of the development process is on Step IV. However, an important side aspect of the development was the possibility to upgrade the design to Step VI. Step VI is presently expected to commence in 2018[**?**]. Step VI is more challenging to shield than Step IV, due to the presence of the large coupling coils. It is generally accepted that local shielding, as described in Section 5, will not work in all likelihood. A limited effort was therefore made to show that the partial return yoke can also be implemented for Step VI. A potential geometry of the partial return yoke is shown in Figure 82. The residual stray field at a radius of 1.8 m, which is just behind the shield, is shown in Figure 83. The figure illustrates that a similar shielding efficiency can be obtained for Step VI as well.

In general it was tried to recycle as much as possible of Step IV; the region in Step VI which offers itself to this is the tracker region, where the iron panels of the Step IV shield can be reused. Around the coupling coils new iron panels (which have not been fully developed) would need to be installed. Preliminary simulations showed that the iron near the coupling coils needs to be at least 30 cm thick for sufficient shielding. The increase in thickness is due to the significantly larger amount of magnetic flux generated in this area. Figures 84 and 85 show the extent of the 5 G surface in 3D iso-surface plots.

The figures illustrate that the shield can reduce the stray field in the MICE hall effectively: longitudinally, the 5 G line shifts from ± 20 m to ± 7.5 m and finishes with the MICE experiment. In the vertical direction, the extent of the fringe field is reduced from 15 to 4 m. Horizontally, the 5 G surface moves effectively to the position of the shield, that is the fringe field in the hall is reduced to 5 G or less.

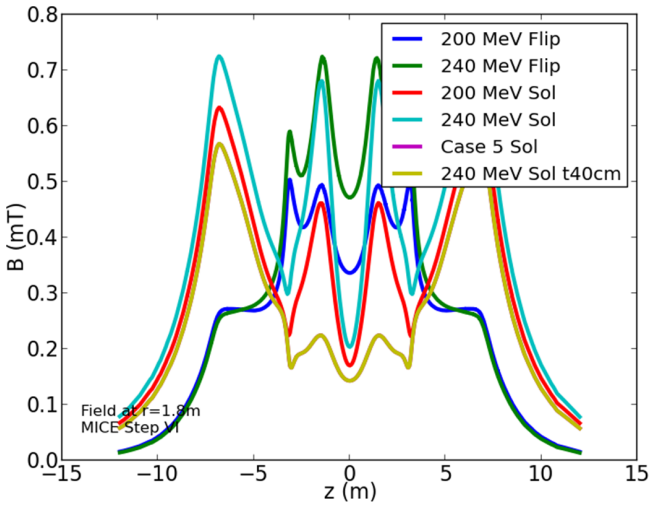

Figure 83: Residual stray field (modulus) at a radius of 1.8 m for the various cases of Step VI.

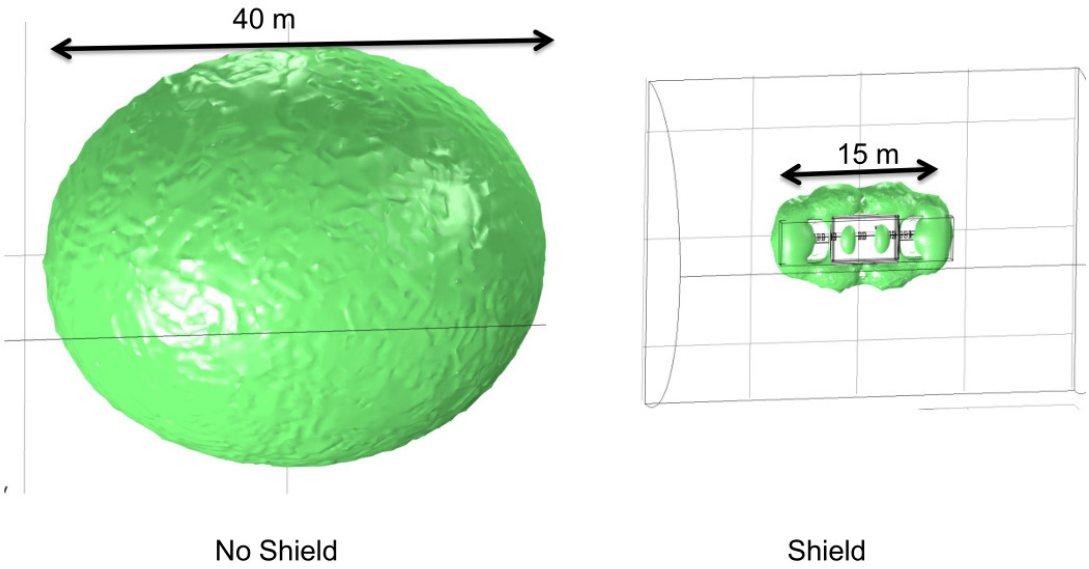

Figure 84: Step VI: iso-surface plot of the 5 G line (with and without shield).

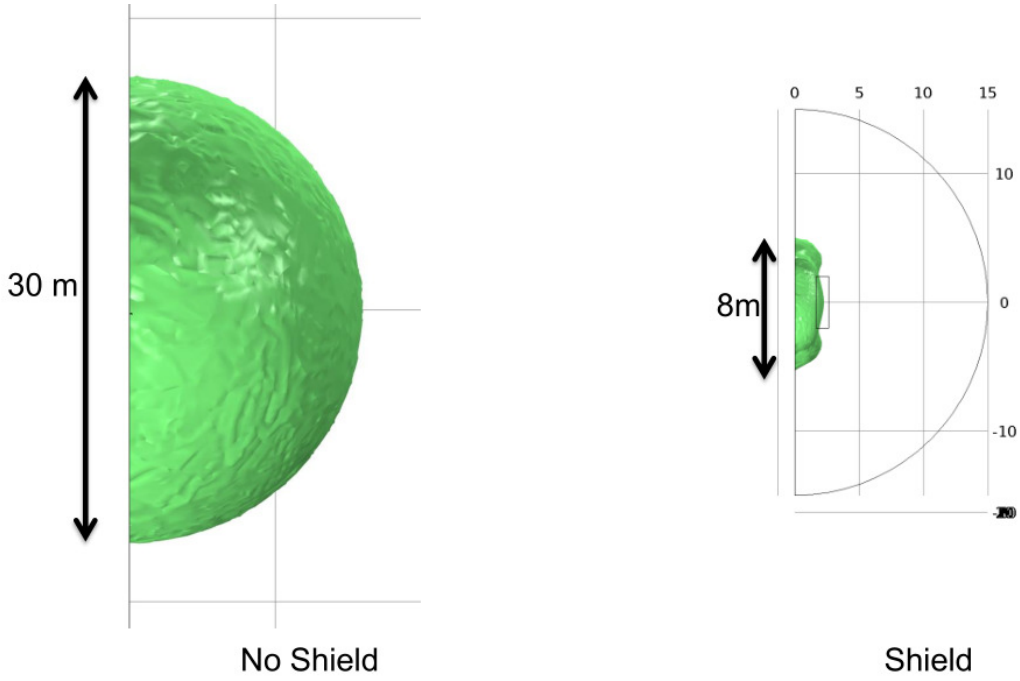

Figure 85: Step VI: iso-surface plot (frontal view) of the 5 G line (with and without shield).

6.4 Implementation in the MICE Hall

The space available in the MICE Hall, prior to the requirement of the magnetic field mitigation changes, was adequate but not excessive. These changes require additional space, for the movement of sensitive equipment and the implementation of magnetic shielding.

For the PRY, there are a significant number of environmental constraints; based on structures, equipment and services (that have already been installed or are planned to be installed) for the operation of the experiment. The following details highlight these constraints and show how they can be dealt with in each case, either by configuration of the PRY to fit with the constraint or a change to the environment to accommodate the PRY.

6.4.1 Experimental Devices & Detectors

Spectrometer Solenoid (SS)

Drawings
TD-1189-1603 Step IV with Yoke (Mod) [**?**]
TD-1189-1455 Upstream SS with Yoke [**?**]
TD-1189-XXXX Downstream SS with Yoke [**?**]

6.5 Summary

Lead author: JT/HW

7 Cost, schedule and risk

7.1 Baseline

Lead author: CM/JT/KL/RP/AG

7.2 Yoke

Lead author: HW/JT/KL/RP/AG

8 Recommended action

Lead author: KL

9 Conclusions

Lead author: KL

Appendices

A Hall Model Details

This appendix includes more complete details of the ferrous and non-ferrous items modelled in the MICE Hall model, as described in Section 4.3.

A.1 Ferrous Objects

North and South Shield Walls (NSW and SSW)

The NSW and SSW stand to the North and South of the cooling channel, and consist of a frame, constructed from horizontal and vertical steel I-beams, with a steel plates bolted to both sides of the frame. The walls are modelled as a continuous double skinned wall, each skin composed of 35 mm AISI 1010 steel. The I-beams that support the shield wall are not modelled, this is a significant amount of steelwork but this level of detail could not be supported in the hall model. Also, the model uses a rectangular sheets approximation, which do not completely extend to the floor in various areas where it slopes.

Floor Web and Floor Web Plates

This is an estimate of the lattice steelwork that sits underneath the beamline between the NSW and SSW, as well as some lattice steel work on the North side of the NSW and the steel floor plates on top of it.

Dipole D2

The dipole is modelled as a solid block of steel. The dipole functionality, i.e. the fields it produces, have not been included in the model.

Quadrupoles, Bases and Baseplates

Q4-Q9 have been included in the model, including an estimation of the steelwork in their bases and the baseplates, which was considered significant. Like the dipole, the quad functionality, has not been included in the model. As the quadrupoles have been modelled as a lumped mass of ferrous material their ferrous mass may have been overestimated.

Virostek Plates and Upstream TOF plates

The Virostek plates are designed to shield the photomultiplier tubes in the TOF detectors from the stray magnetic field. The upstream TOF plate sandwiches the TOF1 detector between the TOF plate and the Virostek plate improving the the shielding for the TOF1 photomultipliers.

The Electron Muon Ranger - EMR

A simple frame has been included to represent the EMR steelwork. The framework for the EMR is complex and would have been difficult to model in detail, but the simple frame approximation is expected to be sufficient.

Decay Solenoid Area - DSA

The DSA wall is composed of steel and concrete blocks which separates the decay solenoid, D2 and Q4-Q6 from the rest of the MICE hall. The steelwork that forms the DSA area constitutes a signficant mass of steel and therefore has been included in the MICE hall model.

Beam Dump

The beamdump is a steel and concrete assembly that marks the end of the MICE beamline. The model was based upon the technical drawings, but approximated due to resolution limitations in the model, removing some of the outer steel framing.

South West Distribution Board

Although only a small amount of steel this was included in the hall model as it will directly effect the field estimate for electrical installations attached to the wall.

Linac Shield Wall

The linac wall is a steel loaded concrete wall, which provides shielding from the ISIS linac room, running parallel to the MICE experimental hall. A reduced BH curve was used to model the wall, approximating its reduced gross magnetisation. The curve was approximated by comparing the attractive force of a permanent magnet to the linac wall and the NSW. This is a crude technique but gives a reasonable first approximation to the magnetisation, which was reduced to 15% of the nominal value.

Trench Plates

The plates covering the Trench have been included in the model, as they constitute a significant amount of steel and run in the Z direction. The steelwork supporting the plates has not been included.

Cellar

The model includes eight magnet bases, buried in the MICE hall. Each base is a steel shell, filled with concrete.

North Mezzanine

The north Mezzanine floor runs behind the north shield wall and is currently constructed from steel plate, so these plates were added to the model. The structural steelwork supporting this floor was not added to the model.

Cranes

The two cranes were crudely approximated by two steel beams running North to South at the West end of the MICE hall. This should give a reasonable approximation of their ferrous mass, but no attempt at modelling their complex geometry has been made.

A.2 Missing Ferrous

The missing items which will produce the largest discrepancies in the model are probably:

- I-beams providing structural support for walls and floors.
- Compressors, racks or steel cabinets, such as the magnet power supply racks. Where possible, these are being moved away from the cooling channel, which will minimize their effect on the model.
- The substation in the North West corner. This has been investigated as a separate sub-model, as described in Section 5.2.3).
- The fridge equipment in the South East Corner.

References

[1] V. Baylis *et al.*, "Magnetic Group Report." https://indico.cern.ch/materialDisplay.py?contribId=10&sessionId=0&materialId=slides&confId=190654 , 2012.

[2] Magnetic Shielding Group, "MICE stray field mitigation twiki." https://twiki.stfc.ac.uk/bin/view/Projects/MICEMagneticShielding , 2012.

[3] Magnetic Shielding Group, "MICE Hall Magnetic Models." http://www.hep.shef.ac.uk/research/mice/opera_models/ , 2012.

[4] **MICE collaboration** Collaboration, M. Bogomilov *et al.*, "The MICE Muon Beam on ISIS and the beam-line instrumentation of the Muon Ionization Cooling Experiment," *JINST* **7** (2012) P05009, 1203.4089.

[5] **MICE collaboration** Collaboration, D. Adans *et al.*, "Characterisation of the muon beams for the Muon Ionisation Cooling Experiment," *Submitted to JINST* (2013) 1306.1509.

[6] The MICE collaboration, "MICE: An International Muon Ionization Cooling Experiment,Technical Reference Document." MICE-TRD-2005, 2005.

[7] J. Tarrant, "West Wall Mezzanine–Review of Design." http://mice.iit.edu/micenotes/public/pdf/MICE0402/MICE0402.pdf , 2013. MICE-Note-402.

[8] J. Tarrant, "MICE scintilating-fibre tracker." http://mice.iit.edu/mnp/MICE0403.pdf , 2013. MICE-Note-403.

[9] http://www.comsol.com/.